NASA CR 180848

NASA

LARGE SCALE ADVANCED PROP - FAN
(LAP)
STATIC ROTOR TEST REPORT

By: Charles L. De George

Jay E. Turnberg

Harry S. Wainauski

HAMILTON STANDARD DIVISION
UNITED TECHNOLOGIES CORPORATION

Prepared for

NASA

LARGE SCALE ADVANCED PROP - FAN (LAP)
STATIC ROTOR TEST REPORT

By: Charles L. De George

Jay E. Turnberg

Harry S. Wainauski

HAMILTON STANDARD DIVISION
UNITED TECHNOLOGIES CORPORATION

CONTENTS

CONTENTS (Continued)

ILLUSTRATIONS

ILLUSTRATIONS (Continued)

TABLES

1.0 SUMMARY

This report describes the procedures followed and results obtained during
Static Rotor Testing of the SR-7L Large Scale Advanced Prop-Fan (LAP). The
LAP is a 2.74 meter (9 foot) diameter, 8 bladed advanced propeller designed
to attain high propulsive efficiency at flight speeds up to Mach .85. The
Prop-Fan achieves this superior speed and efficiency by employing thin swept
blades and high disc loading. The Static Rotor Test was conducted on a 7460
kW (10,000 Hp) whirl rig at the Wright Aeronautical Laboratory in Dayton,
Ohio. This test afforded the first opportunity to operate the Prop-Fan with
the SR-7L blades installed.

The purpose of the Static Rotor Test was to evaluate the static ($V_\infty = 0$)
aerodynamic performance and structural behavior of the Prop-Fan and evaluate
the readiness of the LAP and its instrumentation system for follow up wind
tunnel and static engine testing. The Static Rotor Test was accomplished in
four phases. In the first phase the thrust produced and power absorbed by
the Prop-Fan were measured over a range of blade angles from -6° (reverse) to
60° and a range of rotational speeds from 600 RPM to 1900 RPM. Blade vibra-
tory strain data was collected concurrently with the aerodynamic data. This
allowed the static operating envelope to be defined and the calculated blade
natural frequencies to be verified. During the second phase of testing the
blade steady state deflections and stresses were measured at operating condi-
tions for which analytical predictions of the stresses and deflections were
available. One of these operating conditions was a 20% overspeed point,
which was intended to be a proof test of the Prop-Fan structural integrity.
The third phase of testing employed a specially fabricated pressure tap blade
to map the blade surface pressure distribution for a range of operating con-
ditions. The final phase of testing explored the feasibility of measuring
unsteady aerodynamic phenomena with pressure transducers installed on the
surface of the SR-7L blade.

The results of the Static Rotor Test revealed good agreement between measured
and predicted aerodynamic performance at blade angles below 30° but lower
than predicted thrust produced and power absorbed above 30°. The onset of a
stall buffet phenomenon, characterized by elevated blade vibratory stresses,
was also observed as blade angle was increased beyond 30°. The measured dis-
tribution of steady state strains in the blade structure correlated well with
predictions as did the measured blade deflections. The overspeed test veri-
fied the structural integrity of the Prop-Fan and suggested that classical
flutter will not be a problem for flight operating conditions. The steady
surface pressure testing indicated that the blade tips were more highly load-
ed than expected for low blade angles and that the high tip loading dissipat-
ed with increasing blade angle. This observation correlates with the lower
than expected thrust measured at high blade angles. The unsteady pressure
phase of testing verified that unsteady aerodynamic phenomena could be ob-
served on the surface of the SR-7L blade. The unsteady pressure data however
could not be correlated with the stall buffet phenomenon.

2.0 INTRODUCTION

The SR-7L Large Scale Advanced Prop-Fan (LAP) is the culmination of over ten years of effort to extend the operating envelope of the propeller from the Mach .6 speeds attained by contemporary turboprop aircraft to the Mach .85 speeds of today's turbofan powered commercial airliners. The impetus for this effort is fuel efficiency.

Studies have shown that by applying thin swept wing technology to the design of propeller blades and by achieving higher disc loadings through the use of a greater number of blades, the inherent fuel efficiency of the propeller can be extended to speeds up to Mach .85. Prop-Fan propulsion should allow aircraft to be designed that are 15% to 25% more fuel (reference 1) efficient than todays most technologically advanced turbofan powered airliners.

NASA and Hamilton Standard have collaborated for over 10 years on Prop-Fan research. During this period of time a series of Prop-Fan models were tested in NASA and United Technologies Corporation wind tunnels. These models were used to evaluate the aerodynamic performance and structural dynamic behavior of various Prop-Fan designs (references 2 and 3). The data accumulated from these wind tunnel model tests resulted in the design of the Large Scale Advanced Prop-Fan (LAP)

The LAP is a 2.74 meter (9 foot) diameter, 8 bladed, single rotation tractor Prop-Fan. It has many of the features found on commercial and military propellers produced today by Hamilton Standard. The LAP in effect represents the evolution of Prop-Fan technology from wind tunnel models to a full size propulsion system.

The NASA Lewis Research Center, through its sponsorship of the Large Scale Advanced Prop-Fan (LAP) Program and the follow-on Prop-Fan Test Assessment (PTA) Program, has established a series of tests that take the LAP from initial mechanical checkout through flight test (reference 4). This report presents the test procedures followed and results obtained for the LAP Static Rotor Test conducted at the Wright Aeronautical Laboratory at Wright Patterson Air Force Base in Dayton, Ohio.

The Static Rotor Test was the first test of the Large Scale Advanced Prop-Fan as a complete assembly. The purpose of the test was to measure various Prop-Fan performance characteristics at static operating conditions $(V \infty = 0)$. The specific goals of the test program were as listed below.

- Determine the static thrust produced and power absorbed by the Prop-Fan over a range of blade pitch angles and rotational speeds.

- Determine the stall flutter or stall buffet restrictions, if any, on the LAP static operating envelope and verify the calculated blade natural frequencies.

3

2.0 (Continued)

- Measure the steady state stresses and deflections of the blade structure and compare these stresses and deflections with analytical predictions.

- Establish the structural integrity of the Prop-Fan by conducting an overspeed test per MIL-P-26366A.

- Measure the steady pressure distribution on the surface of the SR-7L Prop-Fan blade for a range of blade angles and Prop-Fan rotational speeds.

- Evaluate the performance of high frequency response transducers, installed on the SR-7L blade, in measuring time varying pressures on the blade surface.

Testing was conducted on a 7460 kW (10,000 HP) electric motor driven indoor whirl rig. No relative air velocity was supplied to the Prop-Fan rotor disc. The test procedure consisted of running a series of rotational speeds with the Prop-Fan operating in a fixed pitch mode. Conditions were allowed to stabilize at each speed and then data was recorded for a minimum of thirty seconds. The blade angle was then changed and the procedure was repeated.

The Static Rotor Test provided a thorough evaluation of the static performance of the Large Scale Advanced Prop-Fan and verified the system's readiness to proceed with wind tunnel and static engine testing.

4

3.0 PROP-FAN DESCRIPTION

3.1 GENERAL DESCRIPTION

A cutaway view of the Large Scale Advanced Prop-Fan is shown in Figure 3.1. The LAP is a 2.74 meter (9 foot) diameter, 8 bladed tractor type Prop-Fan, rated for 4474 kW (6000 hp) at 1698 RPM. It is designed to be mounted on a standard 60A splined propeller shaft.

3.2 ACTUATOR AND PITCH CONTROL

The LAP has a hydraulically actuated blade pitch change system and a hydro-mechanical pitch control (reference 5). Hydraulic pressure for the actuator was provided by pumps located in the control and driven by the propeller shaft. Static Rotor Testing was conducted with the Prop-Fan operating in a fixed pitch mode and the pitch change system was employed only to change blade pitch angle between test points by controlling the position of the actuator servo valve with a small electric motor. However the pitch change system was functional and producing hydraulic pressure throughout the test. The actuator has an adjustable low pitch stop feature, which allows the minimum blade pitch angle to be set between 40° and -6°. The stop accomplishes this by limiting the travel of the actuator servo valve. The low pitch stop was used to lock the blade angle for portions of the Static Rotor Test. Hydraulic pressure for changing blade pitch angle on the non-rotating Prop-Fan was provided by an electric motor driven auxilliary pump contained in the control.

3.3 SR-7L BLADE

The structural configuration of the SR-7L blade consists of a central aluminum spar, a fiberglass shell which overhangs the leading and trailing edges of the spar and a nickel sheath that covers the leading edge of the outer two thirds of the blade. The remaining internal cavities are filled with low density rigid foam. The fiberglass shell is protected from abrasion and environmental factors by an erosion coating. The erosion coating is a durable paint, which can be stripped and re-applied if deterioration occurs. A cutaway view of the blade is shown in Figure 3.2.

The SR-7L Prop-Fan blade aerodynamic design was accomplished using Hamilton Standard Program H444. This program employs Goldstein's lifting line-vortex theory (reference 6) to determine the blade loading distribution. The blade design makes use of NACA Series 16 airfoils outboard and NACA series 65 Circular Arc airfoils inboard. The blade has an activity factor of 227 with 37° of sweep at the tip. The blade was designed with pre-deflection so that it will assume the desired aerodynamic shape at cruise operating conditions (reference 7).
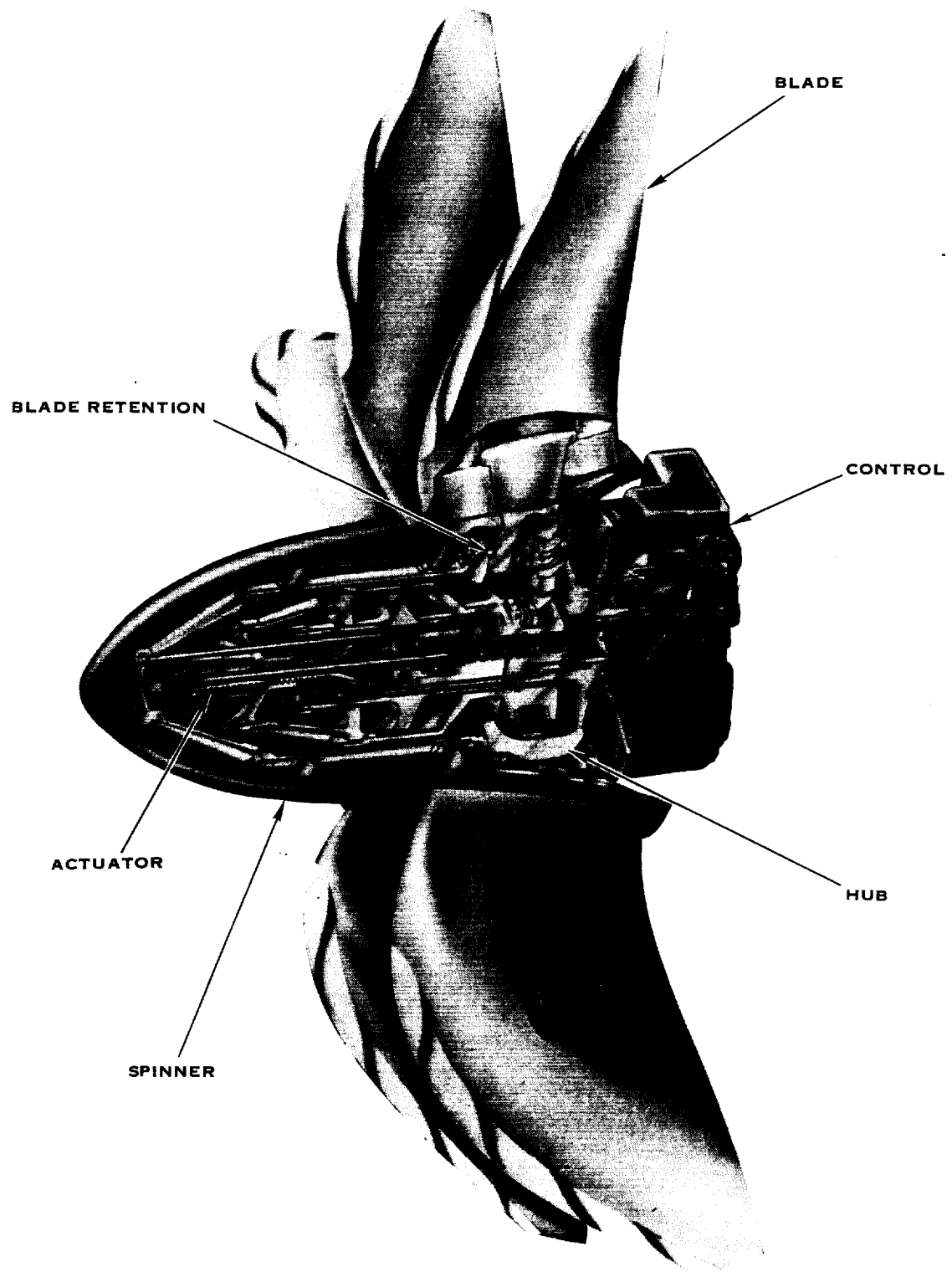
FIGURE 3.1 LARGE SCALE ADVANCED PROP FAN
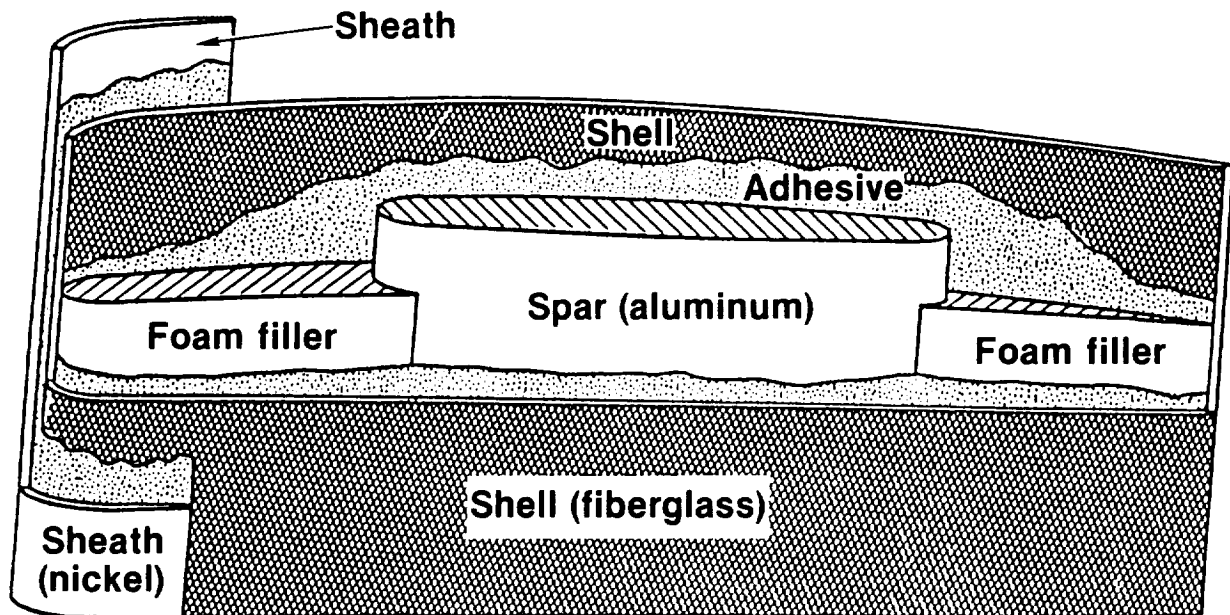
FIGURE 3.2 FEATURES OF SR-7L BLADE CONSTRUCTION

3.4 HUB AND BLADE RETENTION

The hub forms a semi-rigid link between the blades that produce the thrust and the engine shaft which transmits the torque. The hub is a one piece, partially forged part which is carburized, heat treated and machined. The hub is secured to the engine shaft by two cones which are preloaded against each other by the Prop-Fan retaining nut. The hub also supports the blade pitch change actuator, the pitch control and the spinner.

The Prop-Fan blades are retained in the hub by a single row of ball bearings. The balls ride in two hardened steel races. One race is machined into the rim of the hub arm bore and carburized. The other race is a separate part that bears on the blade shank. The ball bearings are kept from contact with each other by a separator. Twisting moments acting on the blades are transmitted to the actuator by a trunnion attached to the blade shank.

3.5 SPINNER

The spinner and bulkhead are essentially a fiberglass shell supported by the hub and actuator. The spinner has an aerodynamic shape to facilitate proper inflow to the Prop-Fan. The bulkhead provides a mounting surface for most of the instrumentation hardware in the rotating field.

4.0 INSTRUMENTATION

4.1 GENERAL DESCRIPTION

The electronic data acquisition system for the LAP provided the capacity to transmit 32 channels of information from transducers on the rotating side of the Prop-Fan to data collection and monitoring equipment in the stationary field (reference 8). These transducers were a combination of strain gages and pressure transducers. A separate pneumatic instrumentation system was also available for measuring the steady pressure distribution on one specially designed blade.

4.2 ELECTRONIC DATA ACQUISITION SYSTEM

Electric power for the electronic data acquisition system and signals from the transducers were transmitted across the rotating/stationary interface by a brush block and slip rings. The physical arrangement of the LAP allowed for only eight slip rings. The need to transmit 32 channels of information therefore necessitated the use of multiplexing. The DC signals from the transducers in the rotating field were divided into two groups of sixteen. The signals were then converted to frequency modulated signals by two groups of voltage controlled oscillators. Each group was then multiplexed by a mixer, allowing thirty two channels to be transmitted through two slip rings. The two groups of sixteen channels were each detranslated in the stationary field to four groups of four multiplexed channels (IRIG Standard 1A thru 4A). Each set of four channels was recorded on one track of a standard Honeywell 101 tape recorder. Simultaneously, eight discriminators were used to demodulate any two groups of four channels for real time monitoring of data. One discriminator was tuned to the center frequency of each channel. A schematic of the electronic data acquisition system is presented in Figure 4.1.

The FM electronic instrumentation system provides inherent noise immunity for data transmission. The frequency response for the system was DC to 1000 HZ. Overall accuracy of the system is $\pm$ 3% RSS. Time correlation between channels was $\pm$13.8 microseconds.

The electronic instrumentation system allowed for up to ten strain gages to be installed on any blade, though a maximum of 32 gages could be active at any one time. A total of sixteen gages could be selected from blades one through four and an additional sixteen gages could be chosen from blades five through eight. Selection of the desired combination of gages was accomplished using eight programmable connectors mounted on the Prop-Fan hub. Programming of the connectors required using jumper wires to connect the sockets of patch boards in the connectors. The bridge completion circuits for the strain gages were located on circuit boards in the blade cuff.

9
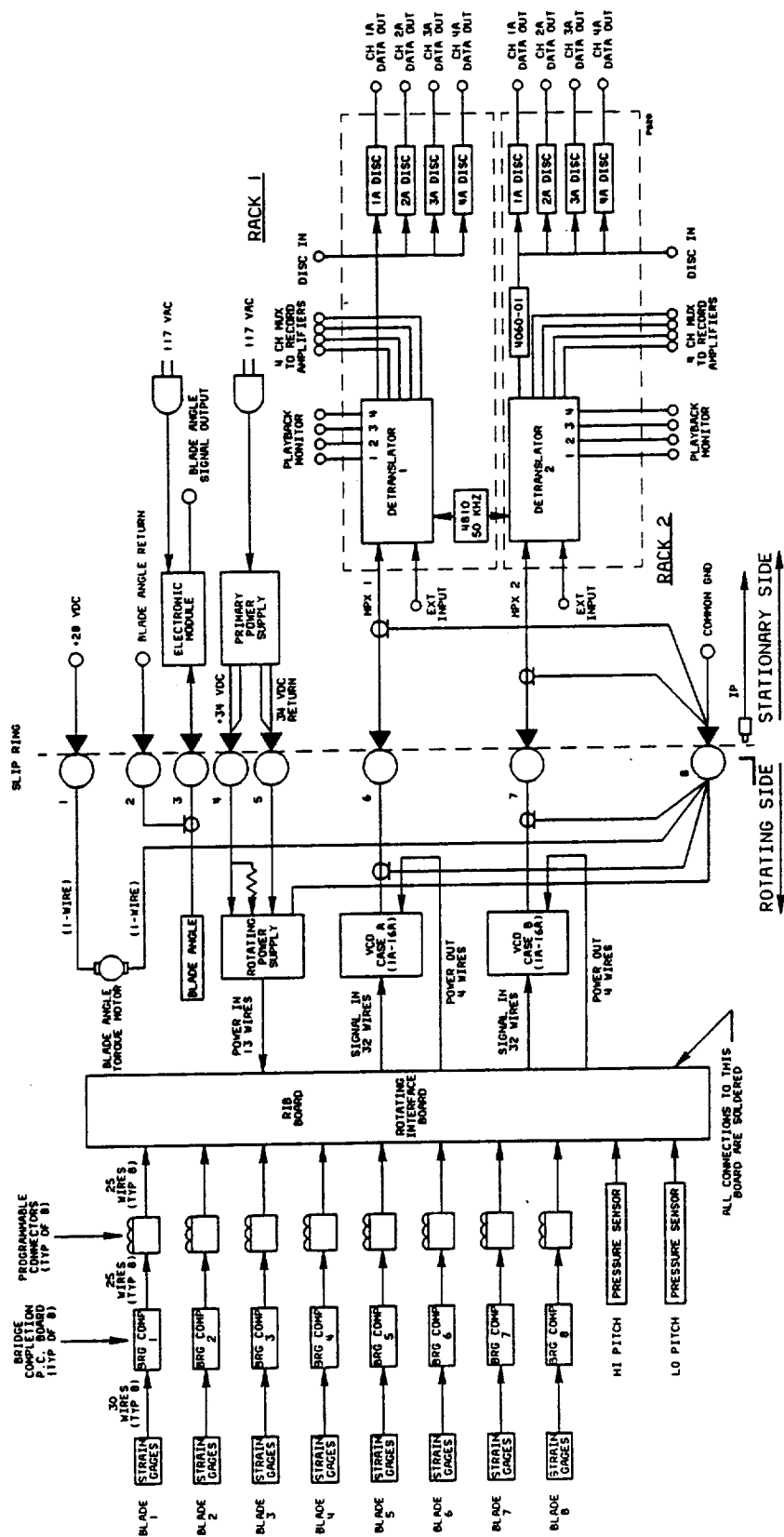
FIGURE 4.1 LAP INSTRUMENTATION BLOCK DIAGRAM

10

4.2 (Continued)

Monitoring of instrumentation during the test was accomplished with an oscilloscope, a spectrum analyzer and a visicorder. The oscilloscope permitted a time domain display of four channels simultaneously. The spectrum analyzer provided the capability to display any one channel in the time or frequency domain. The analyzer also had transient capture and playback features. The visicorder provided a hard copy plot of instrumentation signals versus time.

4.3 STEADY PRESSURE MEASUREMENT SYSTEM

The pneumatic instrumentation system for measuring airfoil surface steady pressures, consisted of a specially fabricated blade with rows of pressure taps installed at ten radial stations and a scanivalve mounted on the nose of the Prop-Fan. The pressure taps were connected to the scanivalve by capillary tubes run along the actuator dome.

The scanivalve provided 36 channels for transmitting pressure data across the rotating/stationary interface. One capillary tube was connected to each channel of the scanivalve. The scanivalve consisted of a rotating and stationary portion. The stationary portion contained a transducer that could monitor one channel at a time. Changing of the scanivalve channel to be monitored was accomplished by a pneumatic signal sent from a control panel to the scanivalve. The scanning rate was adjustable from .1 seconds to 10 seconds per channel. An umbilical cord running from the stationary portion of the scanivalve to a control panel contained wires from the transducer and tubes for transmitting the pneumatic signal. A digital readout of the measured pressure was available on the control panel. The pressure readings were also recorded on magnetic tape.

5.0 TEST FACILITY DESCRIPTION

5.1 WHIRL RIG DESCRIPTION

The SR-7L Large Scale Advanced Prop-Fan is shown mounted on the Wright Aeronautical Laboratory Whirl Rig #1 in Figure 5.1. The whirl rig was driven by a 7460 kW (10,000 hp) synchronous electric motor, which had a speed capability of zero to 1440 RPM. The rotational speed of the synchronous motor was controlled by varying the output frequency of a three phase alternator, that supplied electrical power to the motor. The three phase alternator was driven by two DC electric motors on a common shaft. The rotational speed of the DC motors was controlled by varying the voltage supplied to them from two DC generators. By changing the speed of the two DC motors the output frequency of the 3 phase alternator was also changed. The whirl rig synchronous motor speed achieved is proportional to the output frequency of the 3 phase alternator.

The whirl rig synchronous drive motor could be operated in either a 6 pole or 12 pole configuration. The 12 pole configuration was used for low RPM, high power testing while the 6 pole configuration is used for higher RPM testing. The power available from the rig motor as a function of rotational speed is presented in Figure 5.2 for both the 6 pole and 12 pole configurations. Changing between the 6 and 12 pole configurations simply required that motor rotation be stopped and the position of two power switches be changed.

5.2 SPEED INCREASING GEAR BOX

Static Rotor Testing of the LAP required operation at rotor speeds up to 2038 RPM. The 1440 RPM speed limitation of the whirl rig motor necessitated the use of a speed increasing gearbox to achieve the entire operating speed range of the Prop-Fan. The gear box employed was a coaxial two stage unit, that provided a step up speed ratio of 2.49:1. Power was input to the gearbox by means of a jack shaft and was transmitted to the high speed output shaft by four quill shaft and pinion gear assemblies. The output shaft of the gearbox supported the Prop-Fan and rotated in two pressure fed cylindrical journal bearings. A thrust bearing is incorporated in the gearbox which transmits the Prop-Fan thrust directly to the input jack shaft. The rated power of the gearbox as a function of rotational speed is overlayed on the power curves for the whirl rig in Figure 5.2.

The gearbox was supported at the drive end of the whirl rig and served to keep the spacing between the blade tips and the face of the whirl rig greater than one half the Prop-Fan diameter for all of the blade pitch angles run during the test. Due to the blade sweep, the spacing between the rig and the blades decreased with increasing blade angle. The gearbox casing also has an aerodynamic shape which facilitated well behaved flow downstream of the Prop-Fan Rotor. The juxtaposition of the Prop-Fan and gearbox is illustrated in Figure 5.3.
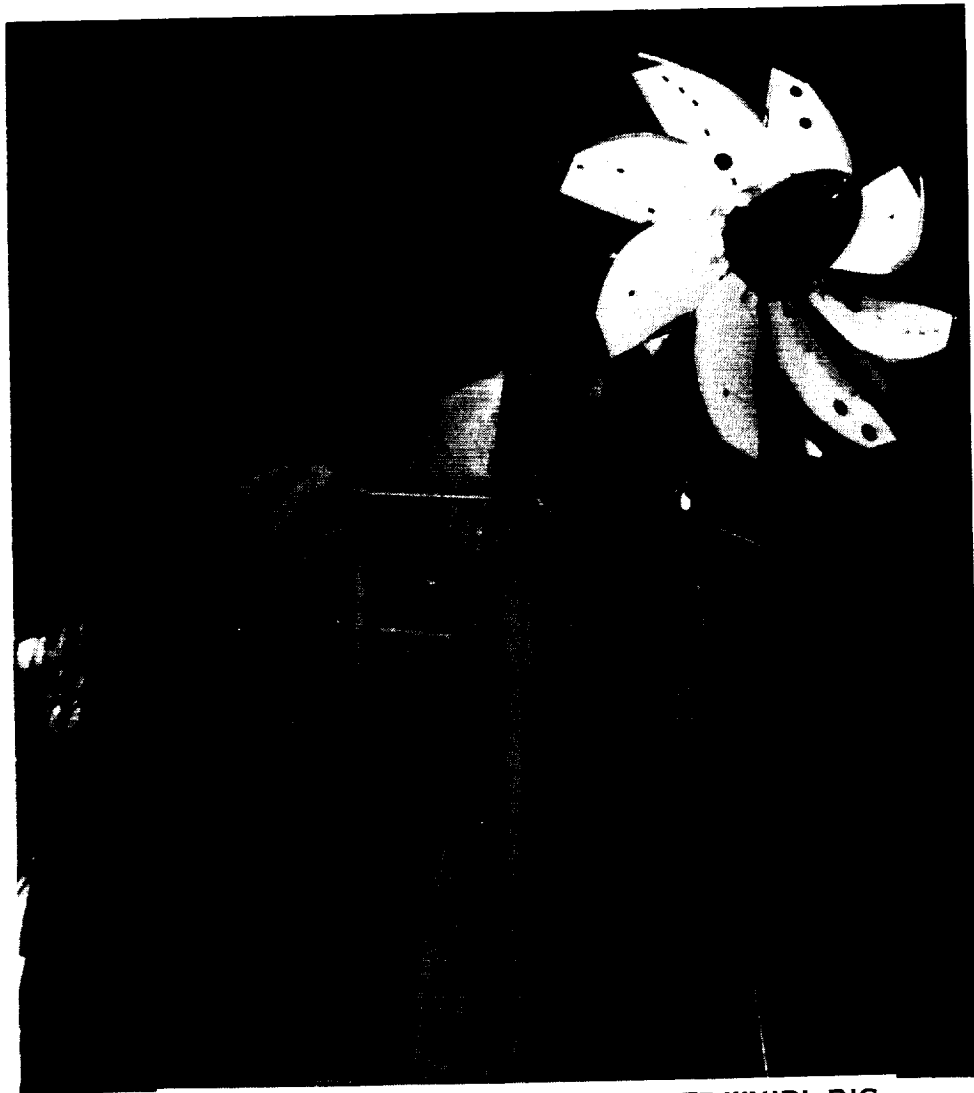
FIGURE 5.1 SR-7L PROP-FAN ON WPAFB WHIRL RIG.

14
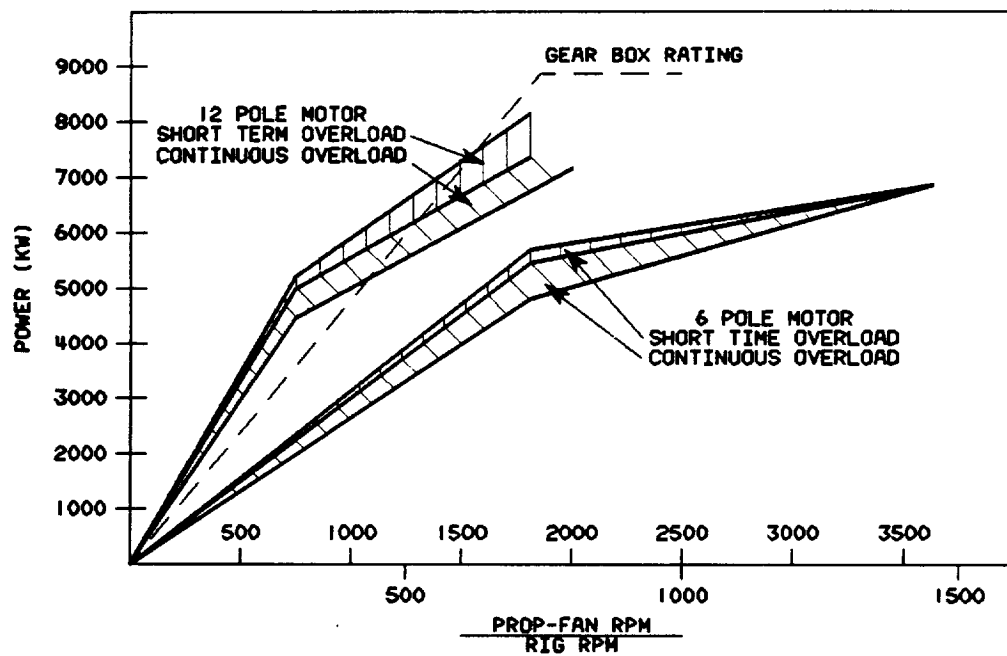
FIGURE 5.2 WHIRL RIG POWER AVAILABLE VS. SPEED

15

ALL DIMENSIONS ARE
SHOWN IN INCHES
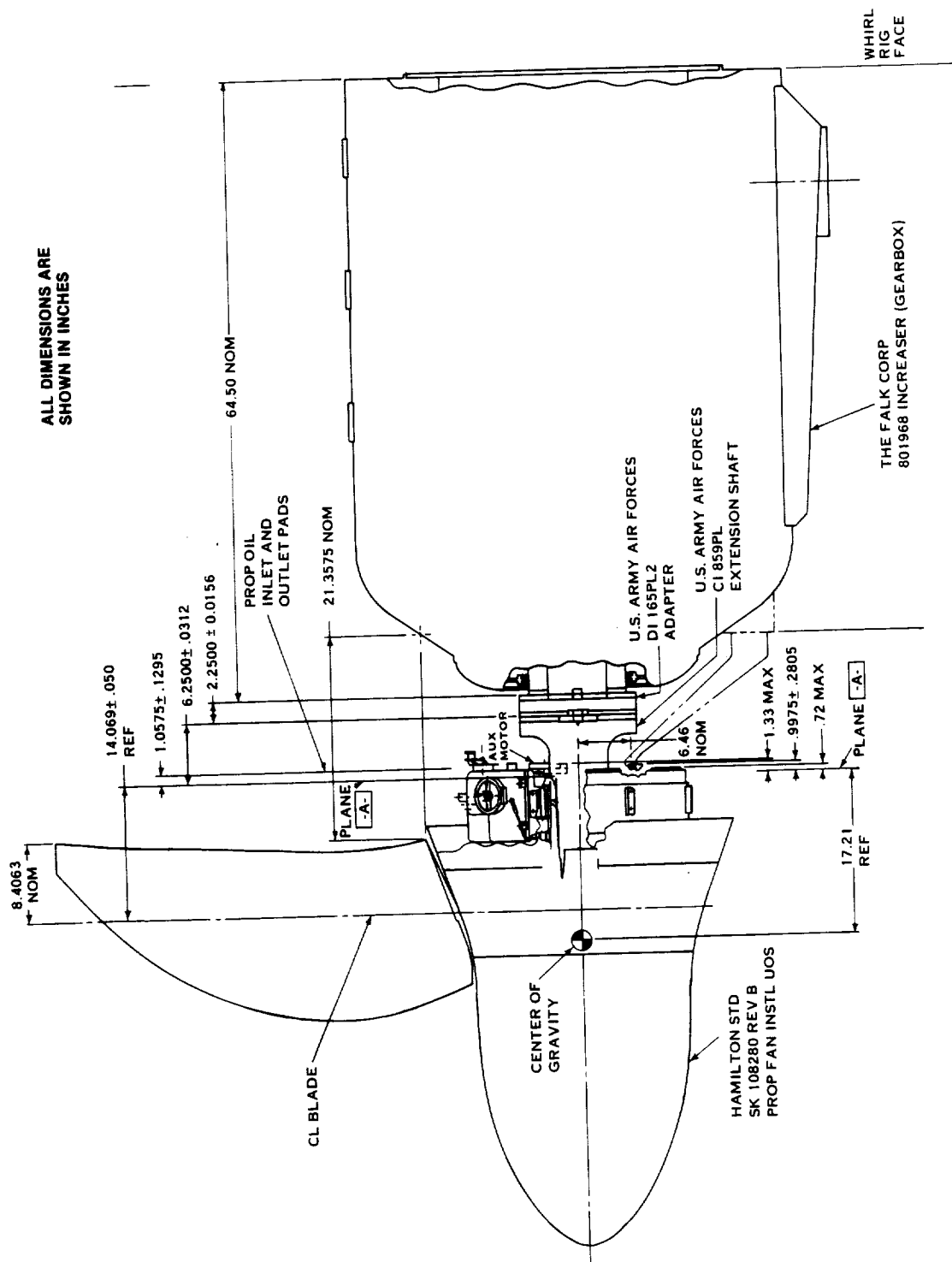
FIGURE 5.3 SR-7L PROP-FAN AND SPEED INCREASING GEARBOX, $\beta 3/4 = 45°$

5.3 WHIRL RIG INSTRUMENTATION

A system, integral to the whirl rig, provided the capability to measure thrust up to 222,400 N (50,000 lb$_f$) in either direction. The system consisted of a hydraulic cell loaded by the whirl rig thrust bearing and an air amplifier. The hydraulic pressure in the load cell was converted to a thrust measurement by the air amplifier system.

Power absorbed by the Prop-Fan was determined by measuring the electrical power supplied to the whirl rig synchronous motor. Empirically determined electrical losses, gearbox mechanical losses and windage losses were subtracted from the electric power measurement to determine the power absorbed by the Prop-Fan. These losses are presented as a function of RPM for the six pole motor in Figures 5.4, 5.5 and 5.6 respectively.

Accelerometers, mounted on the forward and aft ends of the speed increasing gearbox housing were used to monitor Prop-Fan and test rig vibration. The accelerometer signals were integrated twice to yield displacement. A maximum vibratory displacement of .25 mm (.01 inches) was allowable.
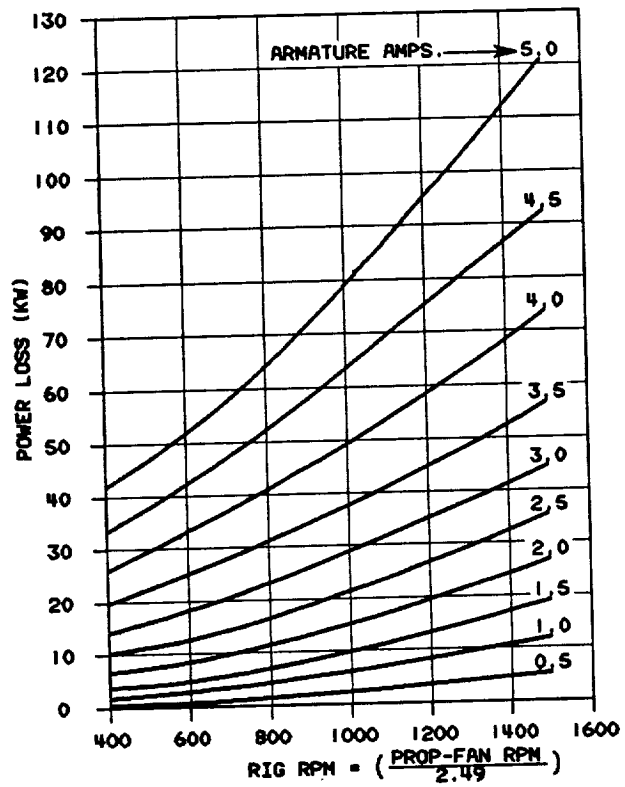
FIGURE 5.4 WHIRL RIG COPPER + LOAD LOSS VS. RPM, 6 POLE MOTOR
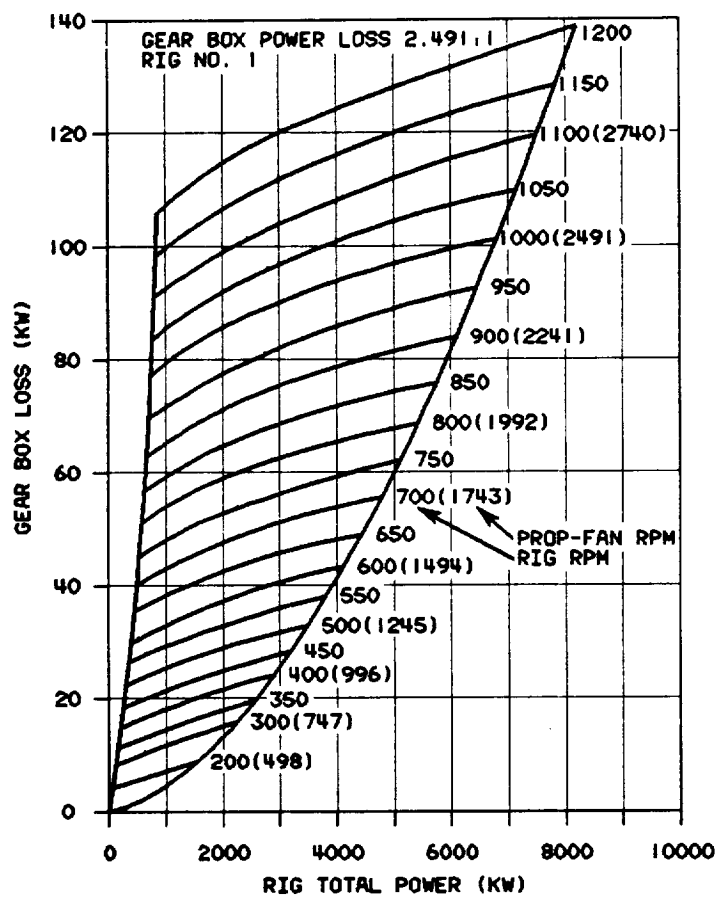
FIGURE 5.5 SPEED INCREASING GEAR BOX LOSS

19
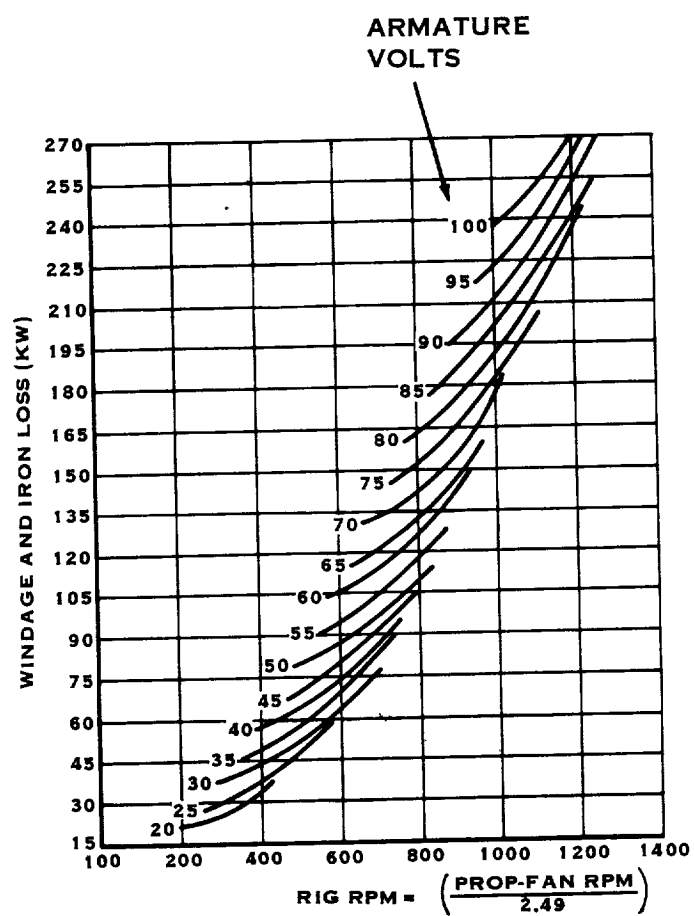
FIGURE 5.6 WHIRL RIG WINDAGE AND IRON LOSS, 6 POLE MOTOR

20

6.0 AERODYNAMIC PERFORMANCE TESTING

6.1 TEST PROCEDURE

The static aerodynamic performance of the SR-7L Prop-Fan was measured concurrently with the gathering of blade structural dynamic data during the Static Rotor Test. The performance data was measured with the Prop-Fan operating in a fixed blade pitch mode.

Prior to the initiation of each test run the blade pitch angle was measured at the 3/4 span blade station, using a hand held protractor and blade template. The blade template was designed to conform to the blade face surface contour and to orient the protractor parallel to the airfoil section chord-line at that station. The angle made by the 3/4 span blade chord line with the plane of rotation defines the blade pitch angle, β 3/4. During the measurement, the blade was loaded by hand toward low pitch to take up the backlash in the actuation system. This reflects the running position of the blade shank, but does not account for airfoil deflections which occur under air and centrifugal loads. The blade angle was remeasured at the completion of each test run.

Ambient temperature and pressure were also recorded at the beginning and end of each test run. Ambient pressure was measured with a Mercury barometer. A correction was applied to the barometer reading to compensate for the effect of temperature on the density of the Mercury.

Static aerodynamic performance data was acquired over a range of blade angles from -6° to 60° and a range of rotational speeds from 600 to 1900 RPM. At blade angles above 30° the maximum RPM was limited by blade vibratory stress levels. The actual test points run are listed in Table 6.1.

TABLE 6.1. TEST POINTS FOR STATIC THRUST, STALL FLUTTER AND CRITICAL SPEEDS

Blade Angle (β 3/4)	RPM
-5.7°	600,700,800,900,1000,1100,1200, 1300,1400,1500,1600,1650,1700,1750, 1800,1850,1900
-2°	600,700,800,900,1000,1100,1200, 1300,1400,1500,1600,1650,1700,1750, 1800,1850,1900
.2°	600,700,800,900,1000,1100,1200, 1300,1400,1500,1600,1650,1700,1750, 1800,1850,1900
2°	600,700,800,900,1000,1100,1200, 1300,1400,1500,1600,1650,1700,1750, 1800,1850,1900

TABLE 6.1.   TEST POINTS FOR STATIC THRUST, STALL FLUTTER AND CRITICAL SPEEDS
(Continued)

Blade Angle (β 3/4)	RPM
6.1°	600,700,800,900,1000,1100,1200, 1300,1400,1500,1600,1650,1700,1750, 1800,1850,1900
10°	600,700,800,900,1000,1100,1200, 1300,1400,1500,1600,1650,1700,1750, 1800,1850,1900
14.1°	600,700,800,900,1000,1100,1200, 1300,1400,1500,1600,1650,1700,1750, 1800,1850,1900
18.2°	600,700,800,900,1000,1100,1200, 1300,1400,1500,1600,1650,1700,1750, 1800,1850,1900
22.1°	600,700,800,900,1000,1100,1200, 1300,1400,1500,1600,1650,1700,1750, 1800,1850,1900
25.8°	600,700,800,900,1000,1100,1200, 1300,1400,1500,1600,1650,1700,1750, 1800,1850,1900
30.3°	600,700,800,900,1000,1100,1200, 1300,1400,1500,1600,1650,1700,1750, 1800,1850,1900
32.1°	700,800,900,1000,1100,1200,1300, 1400,1500,1600,1700
33.5°	700,800,900,1000,1100,1200,1300, 1400,1500,1600,1700
34.3°	600,700,1000,1100,1200,1300
38.1°	600,700,800,900,1000,1100,1200
42°	600,700,800,900,1000,1100,1200
49.9°	600,700,800,900,1000,1100,1200
55°	600,700,800,900,1000,1100
60.1°	600,700,800,900,1000,1100

6.1 (Continued)

At the beginning of each day's testing, Prop-Fan rotational speed was increased to approximately 1000 RPM and allowed to coast to a stop. The thrust measurement apparatus was then zeroed. Following zeroing of the thrust measurement, rotational speed was increased to 600 RPM to begin data acquisition. At each RPM operation was maintained for a sufficient period of time to allow thrust and power readings to stabilize prior to recording data.

6.2 DATA REDUCTION PROCEDURE

Net power absorbed by the Prop-Fan was determined by subtracting electrical and mechanical losses from the measured electrical power supplied to the rig synchronous motor at each test point. These losses had previously been determined experimentally as a function of RPM for the whirl rig and gear box. Net thrust was determined by multiplying the measured thrust by a rig factor determined during thrust calibration. The rig factor was equal to 1.005 for all blade angles and rotational speeds.

Net power and thrust were corrected to standard conditions by multiplying them by the ratio of standard to ambient air density. The air density ratio was computed from the ambient pressure and temperature readings recorded before and after each test run. Corrected and net thrust and power are related by equations 6.1 and 6.2.

$$P_{corr} = P_{net} \frac{p_{amb}}{759.97} \times \frac{288}{t_{amb}} \qquad (6.1)$$

$$T_{corr} = T_{net} \frac{p_{amb}}{759.97} \times \frac{288}{t_{amb}} \qquad (6.2)$$

where:

P_{corr} = corrected power, kW

T_{corr} = corrected thrust, N

P_{net} = net power, kW

T_{net} = net thrust, N

p_{amb} = ambient pressure, mm Hg

t_{amb} = ambient temperature, °K

6.2 (Continued)

The correction equations allow thrust and power data collected for various ambient conditions to be compared on an equal basis.

The power and thrust data were also nondimensionalized to coefficient form for comparison with the analytically predicted static performance. The power and thrust coefficients were computed using equations 6.3 and 6.4 below.

$$\text{(power coefficient)} \qquad C_P = \frac{P_{corr}}{5.674(ND/1000)^3 D^2} \qquad (6.3)$$

$$\text{(thrust coefficient)} \qquad C_T = \frac{T_{corr}}{340.42(ND/1000)^2 D^2} \qquad (6.4)$$

where:

P_{corr} = corrected power, kW

T_{corr} = corrected thrust, N

D = Prop-Fan diameter, 2.74 m

N = rotational speed, RPM

6.3 RESULTS AND DISCUSSION

Curves of corrected power and corrected thrust versus blade angle for a constant RPM are presented in Figures 6.1 and 6.2. Figure 6.3 presents the predicted curve of static power coefficient versus blade pitch angle for the SR-7L Prop-Fan. Figure 6.4 shows the predicted curve of thrust coefficient versus power coefficient. These predicted curves were generated using Hamilton Standard Program H444. Thrust coefficient and power coefficient data are overlayed or the predicted curves.

Examination of Figure 6.2 illustrates the behavior of the static thrust produced by the Prop-Fan as a function of the blade angle. A smooth increase in thrust is observed between blade angles of zero and thirty degrees. Thrust then decreases slightly between blade angle of 30° and 34° and then is essentially constant from 34° to 60°. Figures 6.3 and 6.4 depict an abrupt departure of the power and thrust data from predicted values as blade angle is increased beyond 30°. Both thrust produced and power absorbed by the Prop-Fan are lower than predicted above blade angles of 30°. The calculated SR-7L performance is compared to the measured performance in Table 6.2 below.
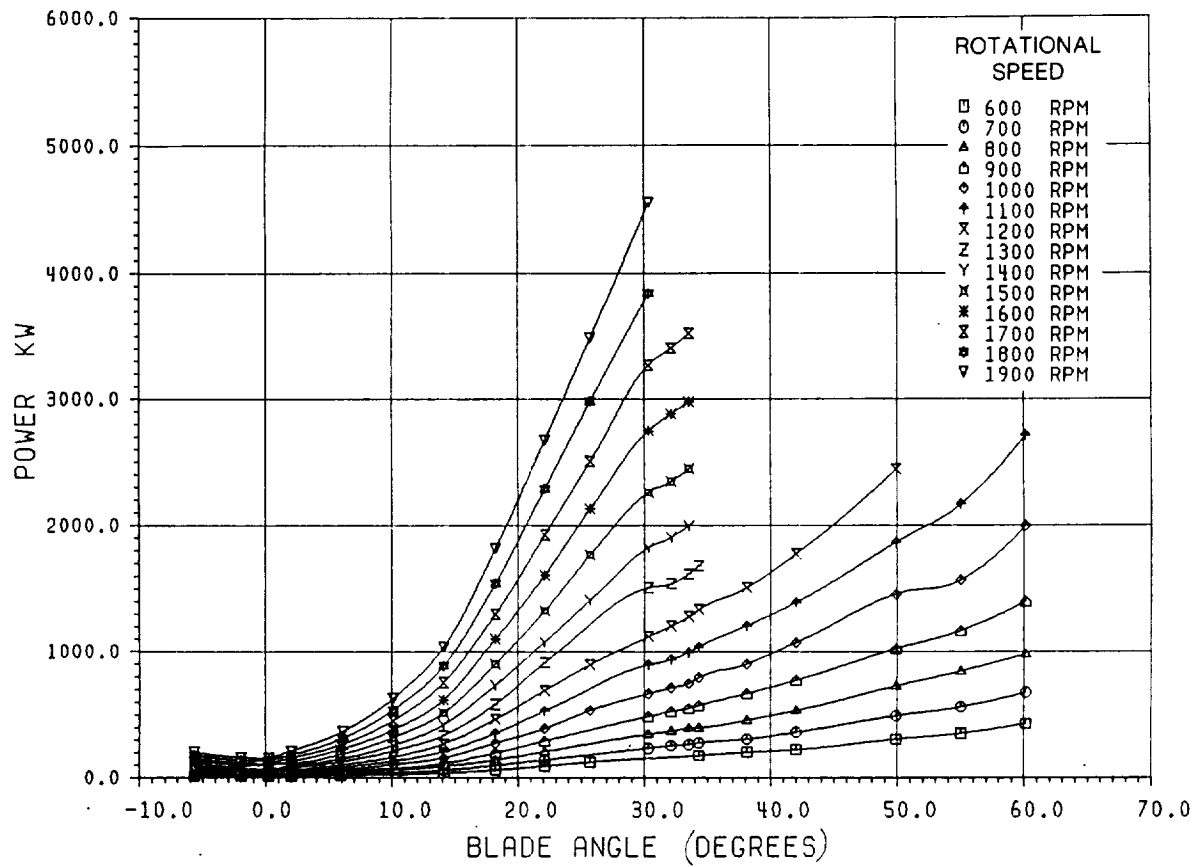
FIGURE 6.1 SR7L PROP-FAN CORRECTED POWER VS BLADE ANGLE
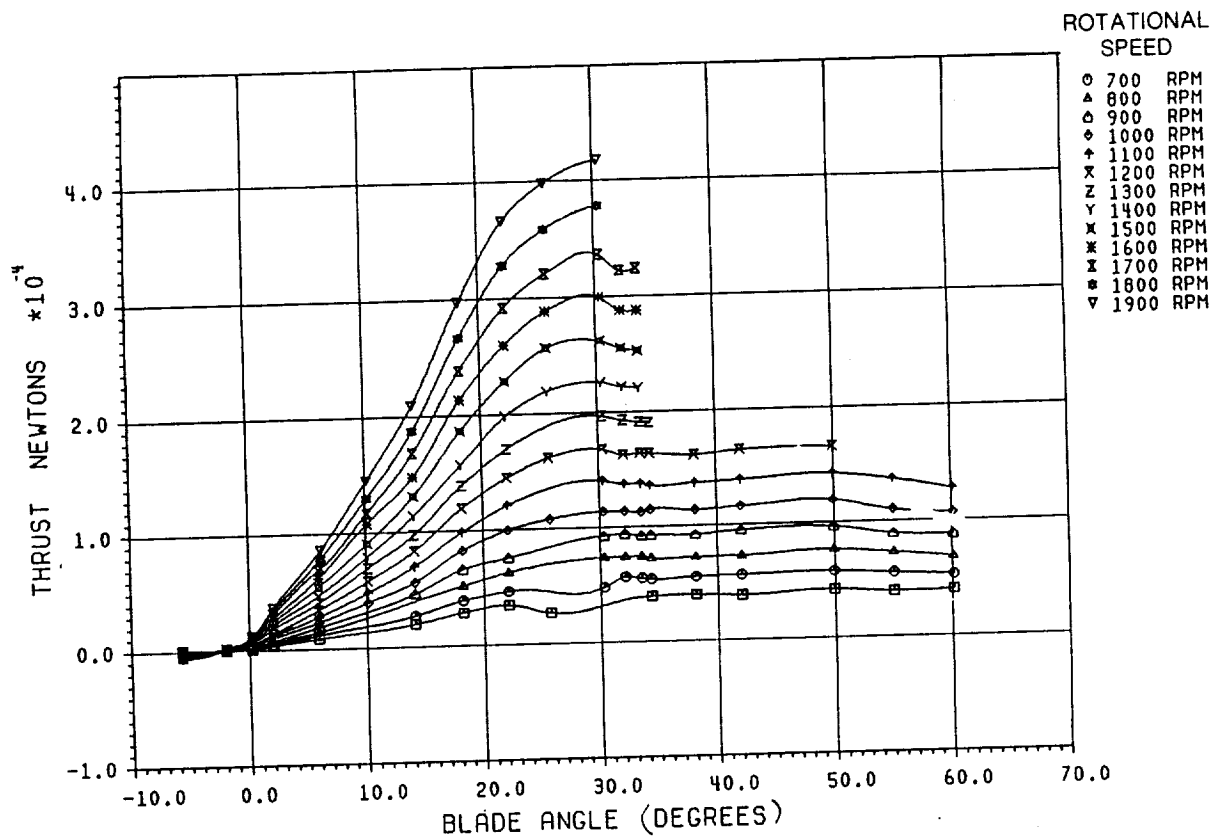
FIGURE 6.2 SR-7L PROP-FAN CORRECTED THRUST VS. BLADE ANGLE $(\beta_{3/4})$, $V_\infty = 0$
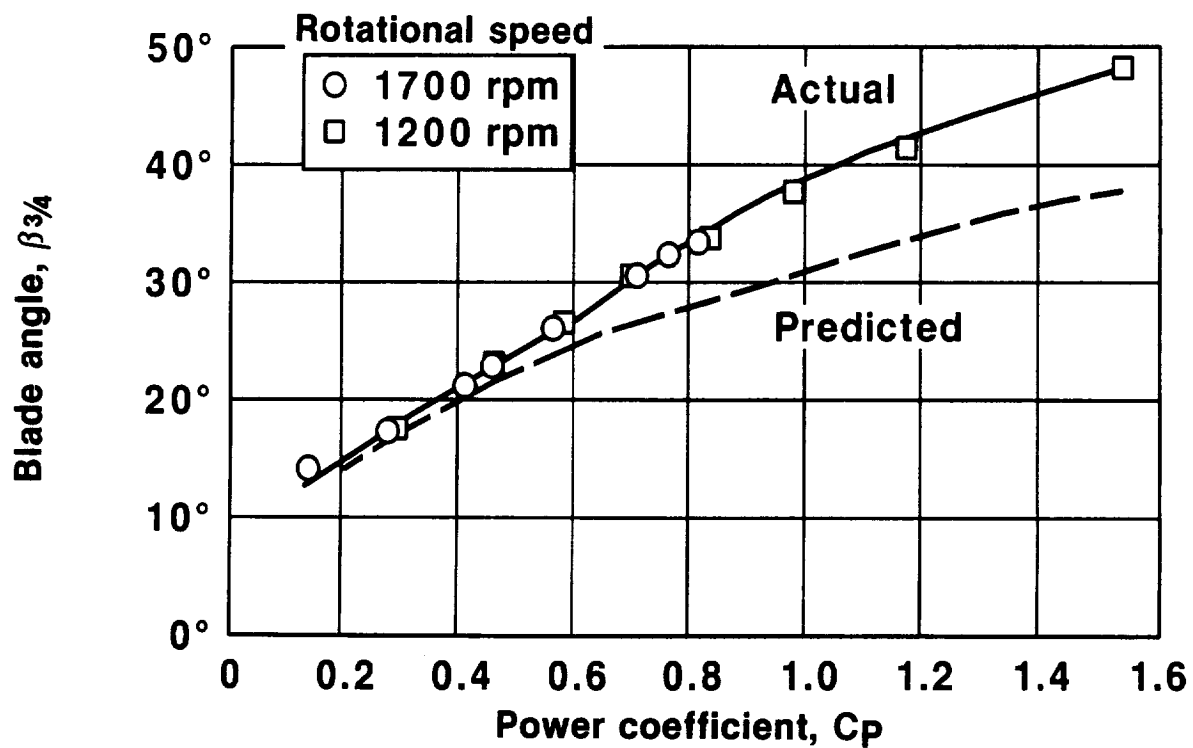
FIGURE 6.3 SR-7L PROP-FAN, COMPARISON OF MEASURED AND PREDICTED CURVES OF BLADE ANGLES VS. POWER COEFFICIENT, $V_\infty = 0$
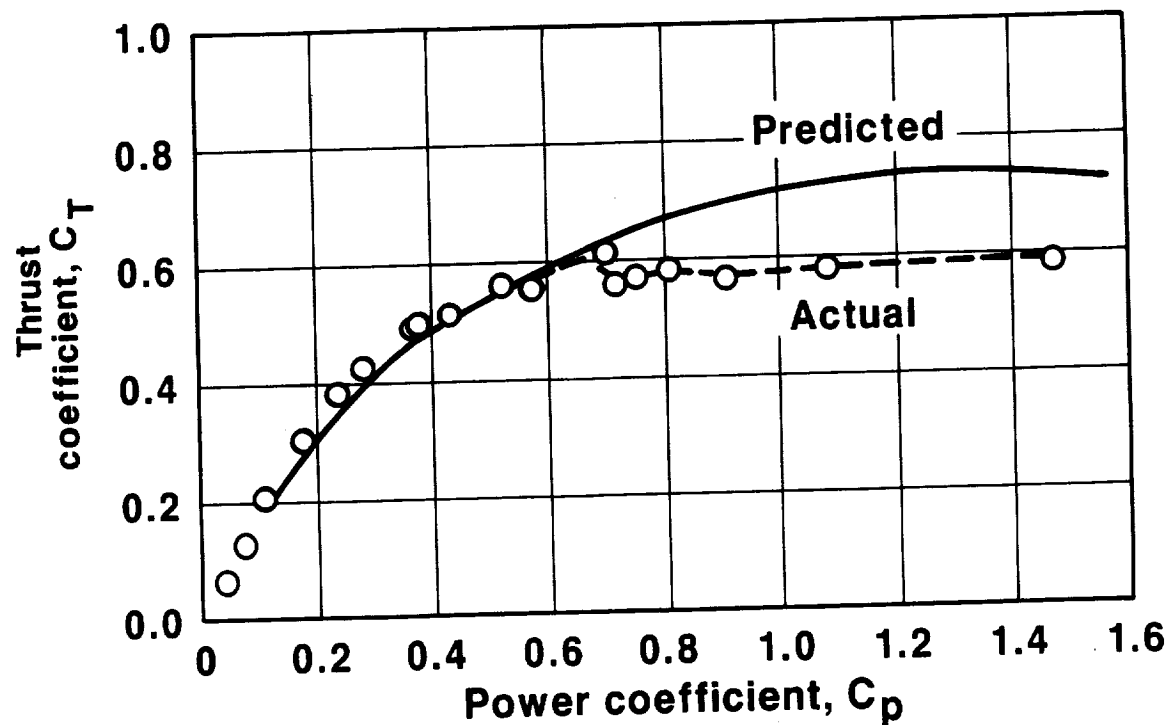
FIGURE 6.4 SR-7L PROP-FAN, COMPARISON OF MEASURED AND PREDICTED CURVES OF THRUST COEFFICIENT VS. POWER COEFFICIENT, $V_\infty = 0$, ROTATIONAL SPEED = 1200 RPM

TABLE 6.2. COMPARISON OF MEASURED AND PREDICTED PERFORMANCE

Predicted Performance	Measured Performance
β 3/4 = 33.3°	β 3/4 = 33.5°
N = 1698 RPM	N = 1702 RPM
Power = 4476 kW (6000 hp)	Power = 3520 kW (4719 hp)
Thrust = 40237 N (9046 lb$_f$)	Thrust = 32337 N (7270 lb$_f$)

The reason for the shortfall in static performance at high blade angle is not
clear from the data presented here. Referring to the thrust versus blade an-
gle data in Figure 6.2, the deviation of the measured and predicted perform-
ance occurs at the same blade angle, independent of the RPM. Since the per-
formance shortfall is observed at rotational speeds as low as 900 RPM, it is
unlikely that it was caused by shock separation or compressibility. The 900
RPM rotational speed results in blade tip speeds in the Mach .3 to Mach .4
range. This type of behavior may be indicative of stall. However, calcula-
tions made with computer program H444 indicate angles of attack well below
stall at the outboard blade sections for β 3/4 angles beyond 34°. The H444
program uses a classical undistorted wake model to obtain variable inflow
distributions for performance predictions. This model may not accurately
represent the actual physical wake geometry for the highly loaded SR-7L
Prop-Fan operating statically at high blade angle. Therefore the angle of
attack distribution along the blade may be very different than was predict-
ed. Computer programs are available that may better handle the cascade ef-
fects between blades, but they require that the geometry of the wake be spec-
ified. Wake geometry data is available for conventional propellers, but not
for Prop-Fans. In order to use these computer programs effectively to
predict static performance, flow visualization studies or wake surveys are
required in order to obtain a better definition of the wake created by
Prop-Fan blades.

In view of the unusual shapes observed in LAP performance curves, the data
from previous static tests of single rotation Prop-Fan wind tunnel models
(reference 9) was carefully reviewed. Under close examination it was found
that the unusual shapes of the C_P versus β 3/4 and C_T versus C_P curves
were present to some degree in all prior test data for single rotation
Prop-Fan configurations including the SR-2, SR-3 and SR-5. Data illustrating
this behavior for the SR-3 Prop-Fan is presented in Figures 6.5 and 6.6. The
SR-3 is most aerodynamically like the SR-7L of the models tested. In general
the performance curves for all Prop-Fans are similar and tend to have a
maximum thrust coefficient of .6 to .7 at power coefficients greater than .7.
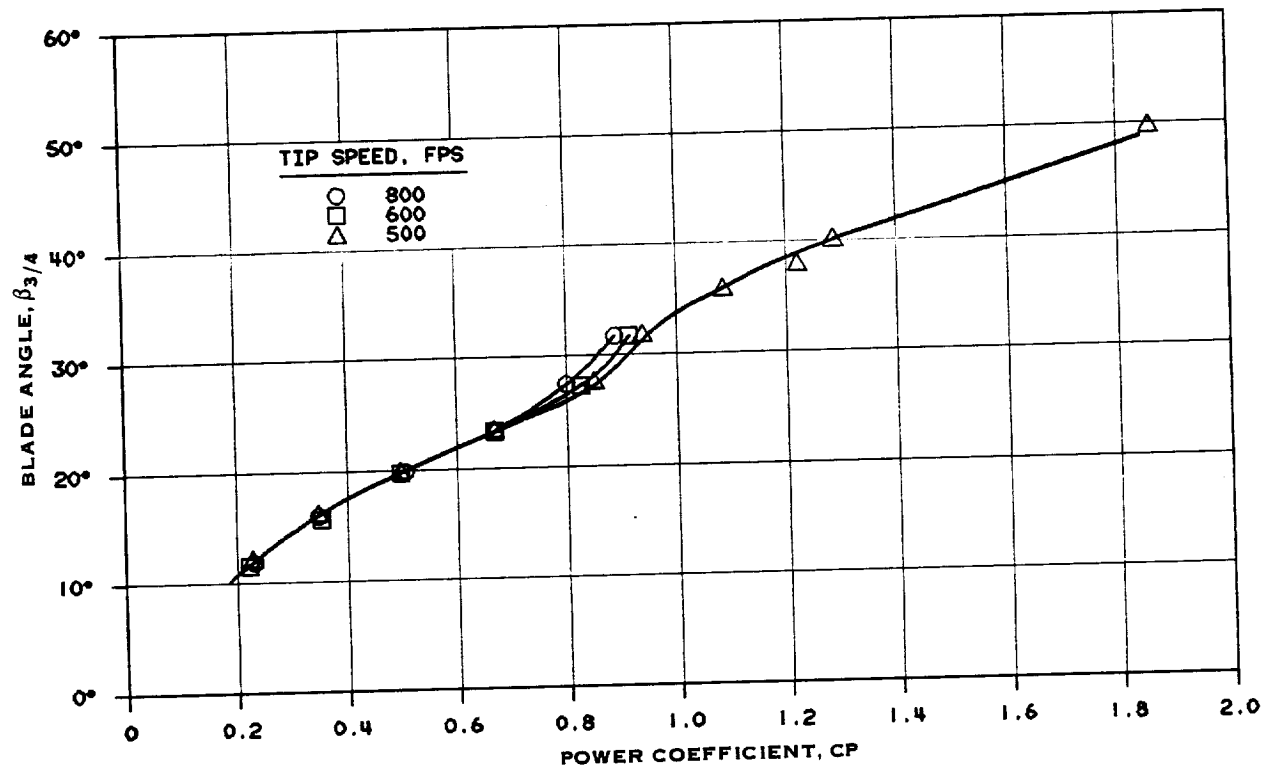
FIGURE 6.5 SR-3 PROP-FAN, BLADE ANGLE VS. POWER COEFFICIENT, $V_\infty = 0$
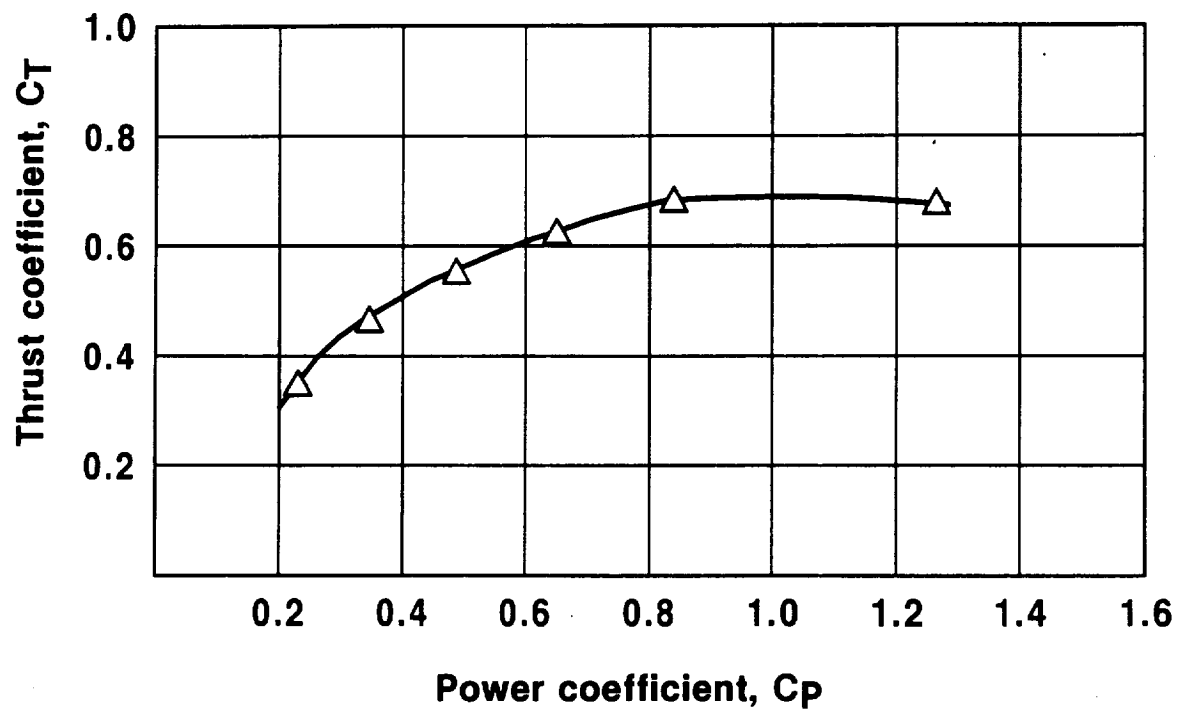
FIGURE 6.6 SR-3 PROP-FAN, THRUST COEFFICIENT VS. POWER COEFFICIENT, $V_\infty = 0$

7.0 STRUCTURAL DYNAMIC, TESTING

7.1 TEST PROCEDURE

Blade structural dynamic data was gathered over the same operating envelope for which aerodynamic performance data was obtained. The actual test points at which structural dynamic data was collected are listed in Table 6.1. Testing allowed the blade natural frequencies to be experimentally determined and the regions of high blade vibratory stress to be mapped as a function of blade angle and RPM. Extensive spectral analysis of the data was also conducted so that the vibration could be characterized as flutter, buffet or resonance.

The LAP electronic data acquisition system provided the capability for extensive strain gaging of the Prop-Fan blades. The strain gage arrangement used for structural dynamic testing is illustrated in Figure 7.1. A total of fifty four gages were applied to the Prop-Fan blades with thirty primary active gages as indicated in the figure. The inactive gages were arranged so they could be employed as backups in the event of primary gage failure. The gages were applied as single bending gages in the radial or chordwise directions, in vee pairs to measure pure shear or in push pull pairs to measure bending moment at the blade shank. One radial bending gage, one chordwise bending gage and one vee pair were combined to form a rosette at certain locations.

The precise location and orientation of the gages on each of the blades is depicted in Figures 7.2 through 7.6. A numbering convention was formulated for the gages, based on the blade number, the gage location and the gage type. The numbering convention is described in Table 7.1.

PAGE 32

Forward to aft view

Blade camber side view
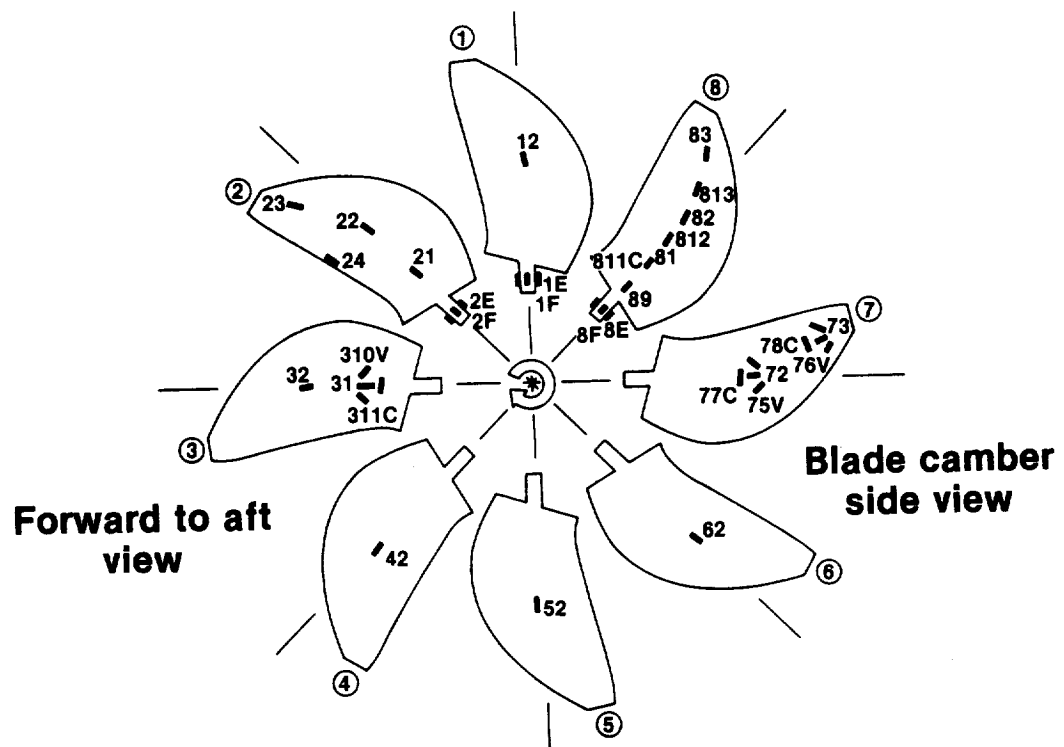
FIGURE 7.1 ACTIVE STRAIN GAGE ARRANGEMENT FOR FLUTTER
AND CRITICAL SPEED TESTING

34
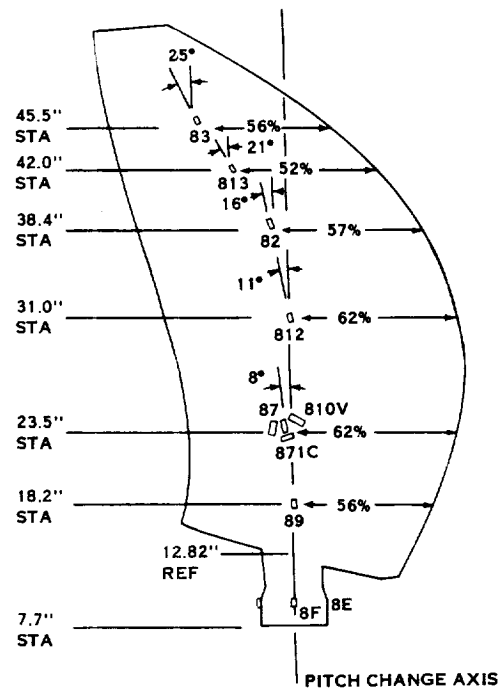
FIGURE 7.2 STRAIN GAGE LOCATIONS FOR BLADES 3 & 8
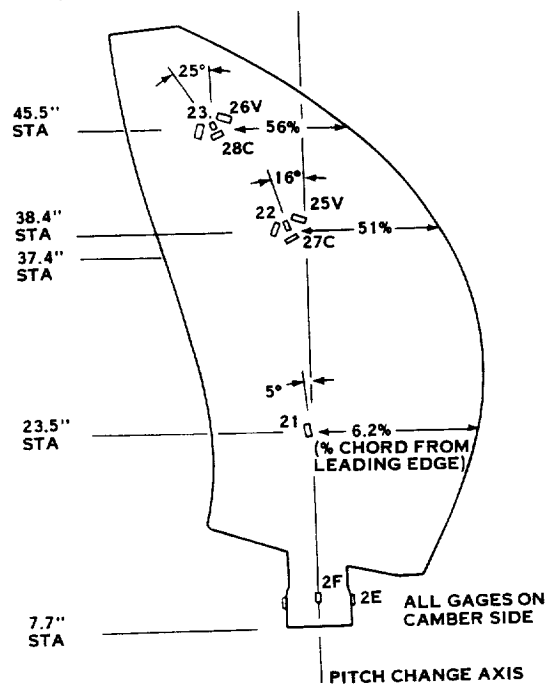
FIGURE 7.3 STRAIN GAGE LOCATIONS FOR BLADES 2 & 7
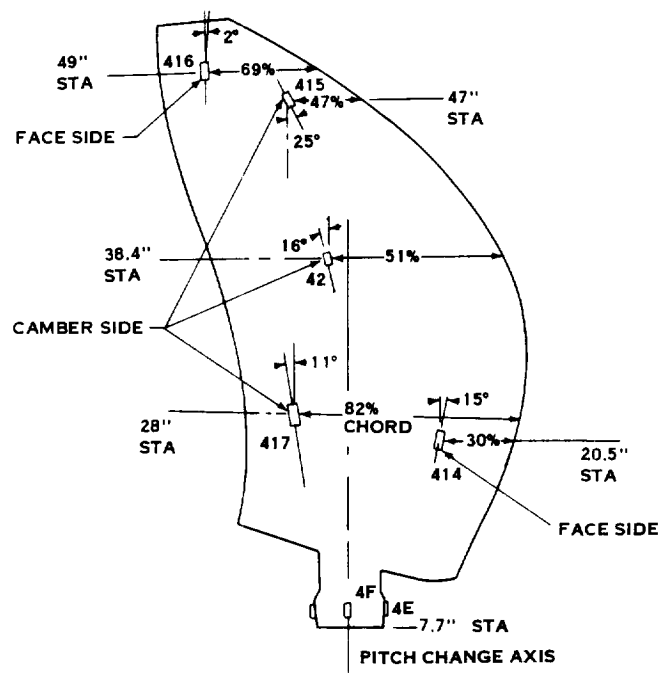
FIGURE 7.4 STRAIN GAGE LOCATIONS FOR BLADE 4
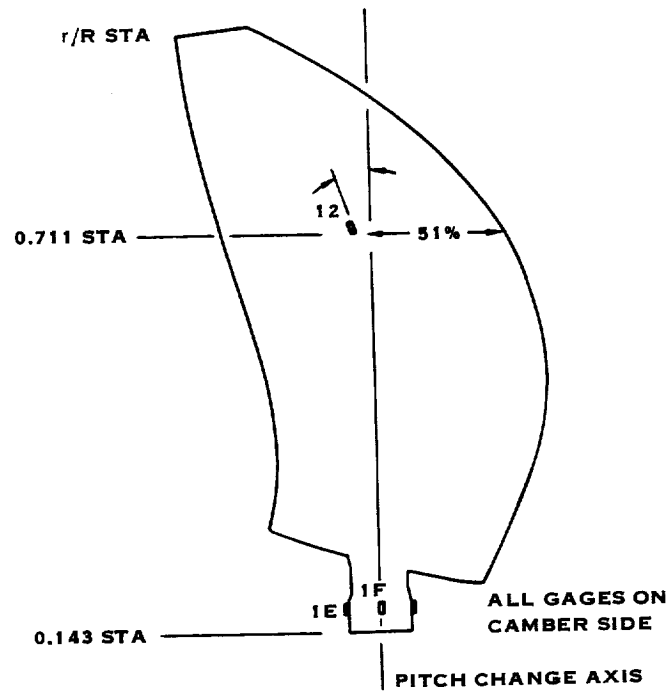
FIGURE 7.5 STRAIN GAGE LOCATIONS FOR BLADES 1, 5 AND 6

11.14" STA

AIRFOIL
SECTION

AXIS X

RETENTION

SHANK

LONGITUDINAL STRAIN GAGE
(4 PLACES)

14.32°

AXIS X

STACKING
PLANE
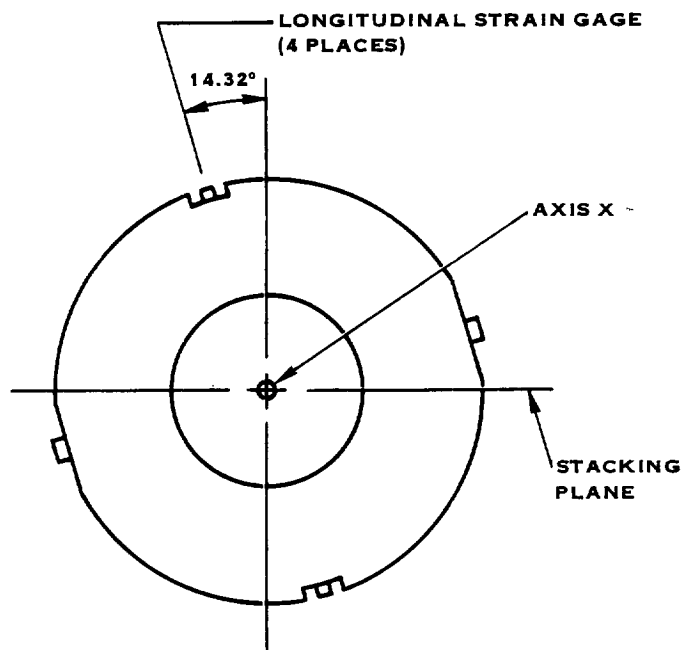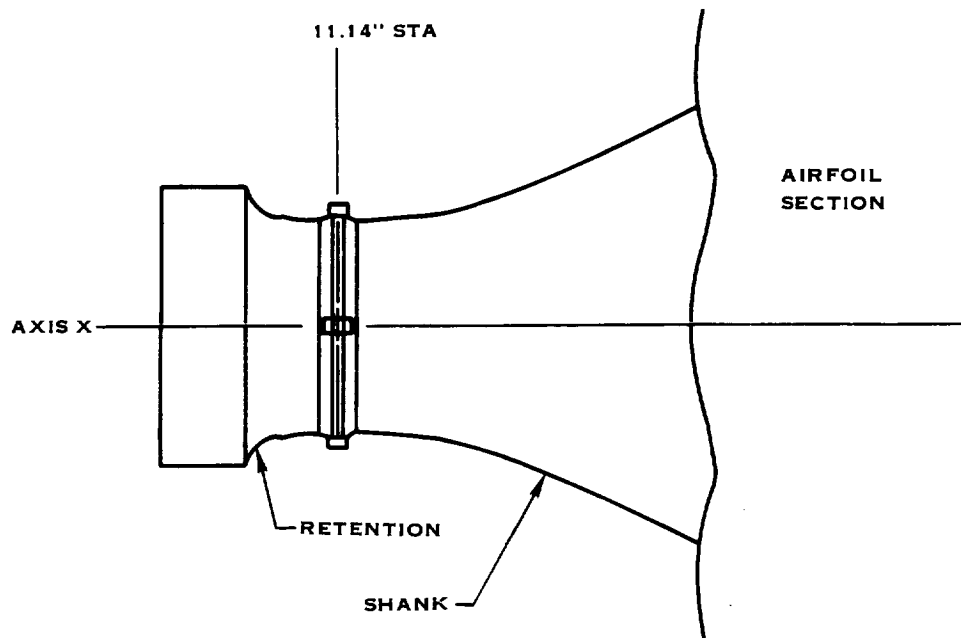
FIGURE 7.6 SHANK STRAIN GAGE LOCATIONS

TABLE 7.1. STRAIN GAGE NUMBERING CONVENTION

Bending gages: 812

   blade location
   gage location

Shear (vee) gages: 76V

   blade location
   gage location
   gage type

Chordwise bending gages: 311C

   blade location
   gage location
   gage type

Shank gages: 1F

   blade location
   gage location

     E - edgewise
     F - flatwise
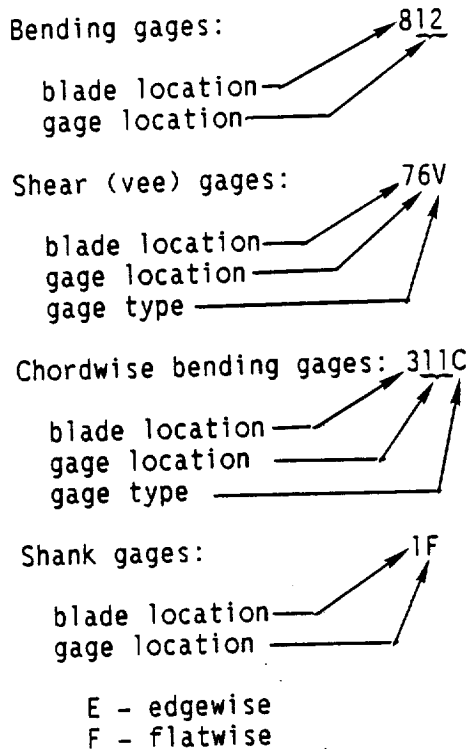
Strain gage locations 1, 2 and 3 were chosen to correspond with the analytically predicted points of maximum vibratory response for the first four blade normal modes. The bending gages were oriented along the predicted principal directions of strain. Analysis indicated that strain gages at location two would see a significant vibratory response for each of the first four normal modes. Therefore an active gage was included at this location on blades 1 through 8. These gages provided the capability to correlate interblade phase information. The gages at location four correspond to a local high stress area on the blade trailing edge.

7.2 DATA REDUCTION PROCEDURES

Reduction of the vibratory strain data began with plotting of the total vibratory strain amplitude versus time for the various combinations of blade angle and RPM at which data was collected. These plots were useful in determining the quality (noise content) of the strain gage signals and also in examining the character of the vibration.

7.2 (Continued)

The total vibratory strain data was also digitized and statistically analyzed to produce tables of mean strain, standard deviation of strain and mean strain plus twice the standard deviation $(\bar{X} + 2\sigma)$. The terminology for the $(\bar{X} + 2\sigma)$ strain is infrequently repeating peak (IRP) strain and is referred to in this report as vibratory strain except where noted. The IRP strain for each data point is presented in Appendix 1.

Spectral analysis of the data was conducted to determine the frequency content of the vibration. The spectral analysis also allowed Campbell plots to be constructed, presenting the blade natural frequencies as a function of RPM. The dependence of the blade natural frequencies on blade angle (ß 3/4) was also determined.

Cross spectral analysis was conducted to determine if a coherent interblade phase angle existed in the vibration data. This analysis technique consisted of forming the product of the vibration signals from two strain gages located in the same position on adjacent blades and performing a spectral analysis of the mixed signal. The cross-spectral analysis algorithm then determined the spectral components of the two signals and the phase relationship between them.

7.3 RESULTS AND DISCUSSION

Testing revealed no significant blade vibratory stress levels for blade angles in the range from -6° to 25° up to rotational speeds of 1900 RPM. The first vibratory stress limit was encountered at a 32° blade angle. An audible change in the sound produced by the Prop-Fan was perceived when the blade angle was increased over 30°. The audible sound level increased and the tonal frequency decreased. No acoustic measurements were taken during the tests to confirm these observations. The Prop-Fan speed was limited for blade angles above 30°. Figure 7.7 shows a map of the speeds and blade angles where vibratory stresses were recorded. In addition to the typical RPM traverses a blade angle traverse was attempted in an effort to circumvent the high stress region. As shown in Figure 7.7 the same high stress region was encountered from a different approach. Additional blade angle traverses were not attempted.

7.3.1 Blade Buffet Response

The blade vibratory stress limits were encountered in the blade tip region, at gage locations 23, 24, 73, and 83 (Figure 7.1). The vibratory stress measured at the other gage locations remained below limits when the tip gages reached their respective limits. The high vibratory stress is characterized as buffet rather than flutter because the stress level and frequency content was unsteady in nature. The stress amplitude did not increase suddenly and no mode sustained a sinusoidal response.

41
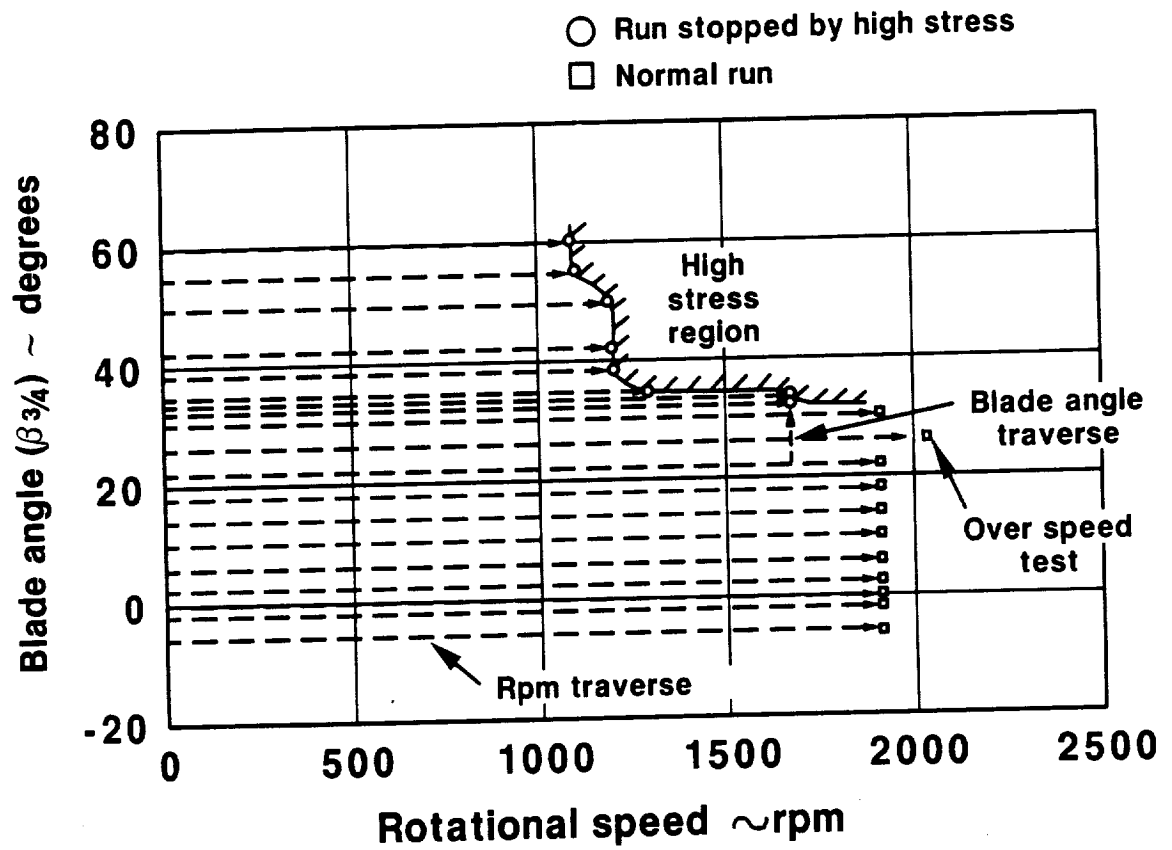
FIGURE 7.7 SR-7L STATIC ROTOR TEST SUMMARY

7.3.1 (Continued)

The transition of blade vibratory response from -2° to 34.2° blade angle is shown in Figure 7.8 for a blade tip bending strain gage. Blade strain changed from near zero response in the blade angle range from -2° to 22° to high response at 34.2°. The response at 34.2° blade angle is unsteady in both amplitude and frequency content. The response is dominated by a frequency of 92.5 Hz which corresponds to the second flatwise natural frequency of the blade. The response is not a sustained sine wave which characterizes flutter, therefore the response is designated as buffet. Buffet is caused by a flow instability, and the structure responds to the broad-band excitation produced by the flow instability.

7.3.2 Blade Vibration Frequency Content

The frequency content of the 34.2° blade angle response is shown by the spectral plot, Figure 7.9. As mentioned previously the dominant frequency is 92.5 Hz which corresponds to the second flatwise blade mode. A Campbell plot for the SR-7L blade is presented in Figure 7.10. The figure shows good agreement between the data and the calculated natural frequencies. The data also, verifies the buffet mode as the second flatwise mode.

The spectral results revealed that the frequency content of the buffet is not independent of blade angle. At blade angles above 39° the response changes from the second flatwise mode to the first flatwise mode of vibration as shown by the spectral plot of the tip bending gage vibratory response for a 55° blade angle in Figure 7.11. The flatwise response at 35 Hz is very close to the 2P first mode critical speed shown in Figure 7.10. Therefore the 2P excitation may be influencing the blade response. High first mode 2P response was not evident below 39° blade angle.

7.3.3 Inter-Blade Phase Angle

The buffet test data for a 34.2° blade angle at 1300 RPM, was examined with cross-spectral analysis and visually with oscillographs to determine if a coherent inter-blade phase angle existed in the buffet response. Although the buffet response was unsteady, the spectral analysis, like that shown in Figure 7.9, indicated that all blades were vibrating at the same frequency, 92.5 Hz. The data analysis showed no coherent inter-blade phase angle during buffet. To investigate why a lack of phase coherence existed with coherent frequency data, zoom spectral analysis was performed on the data to isolate the frequency content. Figure 7.12 shows the results of the zoom spectral analysis, which identified multiple frequency response peaks in the data. The system is not vibrating at a single frequency. Multiple frequencies in the order of 92.5 Hz plus or minus 1 Hz exist. The multiple peaks were not evident in Figure 7.9 because of the resolution of frequency in the spectrum. The multiple peaks show that the Prop-Fan is not responding in a single system mode, therefore no coherent inter-blade phase angle should exist. The
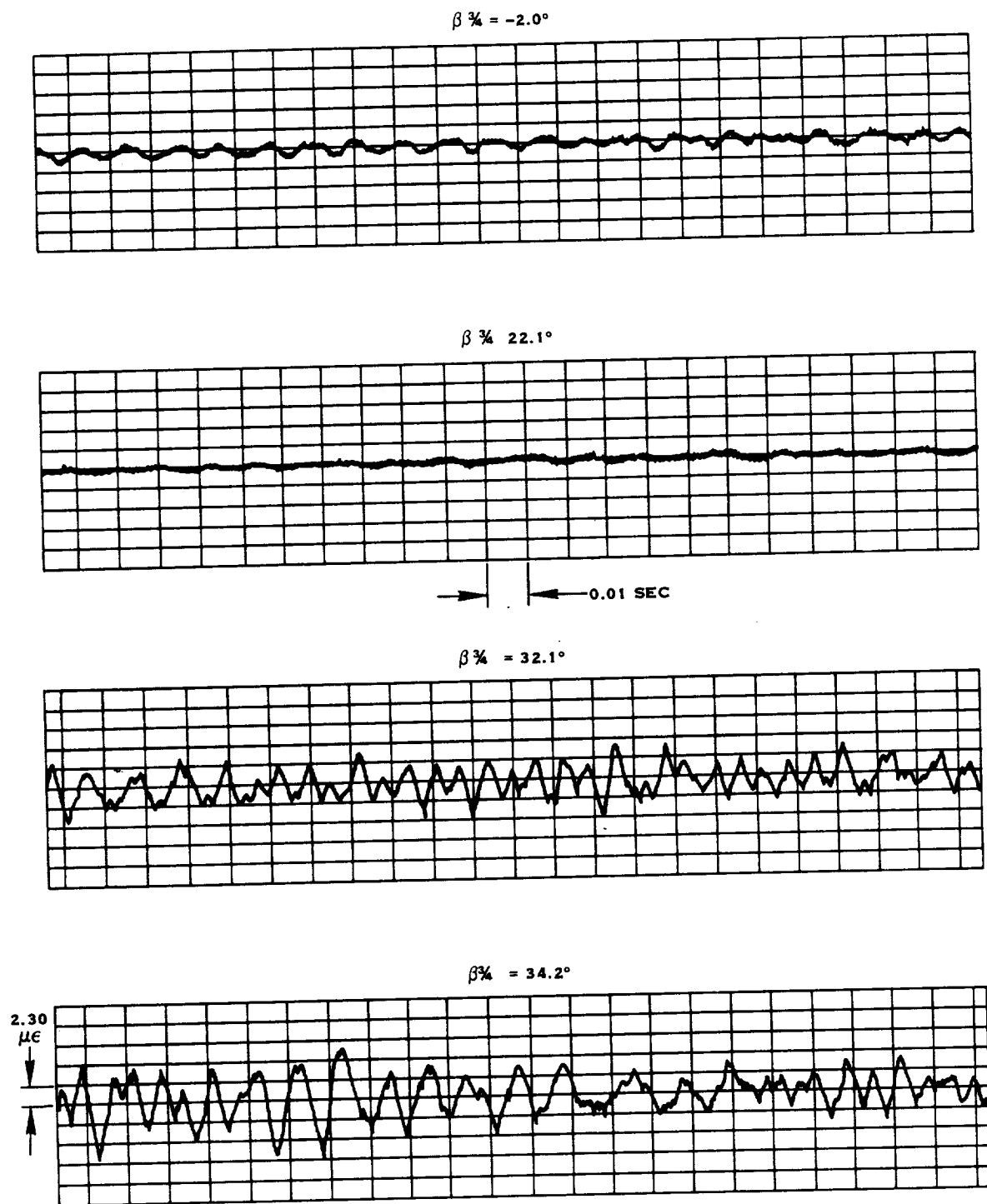
FIGURE 7.8 CHANGE IN THE TIP BENDING GAGE (73) RESPONSE WITH BLADE ANGLE FOR THE SR-7L PROP-FAN AT 1300 RPM
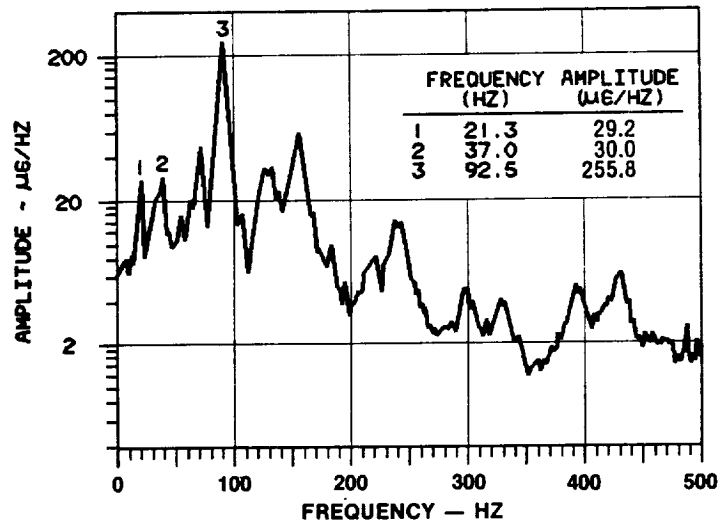
FIGURE 7.9 FREQUENCY CONTENT OF THE TIP BENDING GAGE (73) RESPONSE FOR 1300 RPM, 34.2° BLADE ANGLE
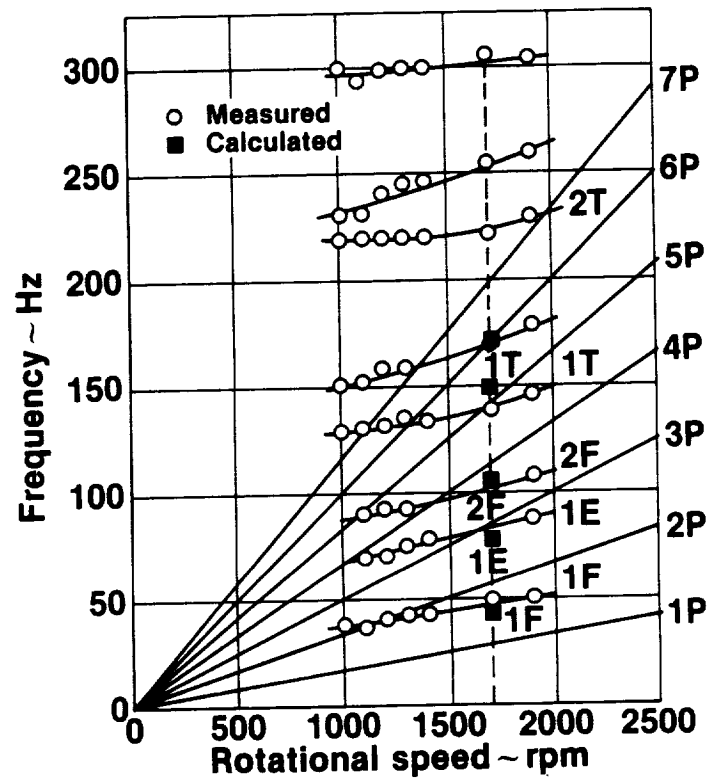
FIGURE 7.10 SR-7L BLADE NATURAL FREQUENCIES

46
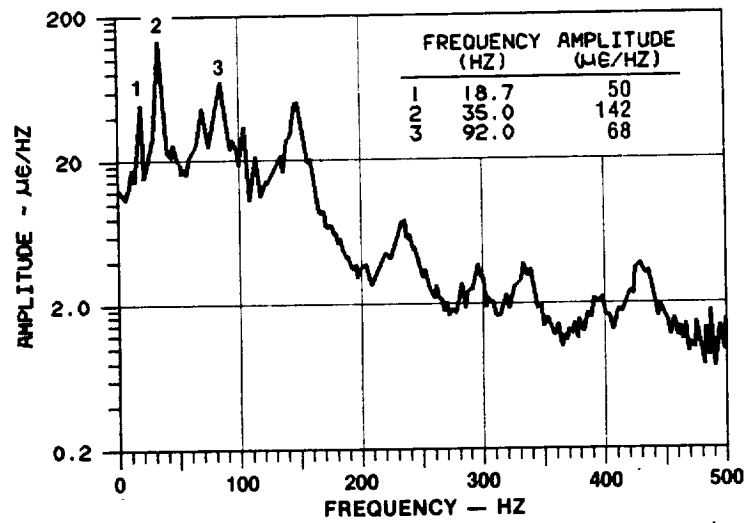
FIGURE 7.11 FREQUENCY CONTENT OF THE TIP BENDING GAGE (73) RESPONSE FOR 1100 RPM, 55° BLADE ANGLE
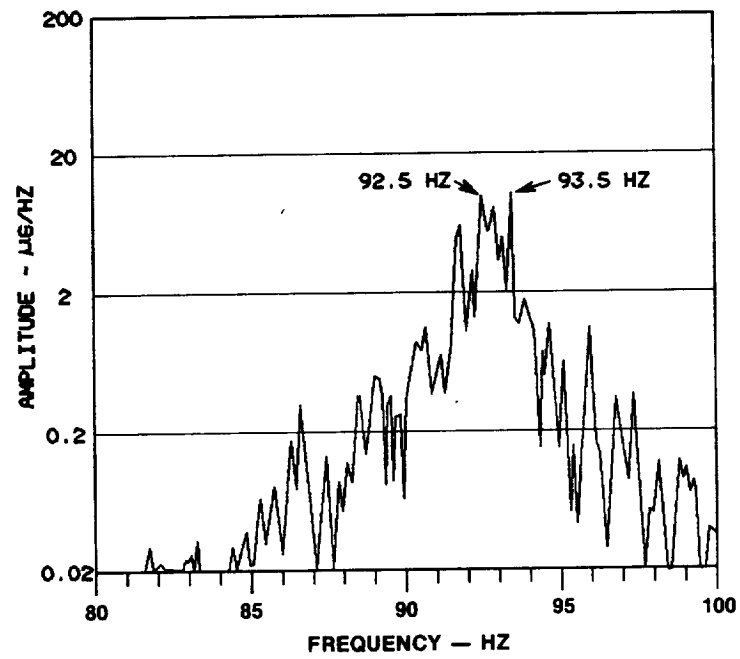
FIGURE 7.12 ZOOM SPECTRAL ANALYSIS OF THE MID-BLADE BENDING GAGE (72) FOR 1300 RPM, 34.2° BLADE ANGLE

48

7.3.3 (Continued)

multiple frequency peaks in the blade response is an indication that the system of blades is mis-tuned. For unstalled flutter, mis-tuning is stabilizing because it prevents the blades from locking into a coherent system mode (reference 10). Evidence of mis-tuning is also apparent when the variation in vibratory amplitude between blades is examined. Figure 7.13 shows the blade to blade variation in mid-blade bending strain between seven of the eight blades. Strain variations on the order of 25% are evident in the data with no blade having consistantly low or high strain levels as the rotational speed changed.

7.3.4 Blade Angle Effect on Natural Frequency

The data presented in the Campbell plot, Figure 7.10, is representative of all the blade angles tested and the condensed scale does not show the effect of blade angle on the blade natural frequency. To examine the blade angle effect the data was replotted versus blade angle in Figure 7.14 for three rotational speeds. Figure 7.14 shows that first and second flatwise bending modes decrease in frequency with increasing blade angle, the first edgewise mode increases in frequency with increasing blade angle, and the first torsion mode remains relatively uneffected by blade angle. These trends in frequency with blade angle are typical for rotating blades. The changes in frequency are caused by the orientation of the blade in the centrifugal field.

The centrifugal field produces a large out-of-plane centrifugal stiffening effect on the blade and a smaller in-plane centrifugal stiffening effect. When a blade is operating at low blade angle conditions, the flatwise natural modes of vibration are increased more than the edgewise modes by the larger out-of-plane centrifugal stiffening effect, because the flatwise motion is primarily out-of-plane. For flatwise modes, as the blade angle is raised the component of out-of-plane motion decreases and the in-plane motion increases so as to reduce the stiffening effect. This causes the blade natural frequency to decrease. The opposite is true for the edgewise natural modes of vibration which have more in-plane motion at low blade angles. Increasing the component of out-of-plane motion with increasing blade angle causes the edgewise mode to increase in frequency with blade angle.

7.3.5 Blade Total Strain Variation

The response of the SR-7L can be subdivided into three regions of differing response characteristics. These regions are low blade angle -5.7° to 25°, moderate blade angle 25° to 40° and high blade angle 40° to 60°. These regions were evident when the blade frequency content was examined and they are also evident when the total strain variation is examined for the three blade angle regions.
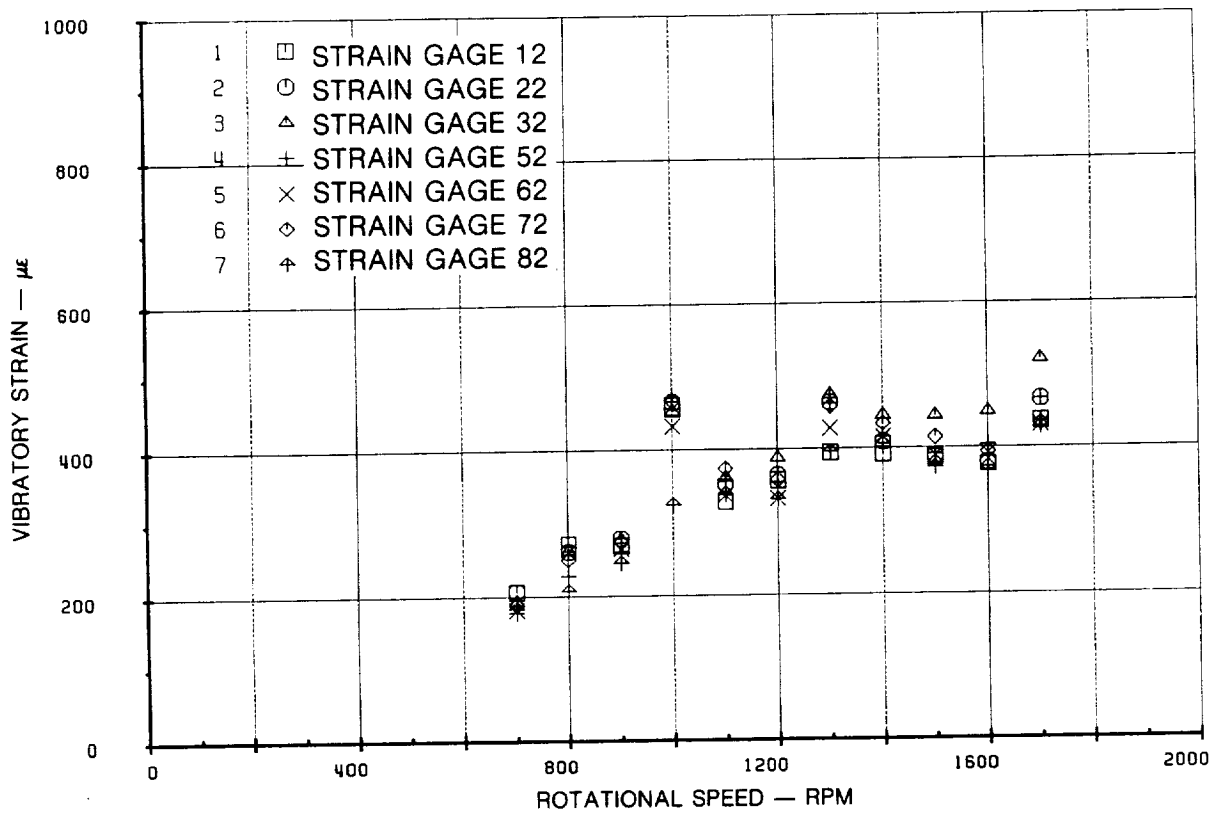
FIGURE 7.13 BLADE TO BLADE VIBRATORY STRAIN VARIATION
FOR THE SR-7L AT 33.5° $\beta_{3/4}$
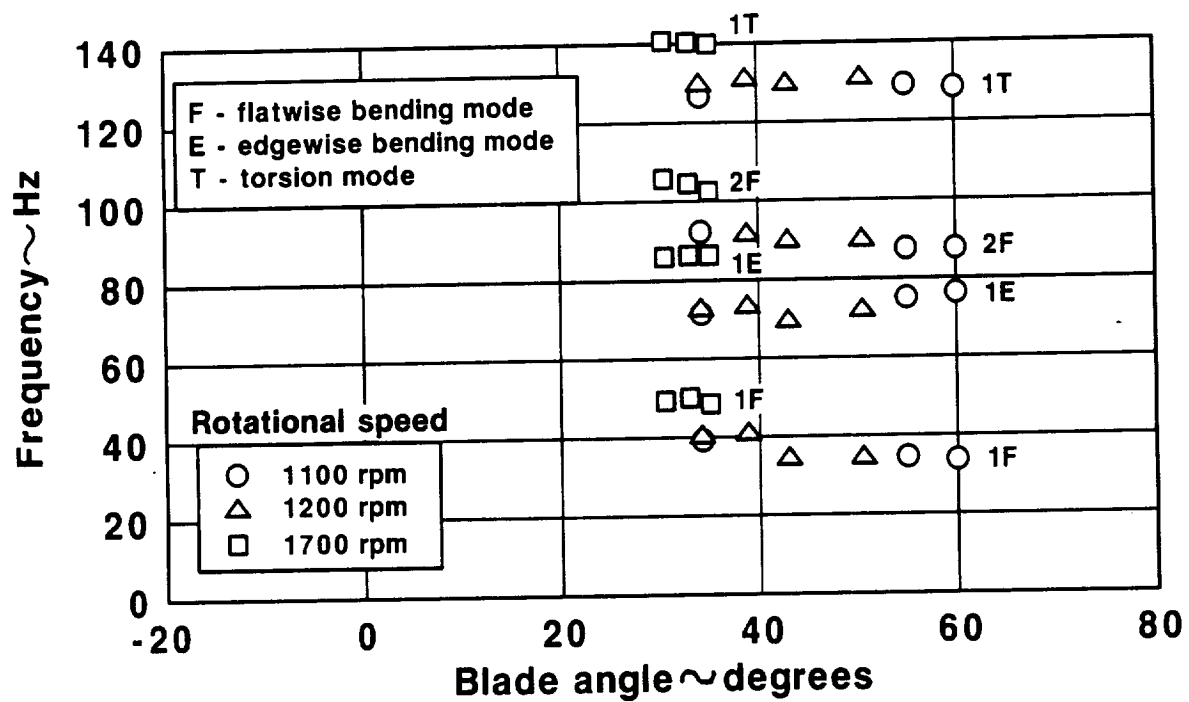
FIGURE 7.14 THE EFFECT OF BLADE ANGLE ON BLADE
NATURAL FREQUENCY FOR THE SR-7L

7.3.5 (Continued)

Figures 7.15, 7.16, and 7.17 show the variation of total strain measured by
the tip bending strain gage for the low, moderate and high blade angle re-
gions respectively. In the low blade angle region, the response is low and
the strain level changes little with rotational speed increase. In the mod-
erate blade angle region, the blade response is very sensitive to both rota-
tional speed and blade angle changes. A critical speed is evident in Figure
7.16 at 1000 RPM. The critical speed involves the first edgewise mode and
four-per-revolution (4P) exitation. At the 34.2° and 38.1° blade angles the
runs had to be stopped at low rotational speeds because the strain was in-
creasing rapidly with increasing rotational speed. The increased sensitivity
of the response to critical speeds in the moderate blade angle region indi-
cates that the damping in these modes has decreased because the external ex-
citation causing harmonic excitation has not changed. The external excita-
tion is due to small perturbations in the flow field. In the high blade an-
gle region the critical speed at 1000 RPM is no longer evident. The strain
at the tip strain gage tends to increase linearly with rotational speed. The
character of the response has changed at high blade angles.

Cross plotting the data in Figure 7.15, 7.16, and 7.17 yields Figure 7.18, a
strain contour plot for the tip bending gage vibratory response. This plot
shows the critical speed at 1000 RPM in the 30° to 40° blade angle region and
the disappearance of the critical speed above 40° blade angle. When the
critical speed effect is ignored, the shape of the constant strain contours
form a pattern of vertical lines at high blade angles and horizontal lines in
the 30° to 35° blade angle region.

Further insight into the changes in response characteristics is gained by ex-
amining the strain at the inboard bending strain gage. Figures 7.19, 7.20
and 7.21 show how the strain at an inboard strain gage changes with increas-
ing rotational speed and blade angle for the three blade angle regions dis-
cussed above. Figures 7.19 and 7.20 show little inboard bending gage re-
sponse at all rotational speeds and blade angles between -5.7° and 38.1°, but
Figure 7.21 shows substantial inboard bending gage response at the high blade
angles, indicating that the response has changed from a second flatwise mode
in the moderate blade angle region to first flatwise response in the high
blade angle region. This feature of the response was shown previously when
the frequency content of the signals was examined.

7.3.6 Blade Strain Distributions

Because the response characteristics changed from the moderate to high blade
angle regions, the distribution of strain along the blade varies from a sec-
ond flatwise distribution to a first flatwise distribution. Figures 7.22 and
7.23 show the distribution of total vibratory strain in the moderate blade
angle region and in the high blade angle region. It is interesting to note
that the shape of the distribution does not change substantially with rota-
tional speed. Only the magnitude of the response increases with increasing
rotational speed. This indicates that the forcing function that drives the
response increases in magnitude with rotational speed but does not change in
character.
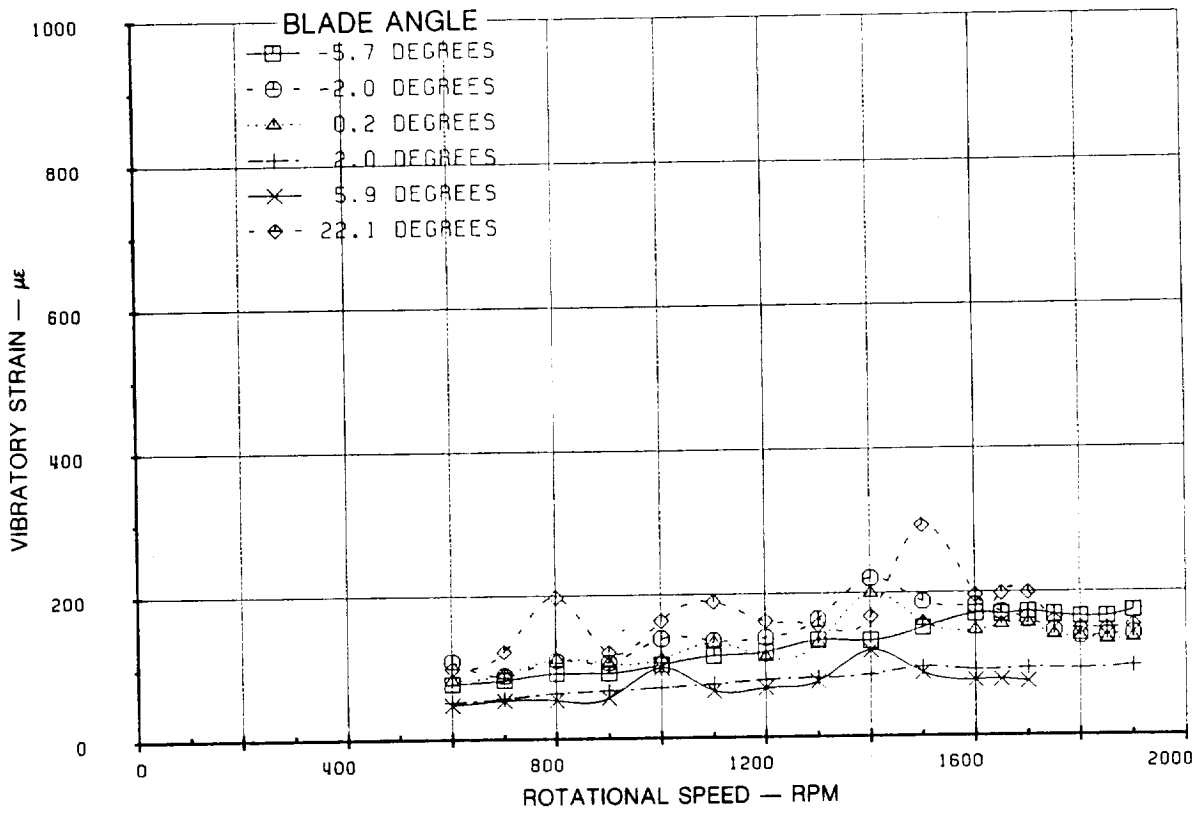
FIGURE 7.15 VIBRATORY STRAIN OF THE SR7L TIP BENDING GAGE (73)
AT LOW BLADE ANGLES

53
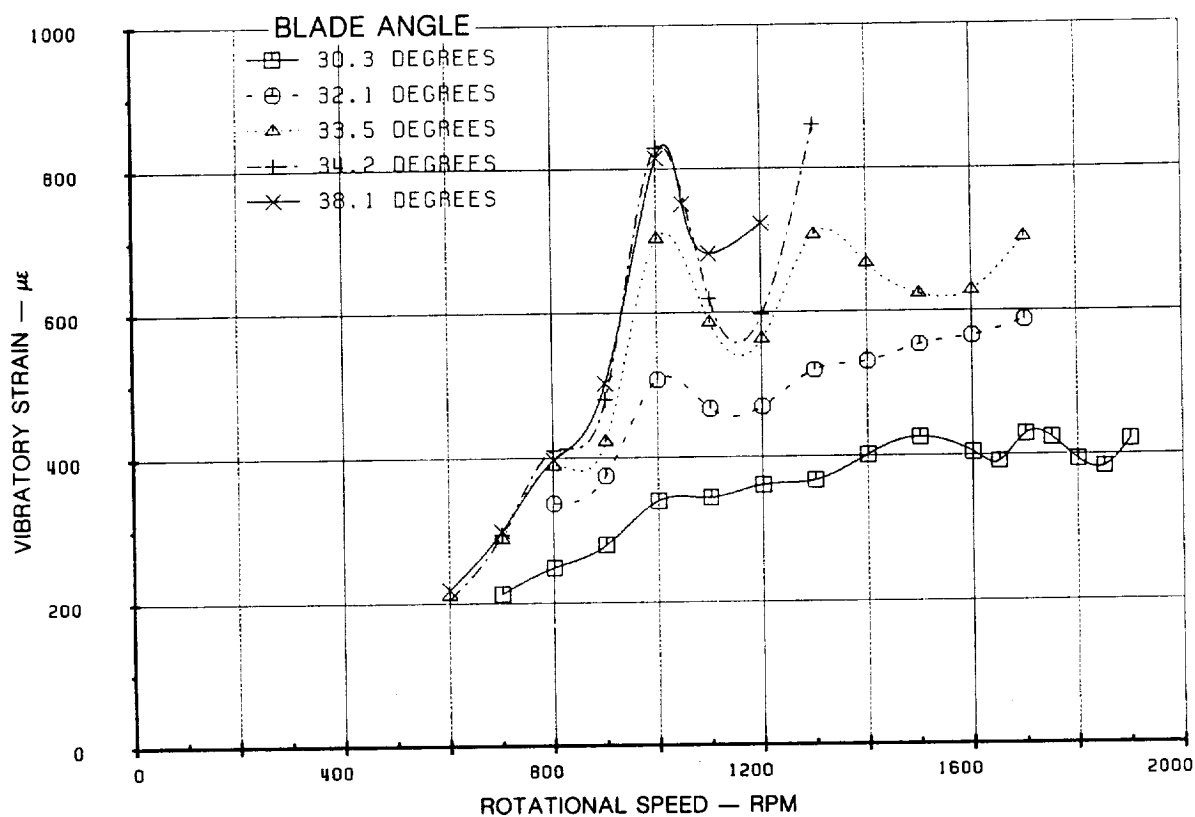
FIGURE 7.16 VIBRATORY STRAIN OF THE SR-7L TIP BENDING GAGE (73) AT MODERATE BLADE ANGLES
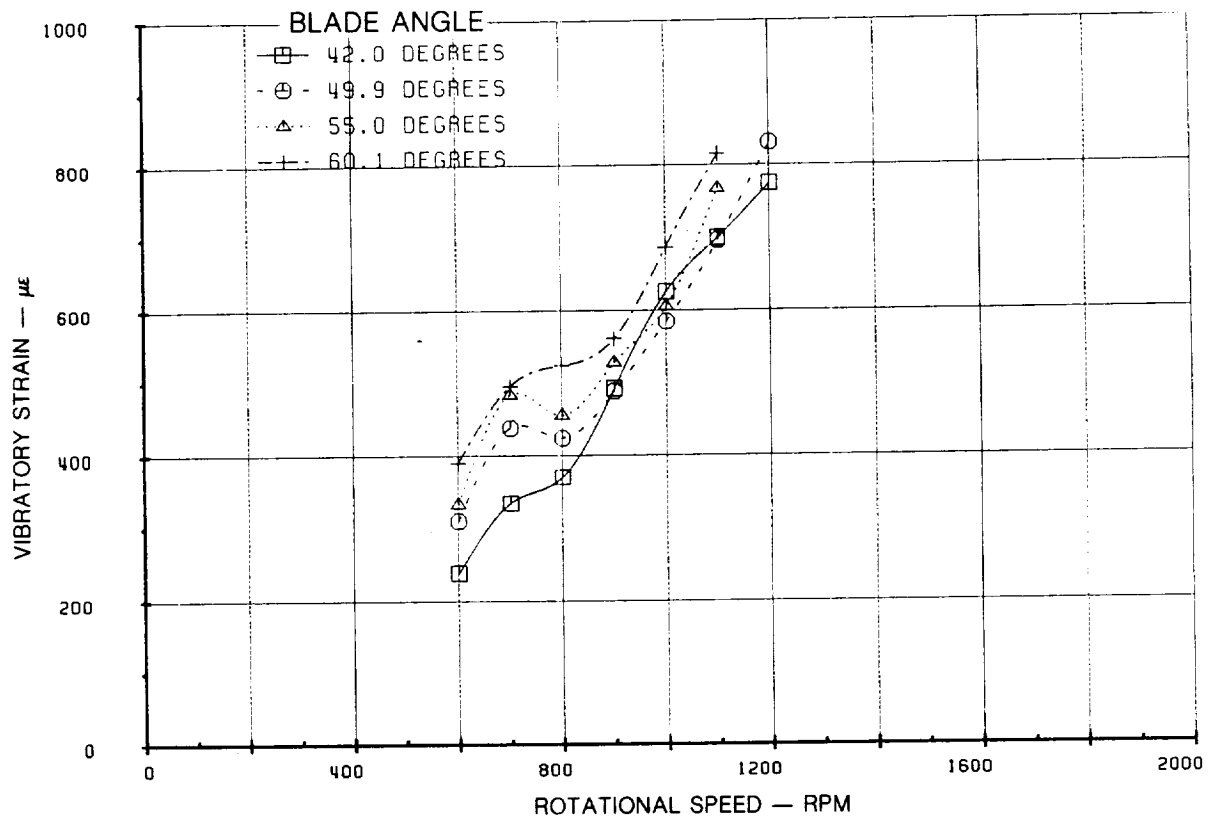
FIGURE 7.17 VIBRATORY STRAIN OF THE SR-7L TIP BENDING GAGE (73)
AT HIGH BLADE ANGLES
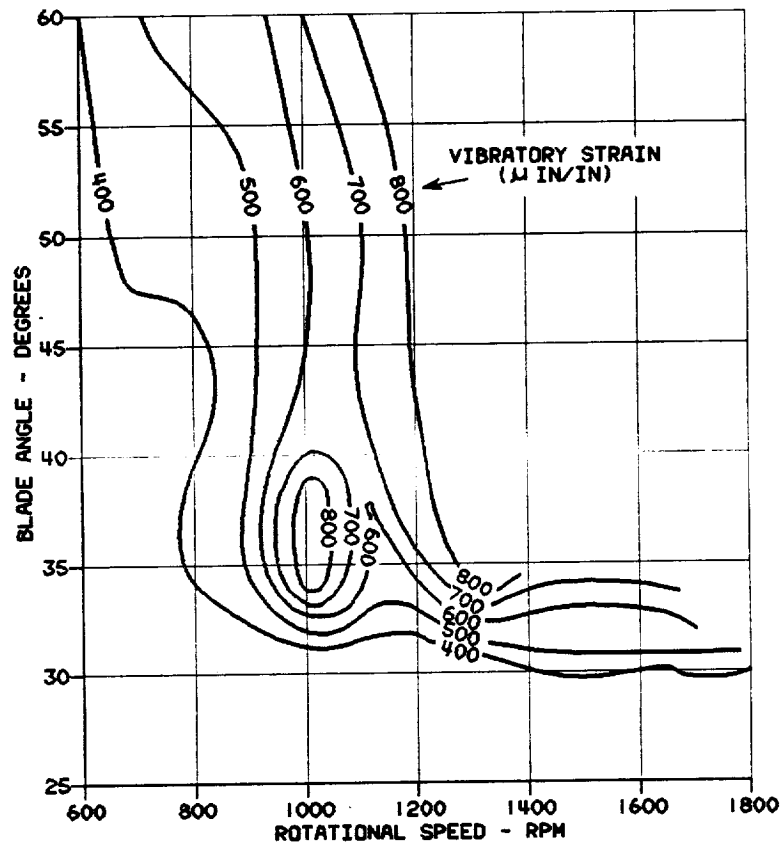
FIGURE 7.18 STRAIN CONTOUR PLOT FOR THE SR-7L
BASED ON GAGE (73) DATA
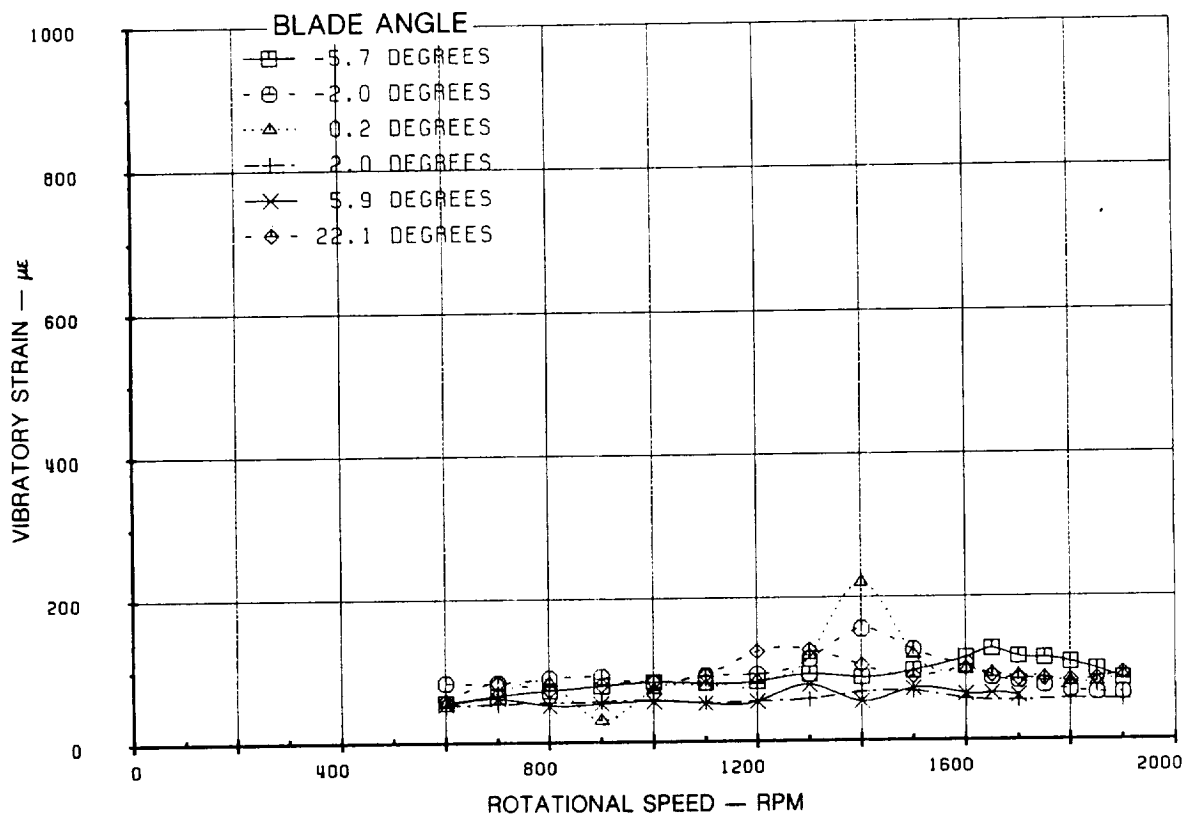
FIGURE 7.19 VIBRATORY STRAIN OF THE SR-7L INBOARD BENDING GAGE (81)
AT LOW BLADE ANGLES
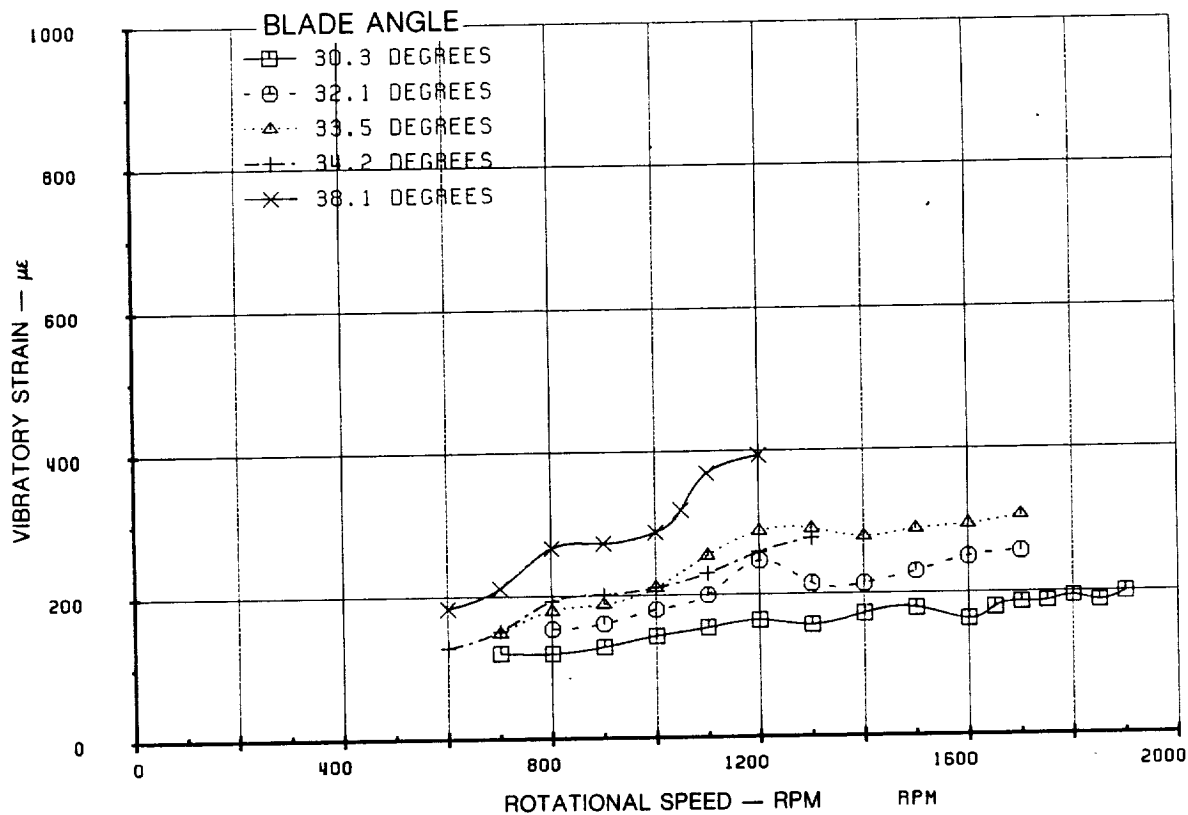
FIGURE 7.20 VIBRATORY STRAIN OF THE SR-7L INBOARD BENDING GAGE (81) AT MODERATE BLADE ANGLES
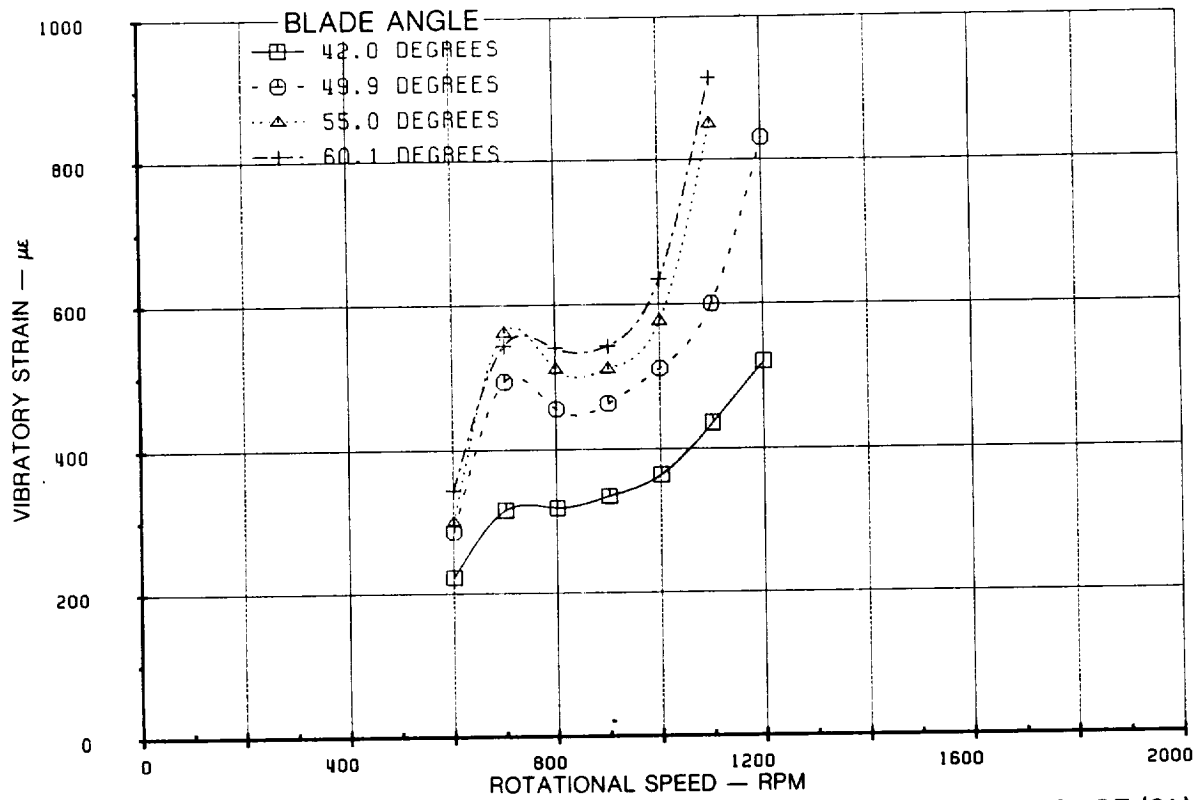
FIGURE 7.21 VIBRATORY STRAIN OF THE SR7-L INBOARD BENDING GAGE (81)
AT HIGH BLADE ANGLES
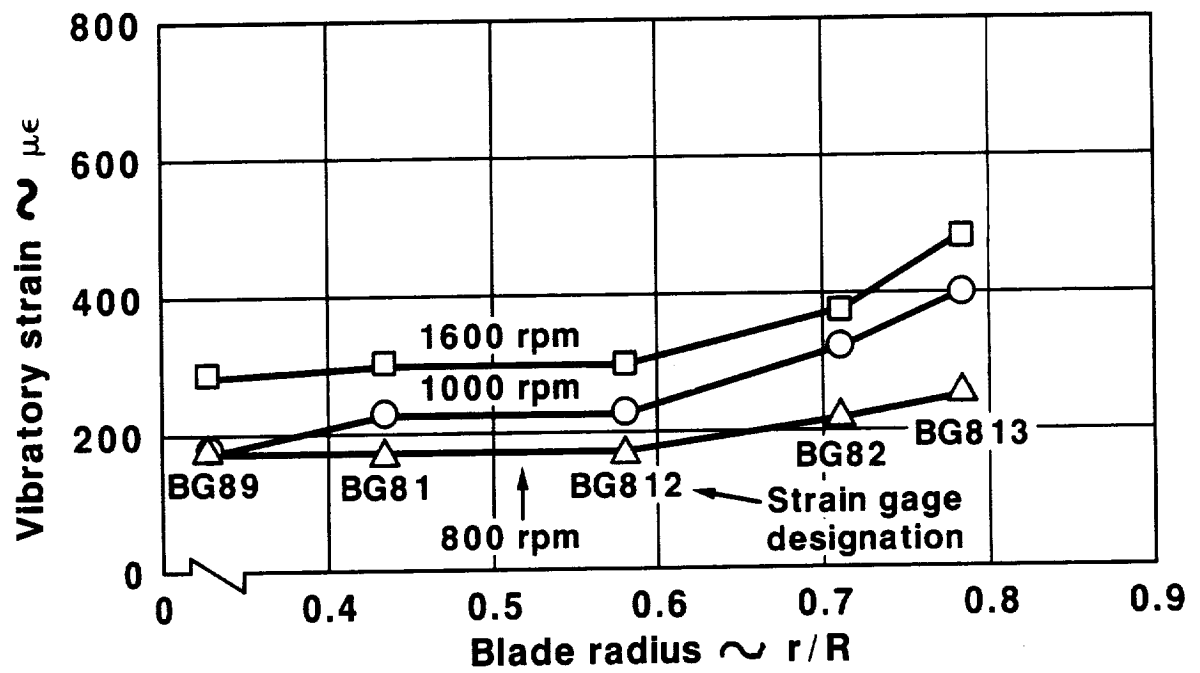
FIGURE 7.22 SR-7L BLADE BENDING STRAIN DISTRIBUTION AT A MODERATE BLADE ANGLE, 33.5°
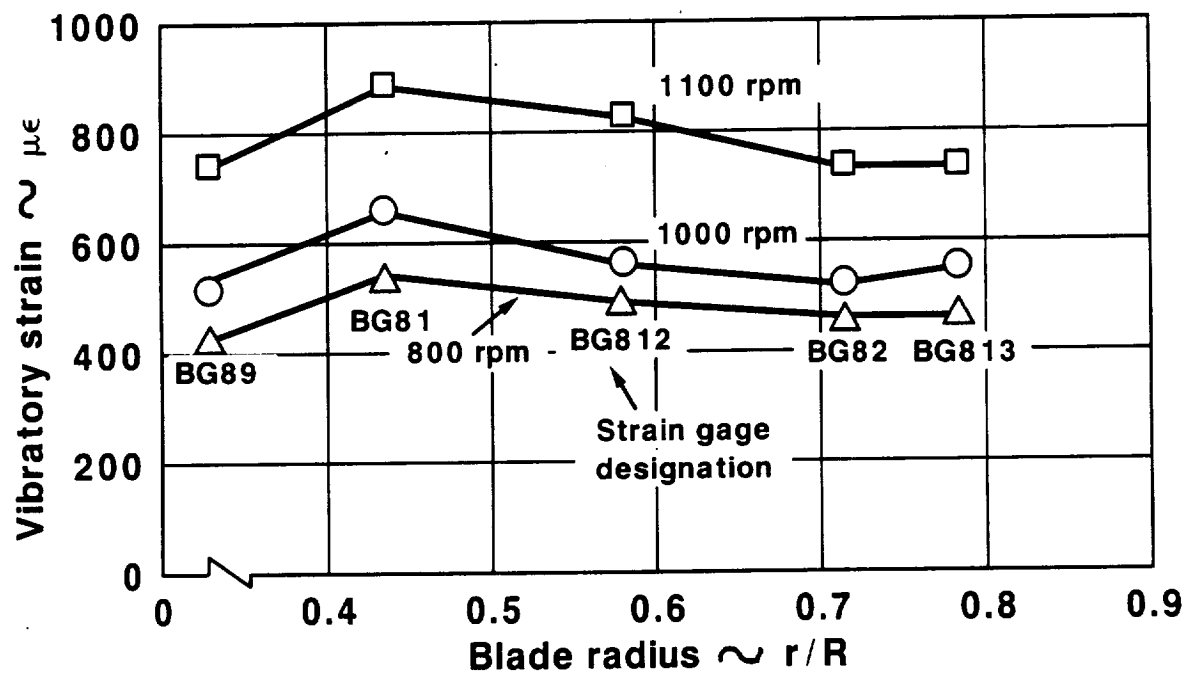
FIGURE 7.23 SR-7L BLADE BENDING STRAIN DISTRIBUTION AT A HIGH
BLADE ANGLE, 60.1°

8.0 BLADE STEADY STATE STRESS AND DEFLECTION MEASUREMENT

8.1 TEST PROCEDURE

This phase of the Static Rotor Test consisted of gathering steady state blade structural data at three operating points for which a static finite element analysis of the blade had been conducted. Acquisition of data at these operating points permitted comparison of analytically and experimentally determined blade stresses and deflections. The test points run are listed in Table 8.1.

TABLE 8.1. STEADY STATE STRESS AND DEFLECTION TEST POINTS

Test Point	Blade Angle (β 3/4)	RPM
1	22°	1700
2	32.1°	1700
3	25.8°	2038

Test point 3 was included as a proof test of the structural integrity of the Prop-Fan blades and mechanical systems. This test point consisted of operation at 120% of the design rotational speed at a blade angle that would allow the Prop-Fan to absorb 100% of its design power at that speed. The total operating time accumulated at the overspeed point was one hour. Test point 3 is in accord with the requirements of military specification MIL-P-26366A for propeller overspeed proof tests.

8.1.1 Analytical Technique

Analysis of the SR-7L blade for the operating points described in Table 8.1 was conducted using the Hamilton Standard in house finite element code BESTRAN. An offset finite element model of the blade was used for this analysis. In the offset model the layers of the blade model are tied together with rigid elements instead of elastic links, thus greatly reducing solution time. A One-Step plus Differential Stiffening approach was used in running the finite element analysis. This is a two step solution. During the first step a differential stiffening matrix is calculated, which accounts for the change in element bending stiffness as the element membrane stresses change. The blade is then reanalyzed including the effect of the differential stiffness matrix calculated in the first step (reference 7).

8.1.2 Steady Stress Measurement

Comparison of measured and predicted blade stresses permits the accuracy of the analytical tools used in the blade design, as well as the structural adequacy of the blade to be evaluated.

PAGE 6 2 INTENTIONALLY

8.1.2 (Continued)

The blade strain gage arrangement used during the steady state stress and deflection portion of the test is shown in Figure 8.1. The locations of gages 414 and 416 were chosen to correspond with the points of predicted maximum steady compressive and tensile stress respectively on the face side of the blade. The location of gages 415 and 417 correspond with the points of predicted maximum steady compressive and tensile stress respectively on the camber side of the blade. Strain gages 89, 81, 82, 813 and 83 provided the capability to determine the radial distribution of stress along the blade. The strain gage arrangement also allowed the blade vibratory stresses to be adequately monitored.

8.1.3 Blade Deflection Measurement

The SR-7L blade was designed so that it would assume the correct aerodynamic shape, when subjected to design centrifugal and air loads. Therefore comparison of measured and predicted deflections provides information, which can be useful in evaluating aerodynamic performance data.

Blade deflection measurements were made using two separate systems, an optical system and a laser based system. The optical system consisted of a transit type telescope mounted on a carriage and track assembly, a linear scale and a strobe light. The scope was located beneath the Prop-Fan and viewed upward at the advancing blades passing through horizontal. The carriage allowed the scope to be moved back and forth parallel to the axis of rotation, as well as laterally. The axial movement of the scope was controlled by a handwheel and worm gear mechanism, which allowed precise adjustment of the scope position. The axial position of the scope was measured with the linear scale. The strobe light was triggered by the rotation of the . whirl rig shaft. The phase could be adjusted to freeze the rotor with blade number one in the horizontal position.

The axial location of the blade leading and trailing edges at any station were determined by adjusting the position of the scope until the crosshairs were aligned with these points. Chordwise stripes were located on the surface of blade number one at the stations where deflection measurements were made to facilitate alignment of the scope. The zero points for blade deflection were taken with the Prop-Fan rotating at 700 RPM. Operation at this speed eliminated backlash in the actuator and retention system, but did not result in significant blade deflection. The blade deflection was determined at each test point by measuring the axial displacement of the blade leading and trailing edges from the zero point.

The laser deflection measurement system consisted of four helium-neon lasers and four photodetectors. One laser is reflected from a mirror on the Prop-Fan spinner back to a detector to provide a once per revolution indication. The remaining three lasers were oriented so that their beams passed obliquely

Forward to aft view

Blade camber side view
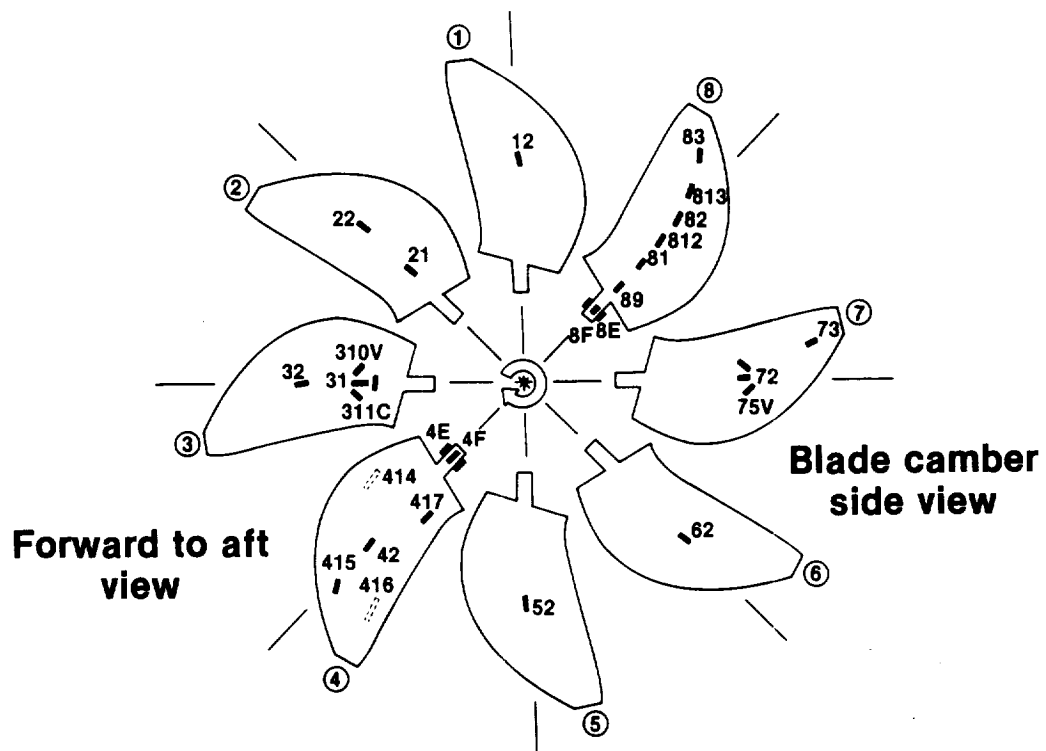
FIGURE 8.1 ACTIVE STRAIN GAGE ARRANGEMENT FOR OVERSPEED AND BLADE DEFLECTION TESTING

8.1.3 (Continued)

through the Prop-Fan rotor disc and were received at three additional photo-detectors. These laser beams intersected the blade in the six o'clock position at the 50% span, 75% span and tip stations. As the blade intersects the beams, light going to the detectors is blocked and the detector output goes low. After the blade trailing edge passes the beam, light going to the detector is restored and the detector output goes high. Therefore the outputs of the detectors are rectangular wave forms when the Prop-Fan is rotating. The deflection of the blade is determined by relating changes in the timing of the waveforms to changes in the geometry of the blade.

8.1.4 Overspeed Test Point

The overspeed test point was run for one hour at 120% of the design speed (2038 RPM) and at a blade angle that absorbed 100% of the design power (6000 HP) at that speed. The test was stopped once after twenty minutes to check the blades.

8.2 DATA REDUCTION

8.2.1 Steady Strain Data Reduction

The devices used for on line monitoring of strain data during test were primarily intended to be used for observing the vibratory component of strain. Therefore the steady strains were not continuously monitored. Several DC shifts occurred in the strain data during test, but were not noticed until the data was played back. These shifts were not the result of a change in the steady strain levels, but occurred due to changes in the instrumentation DC voltage levels. DC shifts of the same magnitude occurred on every strain gage.

The data shifts did not render the steady strain data useless. Since the magnitude of the DC shift was the same for all of the strain gages, the data could be normalized to a selected strain measurement and this normalized data could be compared to similarly normalized analytical predictions to verify trends in the data. The strain reading of gage 417 at 2038 RPM and a 25.8° blade angle was used to normalize all of the strain data for evaluation of data trends.

8.2.2 Blade Deflection Data Reduction

The calculation of the section twist deflection from the optical deflection data is illustrated in Figure 8.2. The pitch angle of the blade section of interest is assumed to be proportional to the projected length of the section as described by equation 8.1. The change in projected length of the section

$$\beta_1 = b/a \; \beta_0 \tag{8.1}$$

is equal to the axial deflection of the leading edge minus the axial deflection of the trailing edge, which yields equation 8.2. Equations 8.1 and

$$b = a + (d_2 - d_1) \tag{8.2}$$

8.2 can then be combined to form equation 8.3 and the twist deflection of the section is computed from equation 8.4,

$$\beta_1 = \left[\frac{a + (d_2 - d_1)}{a} \right] \beta_0 \tag{8.3}$$

$$\Delta\beta = \beta_1 - \beta_0$$

$$\Delta\beta = \left[\frac{a + (d_2 - d_1)}{a} \right] \beta_0 - \beta_0$$

$$\Delta\beta = \beta_0 + \frac{(d_2 - d_1)}{a} \beta_0 - \beta_0$$

$$\Delta\beta = \left[\frac{d_2 - d_1}{a} \right] \beta_0 \tag{8.4}$$
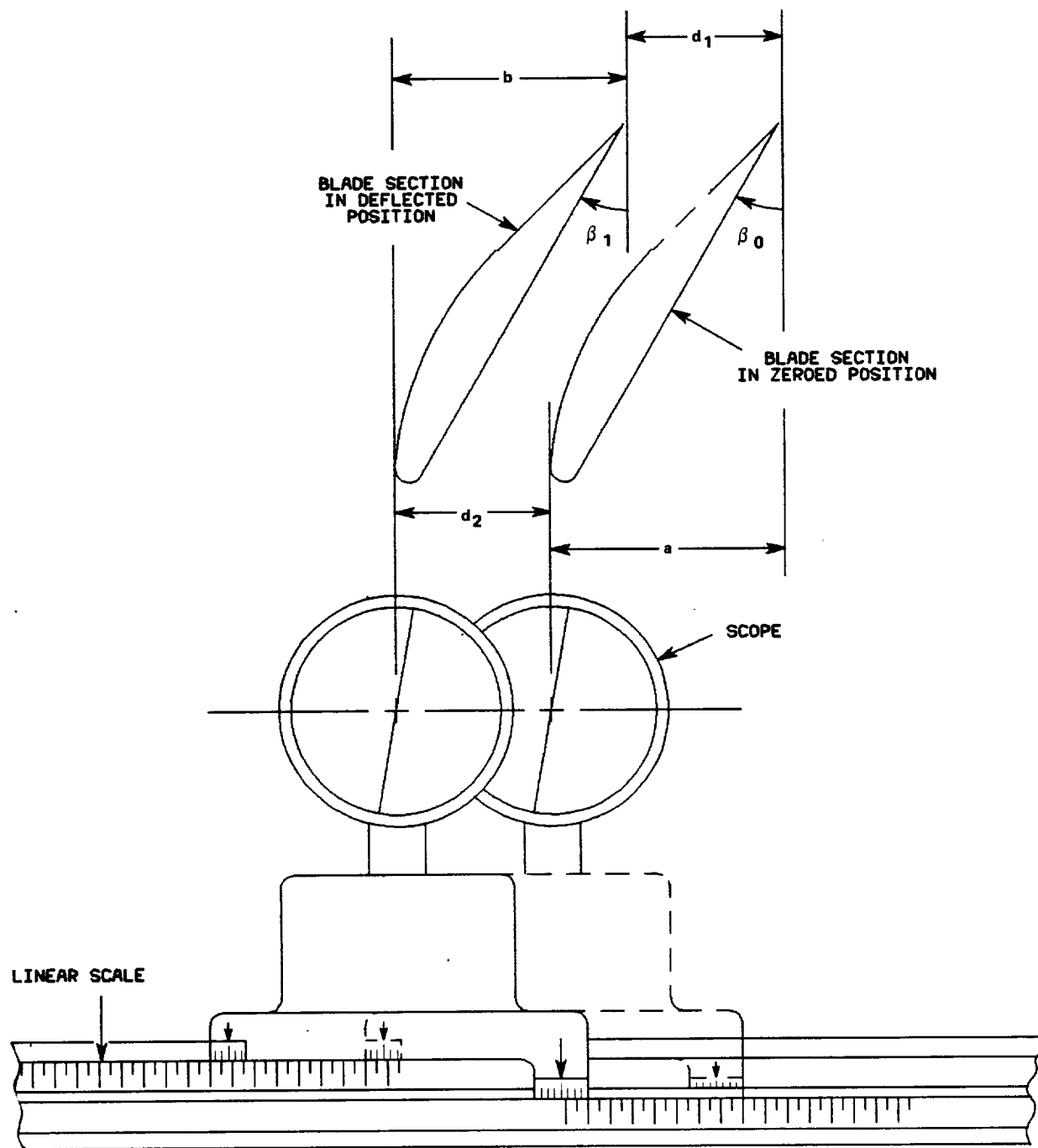
FIGURE 8.2 OPTICAL BLADE DEFLECTION MEASUREMENT SYSTEM

68

8.3 TEST RESULTS AND DISCUSSION

8.3.1 Prop-Fan Performance

Table 8.2 shows a comparison of the predicted and measured thrust for the test points run. The comparison of the measured and predicted thrust and horsepower is indicative of how close the actual aerodynamic loads seen by the blades were to the loads used in the blade steady state structural analysis. Good agreement was obtained between measured and predicted thrust and power for test points 1 and 3, which correspond to blade angles of 22° and 25.8° respectively. The thrust and power measured at test point 2 was significantly lower than predicted. Since test point 2 was run at a blade angle of 32°, the low measured power and thrust correlates with the shortfall in measured performance discussed in Section 6.0.

TABLE 8.2. COMPARISON OF MEASURED AND PREDICTED THRUST AND POWER

Test Point	Power (kW)		Thrust (N)	
	Measured	Predicted	Measured	Predicted
1	1924	1826	29183	27546
2	3520	4476	32337	40237
3	4518	4476	49030	46806

8.3.2 Steady Strain Results

Figure 8.3 shows the increase in measured blade strain with rotational speed for strain gages 414, 415, 416 and 417. The strain is shown to increase with approximately the square of the rotational speed. This is expected because the strain is produced by centrifugal and aerodynamic loads that increase with the square of the rotational speed. At the overspeed condition of 2038 RPM and 25.8° blade angle, the normalized radial distribution of strain compares very well with the predicted blade strain as shown in Figure 8.4. The measured distribution is shown to be slightly higher in the inboard portion of the blade than predicted. A more detailed comparison of the strain distribution at all the locations where strain was measured is shown in Figure 8.5. The comparison is very good except for the measurement on the trailing edge of the blade (gage 24) and at the tip of the blade (gage 416). At gage 24 the strain is substantially higher than predicted while at gage 416 the measured strain is lower than predicted.

8.3.3 Steady State Deflection Results

Initial testing accomplished with the optical blade deflection measurement system revealed that the 50% span and 75% span stations on the horizontal blade were obscured from view by the blade in the 45° below horizontal position. Therefore blade deflection data was only collected at the tip blade station using the optical system.
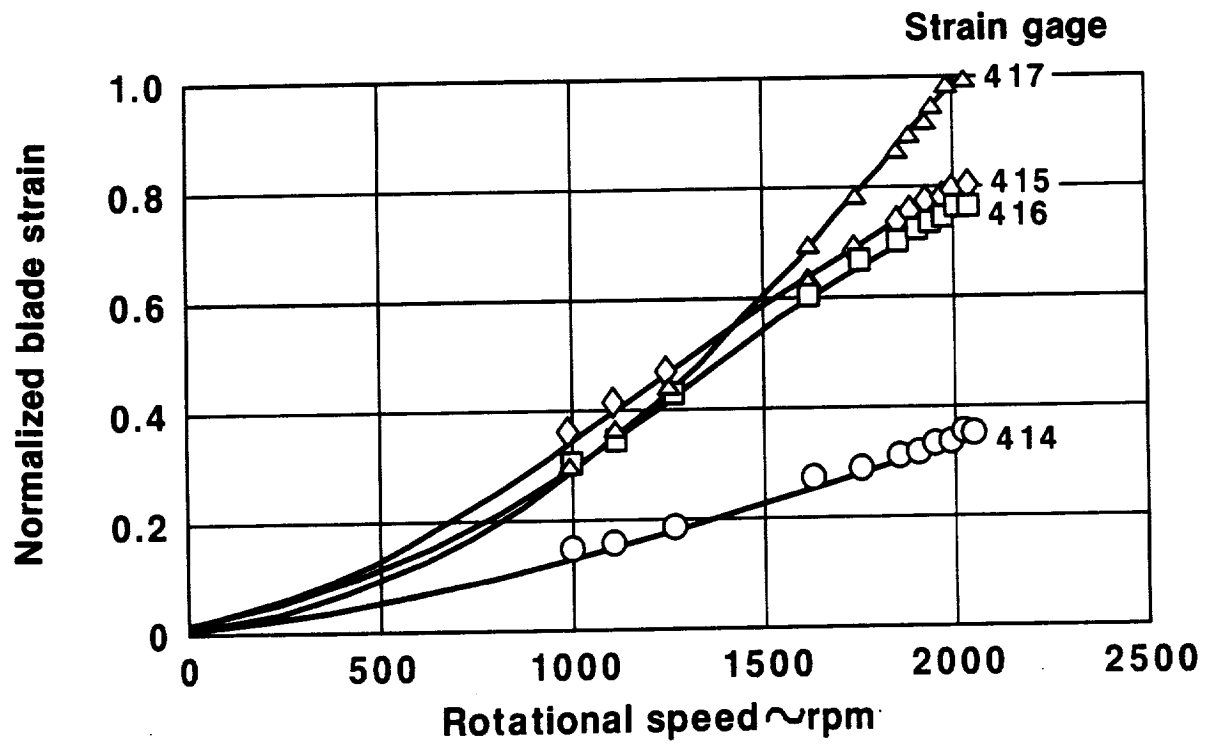
FIGURE 8.3 STRAIN VARIATION WITH ROTATIONAL SPEED, $\beta_{3/4} = 25.8°$, STRAIN NORMALIZED TO MAXIMUM, STRAIN GAGE 417
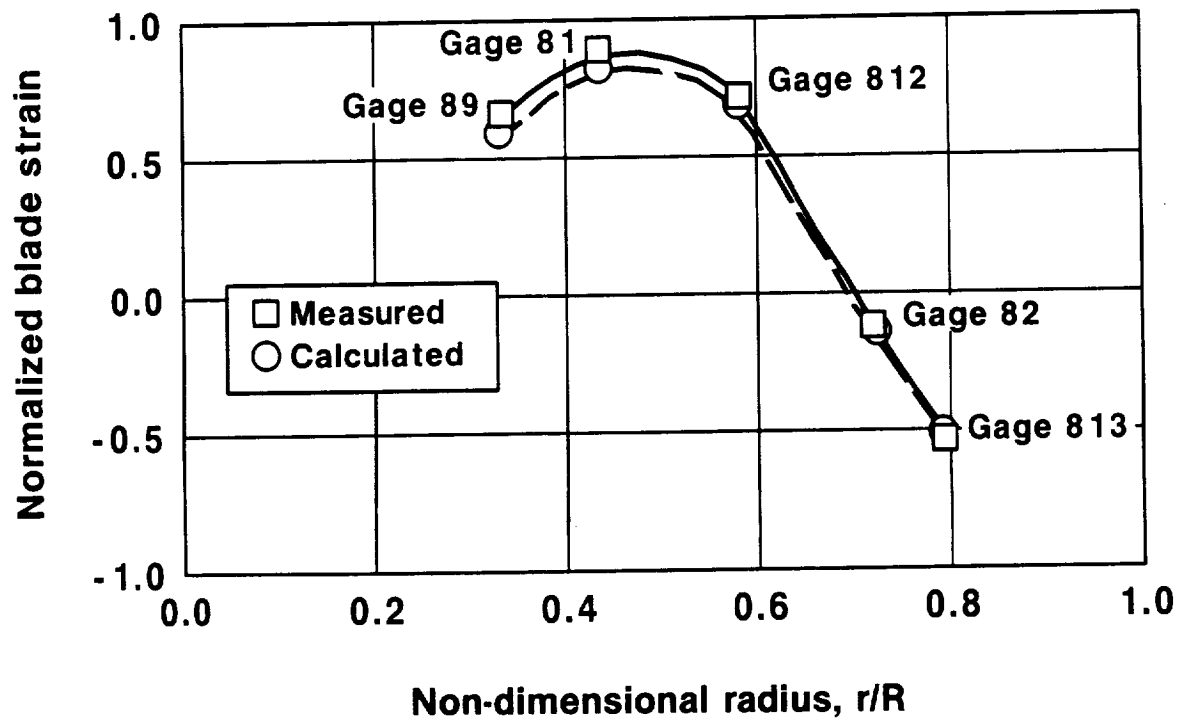
FIGURE 8.4 SR-7L STEADY STRAIN RADIAL DISTRIBUTION DURING WPAFB
OVERSPEED TESTS, TEST POINT NO. 3 (REF. TABLE 8.1), $\beta_{3/4} = 25.8°$,
2038 RPM, STRAIN NORMALIZED TO MAXIMUM STRAIN GAGE 417

FIGURE 8.5 SR-7L STEADY STRAIN DURING THE OVERSPEED TESTS,
TEST POINT NO. 3 (REF TABLE 8.1) $\beta3/4 = 25.8°$, 2038 RPM

8.3.3 (Continued)

Figures 8.6 through 8.8 present the blade tip twist deflection as a function of the square of the Prop-Fan rotational speed. Data acquired both with the optical and laser systems is presented in these figures. The centrifugal and aerodynamic loads on the blades are proportional to the rotational speed squared. Therefore plotting blade deflection versus RPM squared should yield straight lines. Figures 8.9 through 8.11 present the deflection data taken at the 50% span, 75% span and tip blade stations overlayed on the calculated twist deflection distributions.

Examination of the plots of blade deflection versus RPM squared revealed that the data acquired with the laser system is well behaved and approximates a straight line. However a large amount of scatter is seen in the optical data. The scatter may be due to some random fore and aft motion of the blade that was apparent when the blade was viewed through the scope. This unsteadiness made it difficult to accurately align the scope crosshairs with the leading and trailing edges and thus caused uncertainty in the blade deflection measurements.

Figures 8.9 through 8.11 indicate that better correlation of measured and calculated blade deflection was obtained at the tip using the laser system rather than the optical system. Comparing the measured and predicted blade deflection distributions between 50% span and the tip, some large percentage discrepancies are noted. However the actual error in terms of degrees is small, typically on the order of .3° to .4°. The characteristic shape of the spanwise distribution of blade twist also seems to be matched well by the data. It can therefore be concluded that the difference between the desired and actual deflected blade shapes did not significantly effect the aerodynamic performance of the Prop-Fan.

8.3.4 Overspeed Test Results

The overspeed test of the SR-7L produced centrifugal loads that were 1.44 times greater than the centrifugal loads at 100% speed and aerodynamic pressures at the 80% radial station that were 1.8 times greater than those occurring at the design cruise condition due to the higher RPM and air density. The low vibratory response of the blade during overspeed tests shows that no unstalled flutter occurred at this condition and implied that no unstalled flutter will exist during flight testing at the design cruise condition. This implication is drawn because unstalled flutter is inversely proportional to dynamic pressure and the blades encountered higher dynamic pressures during overspeed testing than would occur during flight testing.
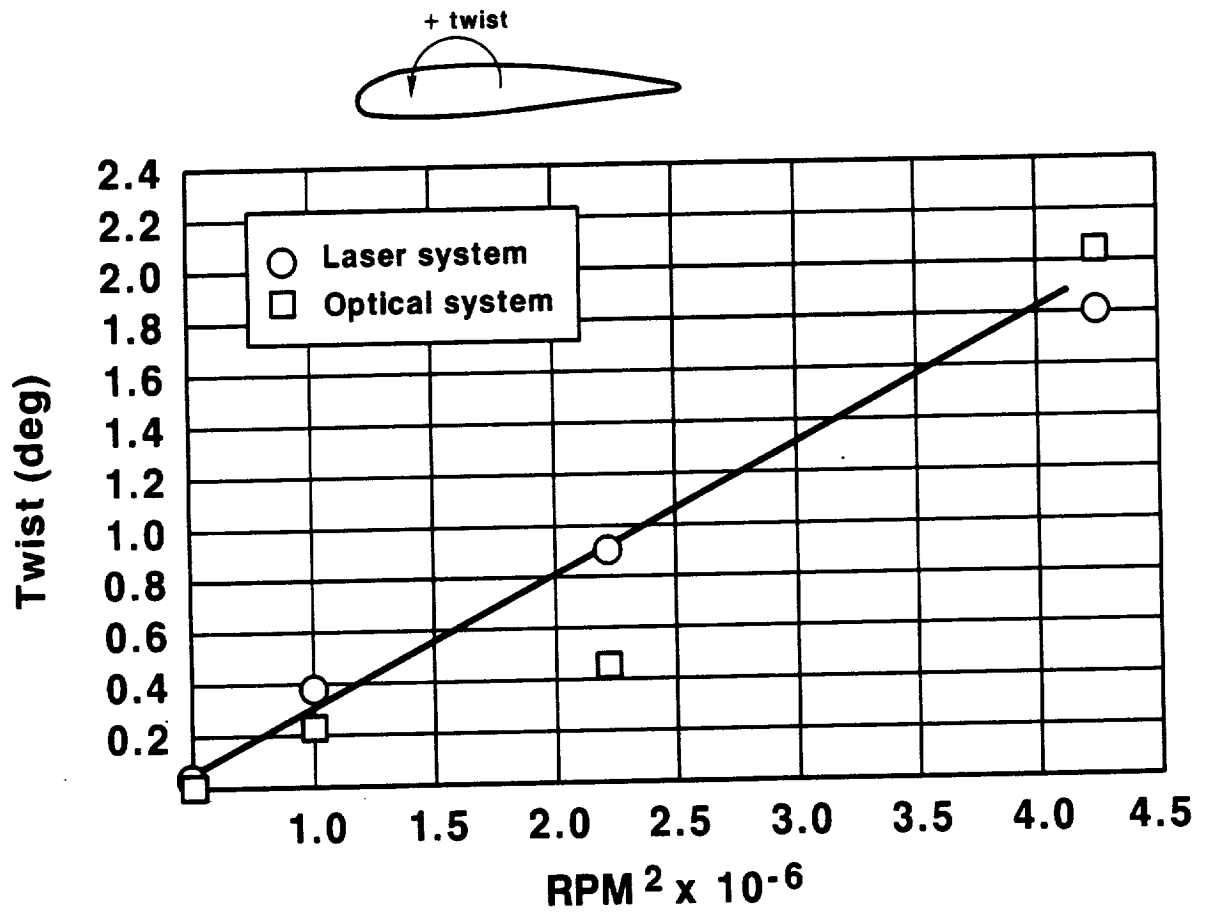
FIGURE 8.6 BLADE TIP TWIST DEFLECTION VS. ROTATIONAL SPEED,
$\beta_{3/4} = 25.8°$
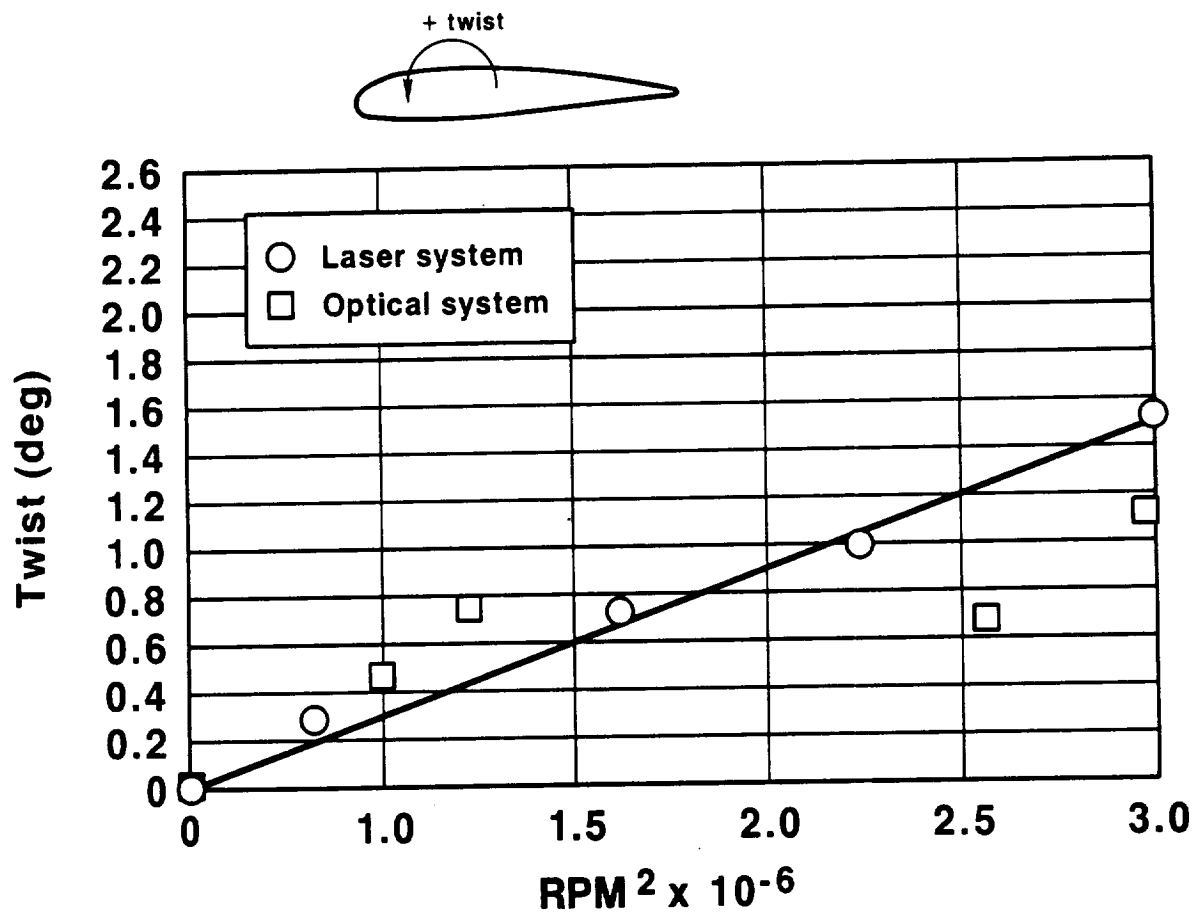
FIGURE 8.7 BLADE TWIST DEFLECTION VS. ROTATIONAL SPEED, $\beta 3/4 = 22°$
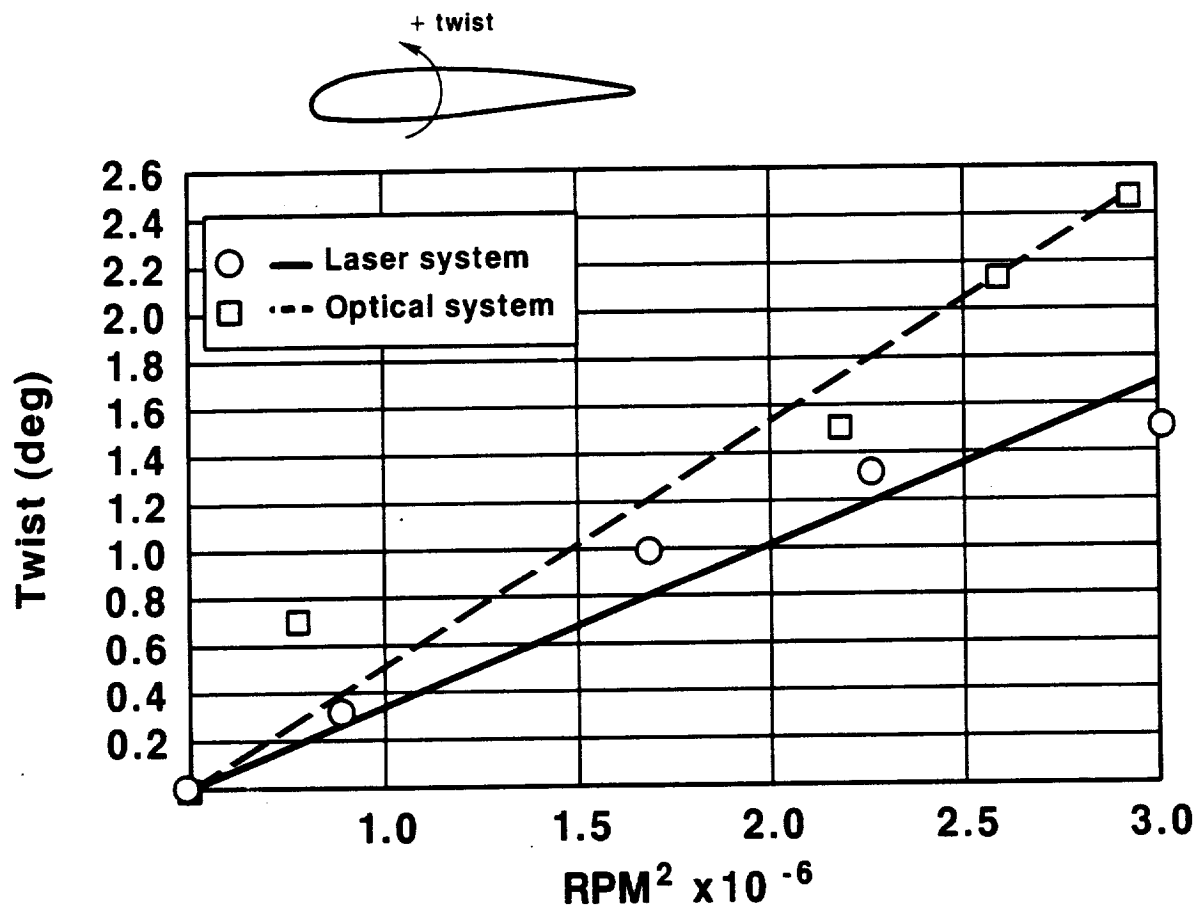
FIGURE 8.8 BLADE TWIST DEFLECTION VS. ROTATIONAL SPEED, β 3/4 = 32°
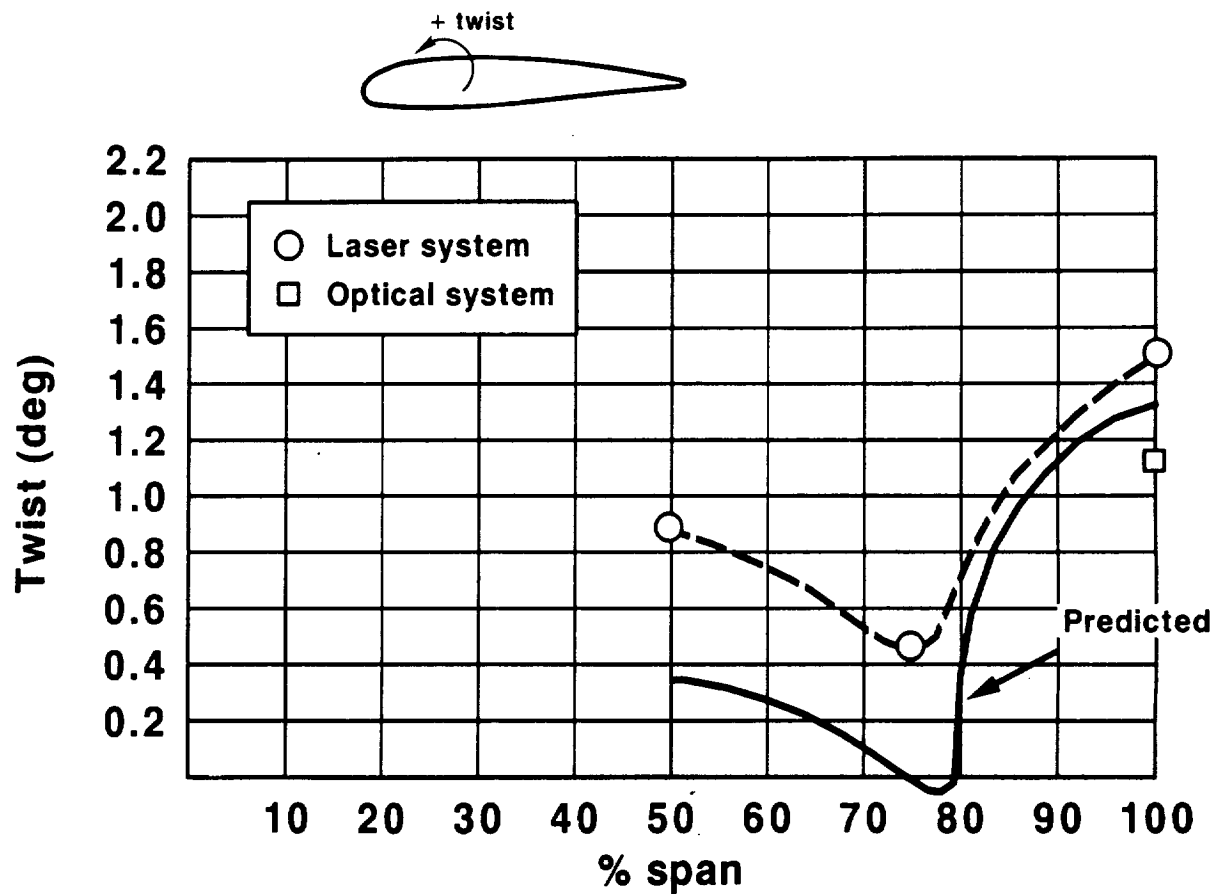
FIGURE 8.9 COMPARISON OF MEASURED & PREDICTED BLADE TWIST DEFLECTION,
TEST POINT NO. 1 (REF. TABLE 8.1) $\beta 3/4 = 22°$, N = 1700 RPM
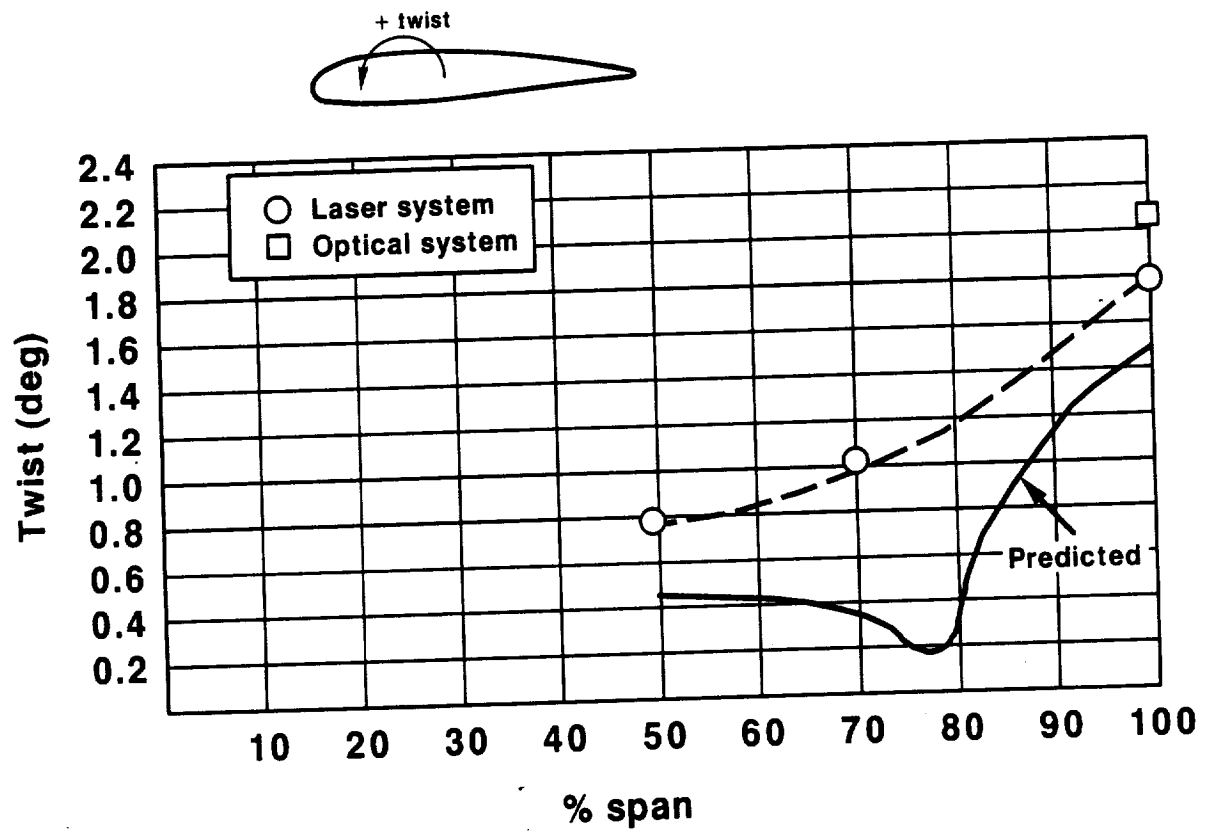
FIGURE 8.10 COMPARISON OF MEASURED & PREDICTED BLADE TWIST DEFLECTION, TEST POINT NO. 3 (REF TABLE 8.1) $\beta_{3/4} = 25.8°$, N = 2038 RPM
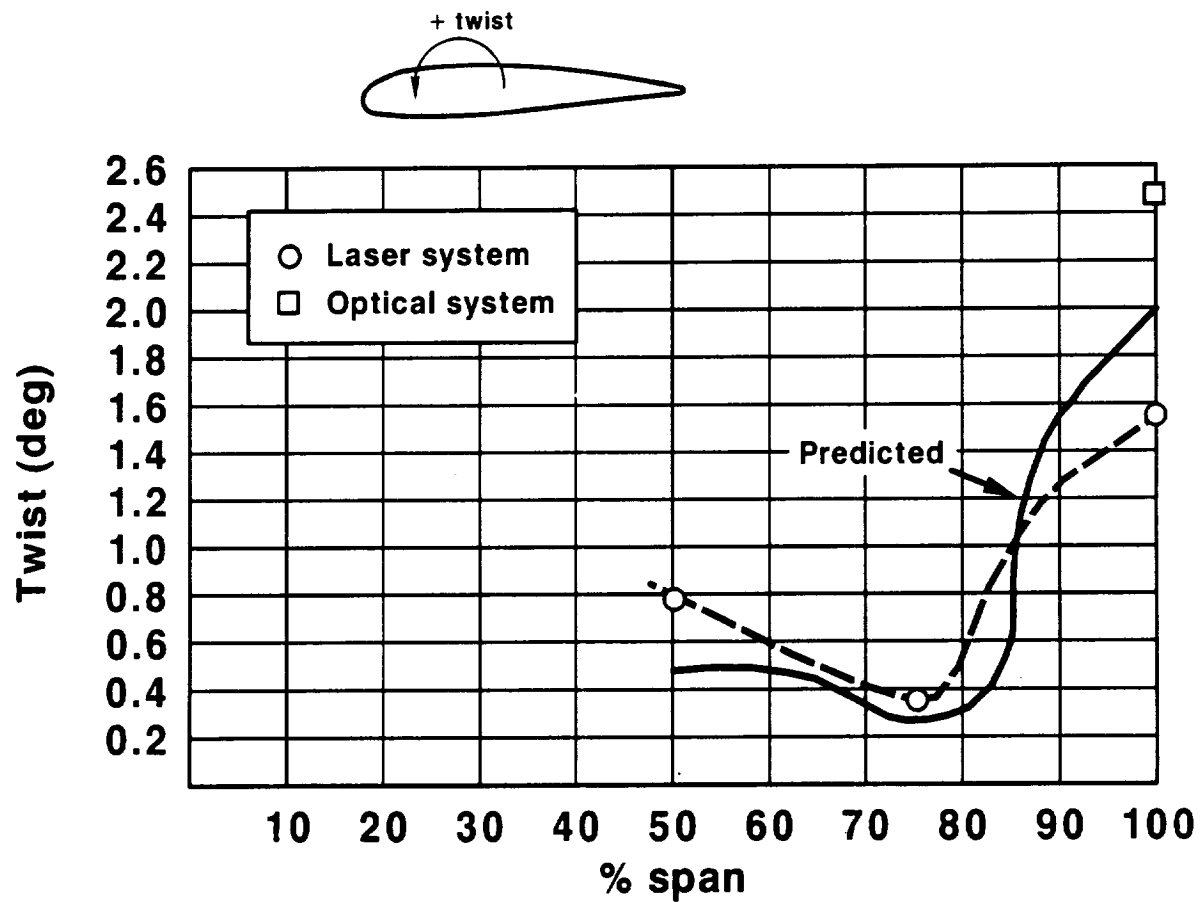
FIGURE 8.11 COMPARISON OF MEASURED & PREDICTED BLADE TWIST DEFLECTION, β 3/4 = 32°, N = 1700 RPM

8.3.4 (Continued)

Inspection of the Prop-Fan at the completion of the test revealed the following:

- Small shell to foam delaminations present in two blades prior to initiation of the test did not grow during the test.

- A new small shell to foam delamination was found in one blade.

- All other hardware was in good condition.

9.0 BLADE SURFACE STEADY PRESSURE MEASUREMENT

9.1 Test Procedure

The purpose of steady surface pressure testing was to determine the pressure distribution around airfoil sections at ten spanwise stations on the SR-7L blade. The pressure distribution was measured over a range of rotational speeds for blade angles of 21.7°, 32° and 38.3°. These blade angles were chosen to aid in the investigation of the stall buffet phenomenon, discussed in section 7.0 of this report and the corresponding reduction and leveling off of thrust with increasing blade angle, discussed in section 6.0. This range of operating conditions allowed surface pressure data to be collected before the onset of stall buffet (ß 3/4 = 21.7°), at the threshold of stall buffet (ß 3/4 = 32°) and with the stall buffet well developed (ß 3/4 = 38.3°).

The locations of the pressure taps on the specially modified blade used for steady pressure measurement are depicted in Figure 9.1. Each column of pressure taps was connected to a radial channel embedded in the surface of the blade and leading to the blade shank. Each column is connected to one channel of the scanivalve. This system required that all pressure taps be capped, except at the spanwise station at which the pressure distribution was being determined. Capping of the pressure taps was accomplished by masking the blade surface with tape at the appropriate spanwise stations. In order to measure the pressure distribution over the entire blade surface for one operating condition, ten separate runs were required.

The test procedure consisted of setting a blade angle and running the desired range of rotational speeds at that angle. Pressure data was recorded from every tap in the exposed chordwise row at each speed. The test rig was shutdown, the exposed row of taps was covered and a new row of taps was uncovered. Data was then taken at the same rotational speeds as the previous run. This procedure ensured that all of the data for a pressure map of the blade at a particular operating condition was gathered at a constant blade angle. This was critical, since the blade surface pressure distribution is sensitive to blade angle. The low pitch stop feature of the blade pitch actuator was also employed to prevent variation of the blade angle during surface pressure testing. Thrust and power were measured for each test point, to ensure that significant variations in these parameters did not occur, between test points at the same blade angle and RPM.

The pressure tap blade was installed in rotor position number one. Due to fabrication constraints for this blade, it was heavier and had a slightly thicker airfoil section than the standard SR-7L blade. A heavier blade was installed in rotor position number five to balance the pressure measurement blade. The extra weight was added to this blade by applying a thicker erosion coating to the aerodynamic surface. Due to the aforementioned changes, the Prop-Fan rotor configuration employed for steady surface pressure testing was not identical to the configuration that was evaluated during structural dynamic testing. Therefore, vibratory strain was monitored throughout testing. The strain gage arrangement used to monitor the vibratory strains was identical to the arrangement illustrated in Figure 7.1, except that the pressure measurement blade in position one was not strain gaged.

81

Camber Side

FFaceSide

			Radius Ratio
4.3°	STA 51.45	0.963	
3.0°	STA 48.78	0.917	
1.8°	STA 46.0	0.861	
0.2°	STA 42.25	0.800	
1.4°	STA 38.83		0.722
3.0°	STA 35.0		0.648
5.0°	STA 30.20		0.556
6.8°	STA 25.25		0.454
9.2°	STA 20.27	0.361	
13.0°	STA 15.5		0.287
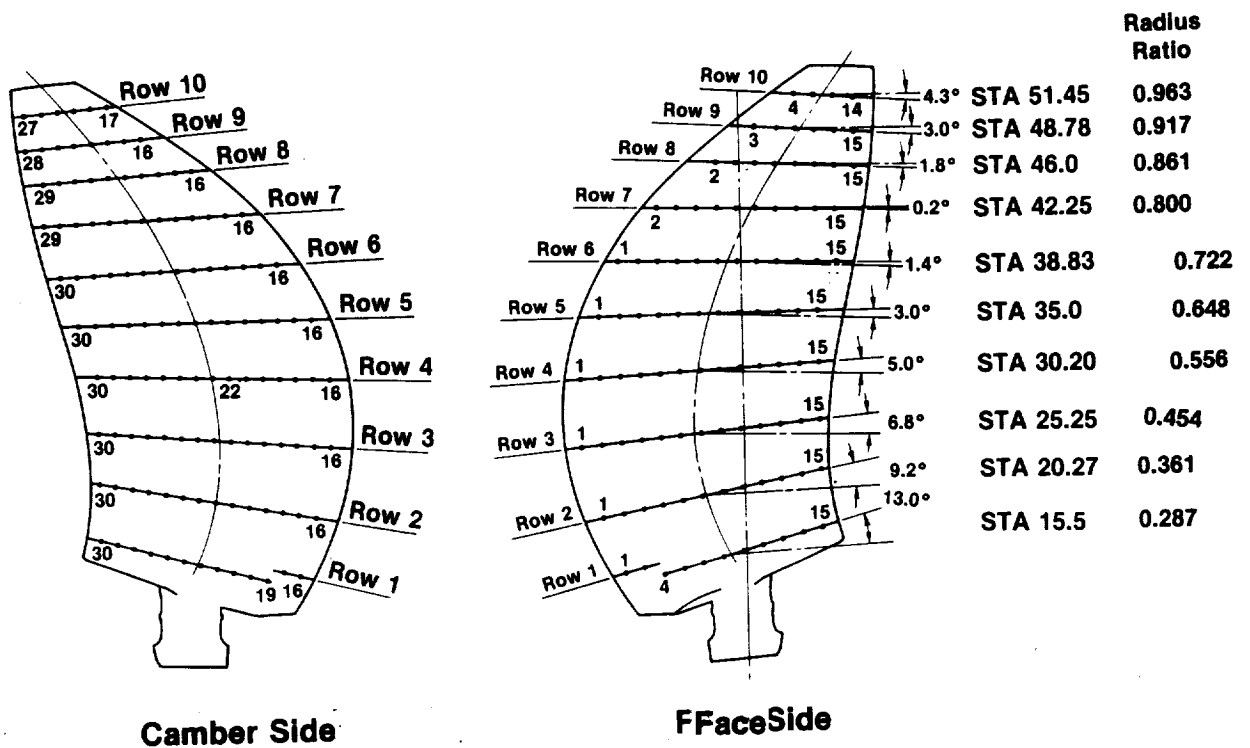
FIGURE 9.1 STEADY PRESSURE BLADE, PRESSURE TAP NUMBERING AND LOCATIONS

82

9.1 (Continued)

The Large Scale Advanced Prop-Fan is shown with the scanivalve and pressure measurement blade installed in Figure 9.2. The stationary portion of the scanivalve was secured against rotation by cables, as shown in the figure.

The steady pressure test points were run at rotational speeds corrected for ambient temperature, so that the pressure data could be compared for a constant blade surface Mach number. Test data was taken at points of constant corrected RPM. The rotational speed correction is calculated per equation 9.1. The test points at which steady pressure data was acquired are listed in Table 9.1.

$$RPM_{act} = RPM_{corr} \sqrt{\frac{273° + t_{amb}}{273° + 15°}} \qquad (9.1)$$

where:

t_{amb} = ambient temperature, °C
RPM_{corr} = corrected RPM
RPM_{act} = actual RPM at which data is taken

TABLE 9.1. STEADY PRESSURE TEST POINTS

Press. Tap Row	β 3/4	Temp (°C)	RPM_{act}
10	21.7°	18	906,1308,1508,1709,1791
9	21.7°	17	903,1305,1505,1705,1786
8	21.7°	16	902,1302,1503,1702,1783
7	21.7°	16	902,1302,1503,1703,1783
6	21.7°	15	900,1300,1500,1700,1780
5	21.7°	16	902,1302,1503,1704,1784
4	21.7°	15	900,1300,1500,1700,1780
3	21.7°	14	898,1298,1497,1697,1777
2	21.7°	13	897,1295,1495,1694,1774
1	21.7°	12	895,1293,1492,1692,1771
10	32.0°	21	909,1313,1516,1717
9	32.0°	21	909,1313,1516,1718
8	32.0°	21	909,1313,1516,1718
7	32.0°	21	909,1313,1516,1718
6	32.0°	21	909,1313,1516,1718
5	32.0°	12	895,1293,1492,1691
4	32.0°	12	895,1293,1492,1691
3	32.0°	12	895,1293,1492,1691
2	32.0°	12	895,1293,1492,1691
1	32.0°	12	895,1293,1492,1691
10	38.3°	24	914
9 thru 1	38.3°	19	906
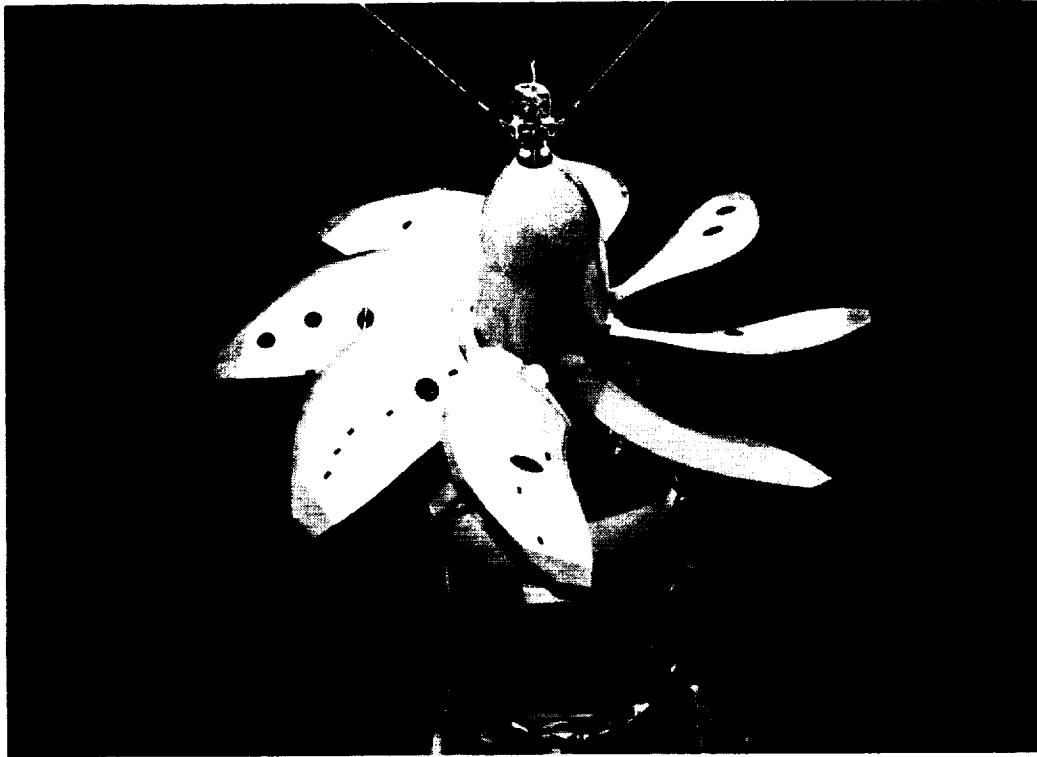
**FIGURE 9.2 SR-7L PROP FAN WITH STEADY PRESSURE BLADE
AND SCANIVALVE INSTALLED**

9.1 (Continued)

Cycling of the scanivalve between channels created pressure pulses in the system that could effect the blade surface pressure data. To alleviate this problem, a settling time of ten seconds was allowed before recording data. This provided sufficient time for the pressure pulse to damp out to a level much lower than the blade surface pressure.

9.2 Data Reduction Procedure

The blade surface pressure data was corrected for centrifugal field effects, nondimensionalized to pressure coefficient form and then plotted versus percent chord for the face and camber surfaces. The pressure coefficient data was integrated to determine the airfoil section normal force coefficient.

Centrifugal corrections to the blade surface pressure data are required because the transducer that measures the pressure is located in the scanivalve on the centerline of rotation, while the pressure taps are located at various radii on the blade surface. Therefore, due to the pressure head created by the centrifugal field, the pressure measured by the transducer is lower than the actual pressure at the tap. The variation of pressure with radius is given by equation 9.2 (reference 11)

$$dp/dr = \rho\omega^2 r \qquad (9.2)$$

where:

ρ = density of air (kg/m^3)
ω = Prop-Fan Speed (1/s)
r = radius to pressure tap (m)

Density is then expressed in terms of pressure and temperature, using the ideal gas law, and substituted into equation 9.2 to yield equation 9.3.

$$dp/dr = \frac{p\omega^2 r}{Rt} \qquad (9.3)$$

Finally, integrating from the centerline to the radial location of the pressure tap of interest, results in equation 9.4

$$p = p_T \exp\left[\frac{\omega^2 r^2}{2Rt}\right] \qquad (9.4)$$

where:

p_T = pressure measured by the transducer, Pa
t = ambient temperature, °K
R = gas constant for air, m^2/s^2 °K
p = actual pressure at tap, Pa
exp = exponential

9.2 (Continued)

The blade surface pressure coefficient was computed from equation 9.5

$$Cp_{u,\ell} = \frac{p - po}{1/2\ \rho\omega^2 r^2}$$
(9.5)

where:

Cp = pressure coefficient
p = local static pressure at tap, Pa
po = ambient static pressure, Pa
ρ = ambient density, kg/m^2
r = radius at tap, m
ω = rotational speed, 1/s
u = upper (camber) surface
ℓ = lower (face)surface

The airfoil section normal force coefficient was computed by numerical integration of the area between the face and camber surface plots of pressure coefficient versus the percent chord. The normal force is defined as the force perpendicular to the airfoil section chord line, resulting from the pressure distribution around the airfoil. The force coefficient is defined by equation 9.6.

$$C_N = \frac{Fn}{qC} = \int_0^{1.0} \frac{\Delta P}{q}\ d\left(\frac{x}{c}\right)$$
(9.6).

where:

$$\frac{\Delta P}{q} = C_{P_u} - C_{P_\ell}$$

C_{P_u} = upper (camber) surface C_P

C_{P_ℓ} = lower (face) surface C_P

C = chord, m

q = 1/2 $\rho\omega^2\ r^2$, Pa

$\frac{x}{c}$ = chordwise position

Fn = section normal force, N/m

9.2 (Continued)

In order to verify that the measured pressure distribution is accurate, the thrust measured by the test rig is compared with the approximate thrust determined by integration of the pressure acting on the blade. Figure 9.3 depicts a typical blade airfoil section. β_{local} is the angle between the section chord line and the plane of rotation of the Prop-Fan at any station. The force acting on the airfoil section is shown resolved into components normal to and coincident with the chord line. The thrust per unit blade span is then given by equation 9.7.

$$T = Fn \cos \beta_{local} - Fc \sin \beta_{local} \qquad (9.7)$$

where: T = thrust per unit blade span, N/m
$\quad\quad F_n$ = section normal force, N/m
$\quad\quad F_c$ = section chordwise force, N/m

For small values of β_{local}, it may be assumed that $Fc \sin \beta_{local}$ is much less than $Fn \cos \beta_{local}$. Therefore the thrust per unit of blade is approximated by equation 9.8.

$$T = Fn \cos \beta_{local} \qquad (9.8)$$

Fn is calculated from the experimentally determined normal force coefficient by equation 9.9.

$$Fn = 1/2 \, \rho\omega^2 \, r^2 \, Cn \, C \qquad (9.9)$$

The thrust is then computed by numerically integrating the thrust per unit span from the blade root to the tip and multiplying by 8, the number of blades.

9.3 RESULTS AND DISCUSSION

The blade surface pressure data obtained was generally well behaved. The shape of the curves of pressure coefficient versus percent chord was reasonable for all of the blade stations at which the data was taken. No significant time dependent variation of surface pressure was noted at the pressure taps located on the face surface of the blades, however unsteady surface pressure behavior was noted at several of the taps on the camber surface of the blade. When the pressure data was plotted versus percent chord, the fluctuation of surface pressure with time caused a few of the points to be inconsistent with the majority of the data. These points were deleted prior to drawing the pressure coefficient distribution curves. All of the pressure coefficient data are tabulated in Appendix II.

Figures 9.4 through 9.13 present the variation of the chordwise pressure coefficient distribution with blade angle for each of the ten blade stations at which data was taken. The data was collected at a rotational speed of 900 RPM and at blade angle of 21.7°, 32° and 38.3 degrees. At some of the outboard stations there were no pressure taps closer than 10% of the chord to the leading edge. Therefore the shape of the pressure coefficient curve in the vicinity of the leading edge was extrapolated, guided by the requirement that the pressure coefficient must equal unity at the stagnation point.
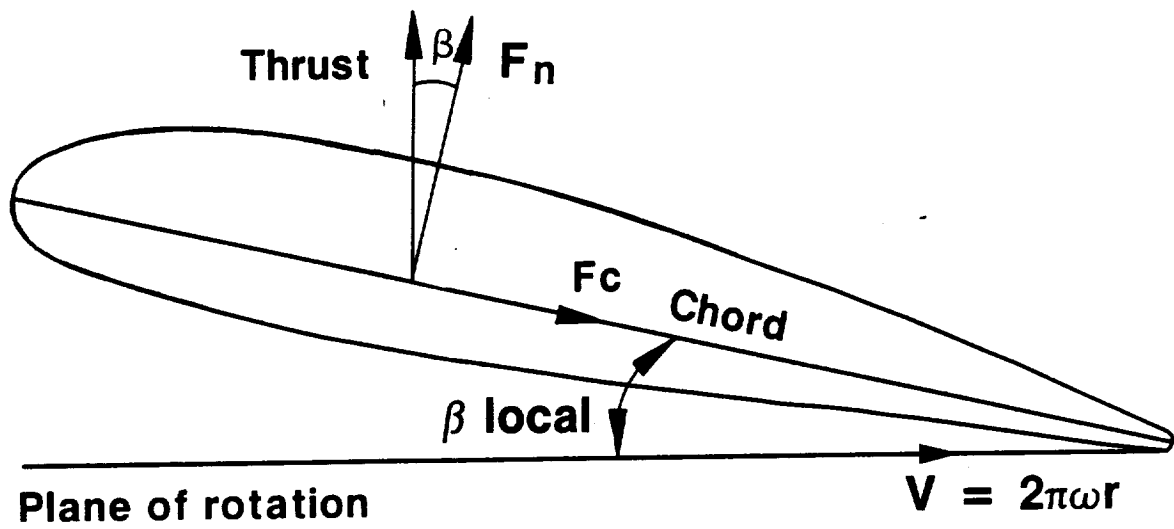
FIGURE 9.3 RESOLUTION OF NORMAL AND CHORDWISE FORCE INTO THRUST
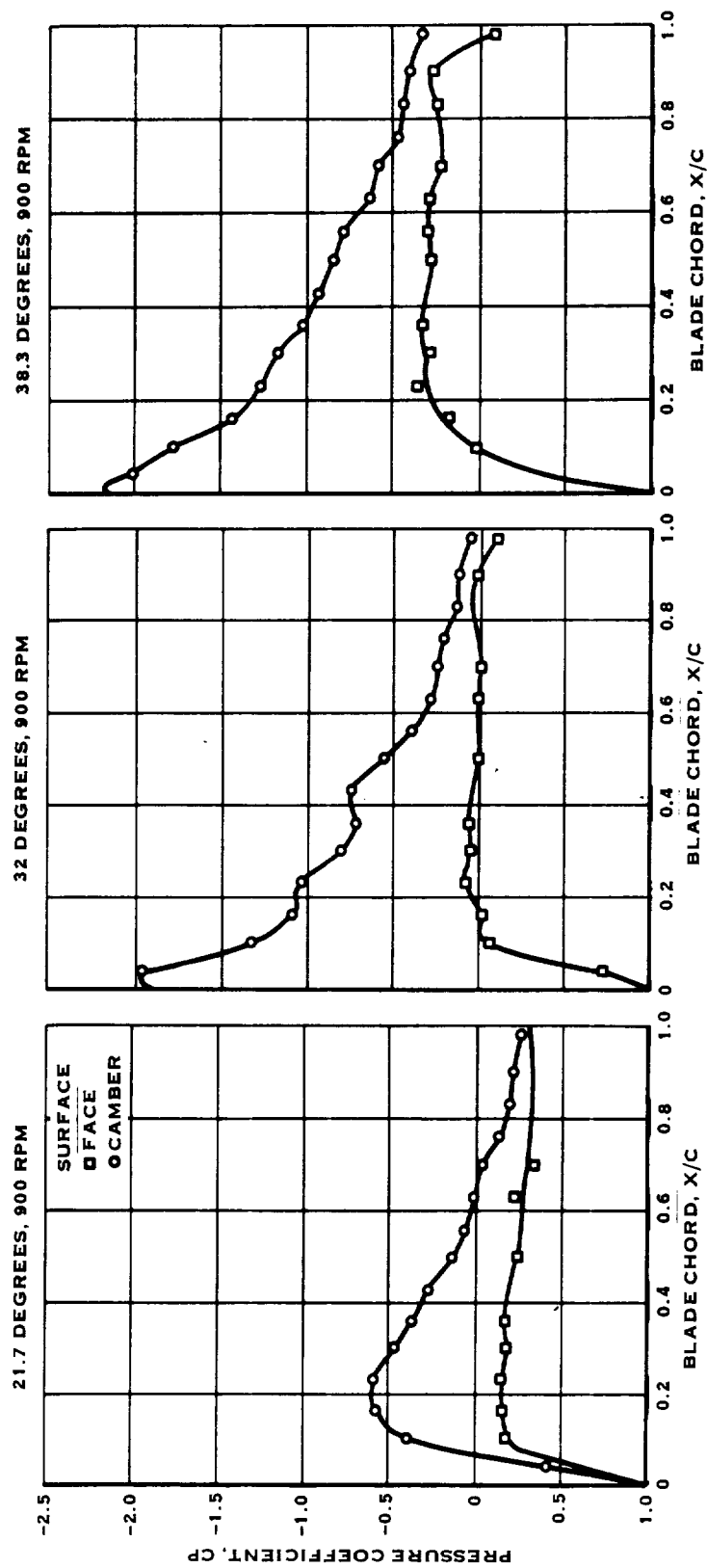
FIGURE 9.4 SR-7 PRESSURE DISTRIBUTION, r/R = 0.287
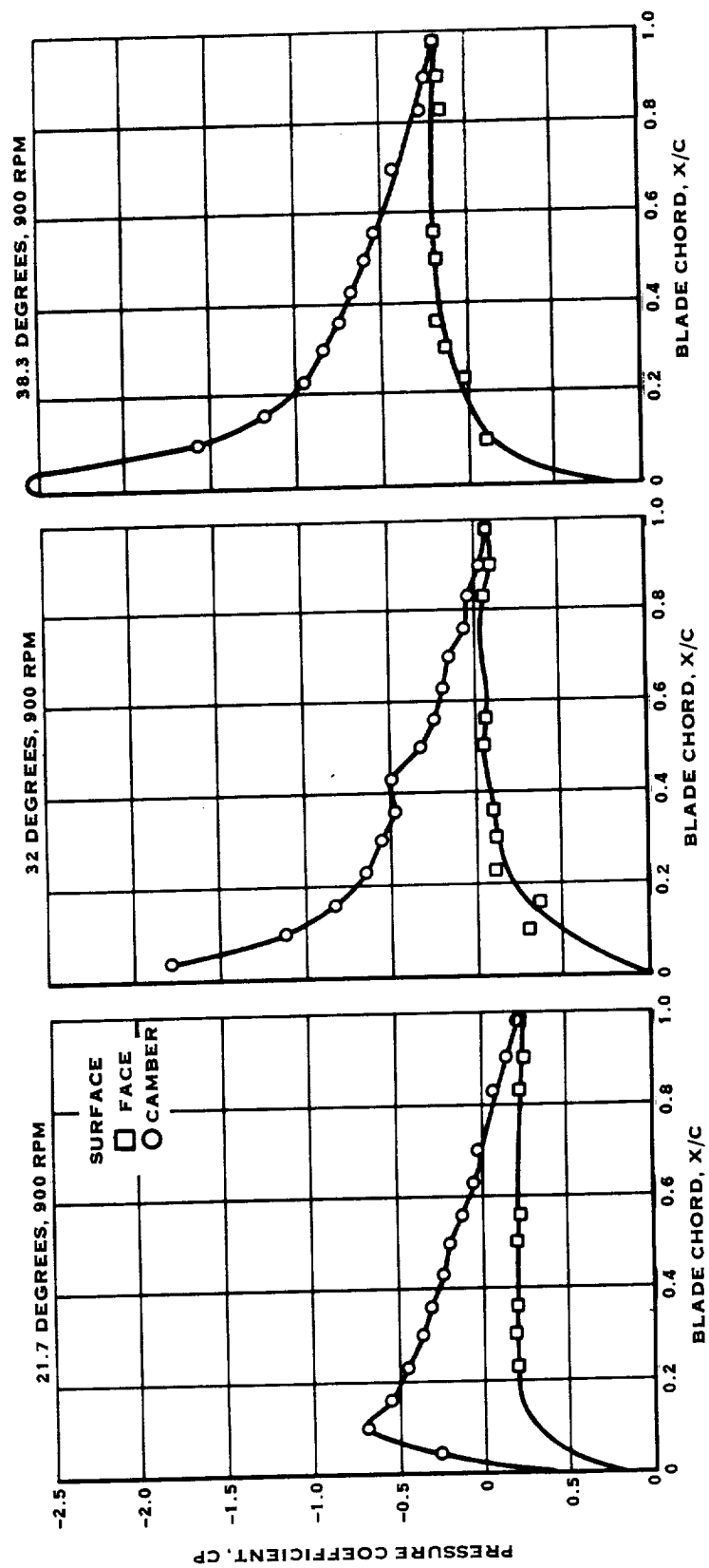
FIGURE 9.5 SR-7 PRESSURE DISTRIBUTION, r/R = 0.361
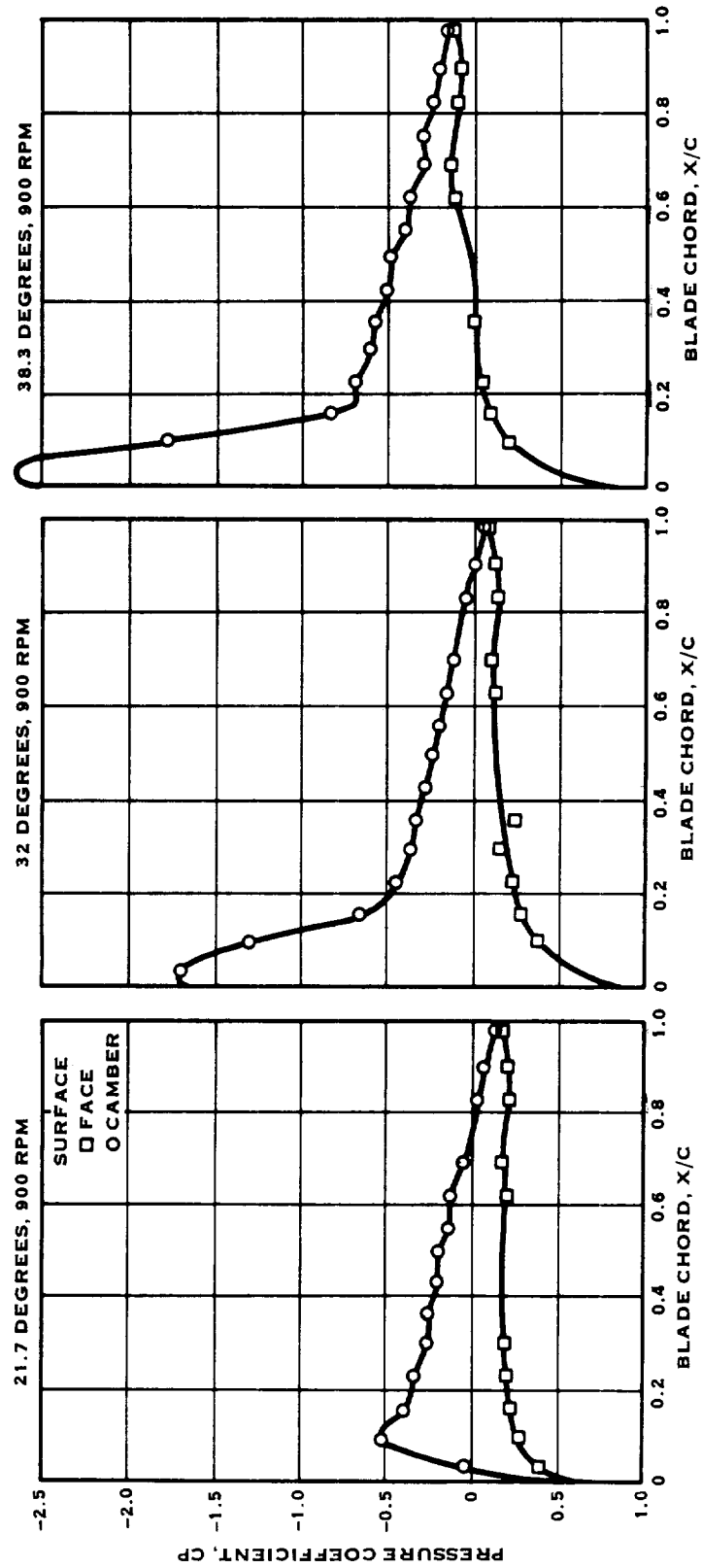
FIGURE 9.6 SR-7 PRESSURE DISTRIBUTION, r/R = 0.454

91
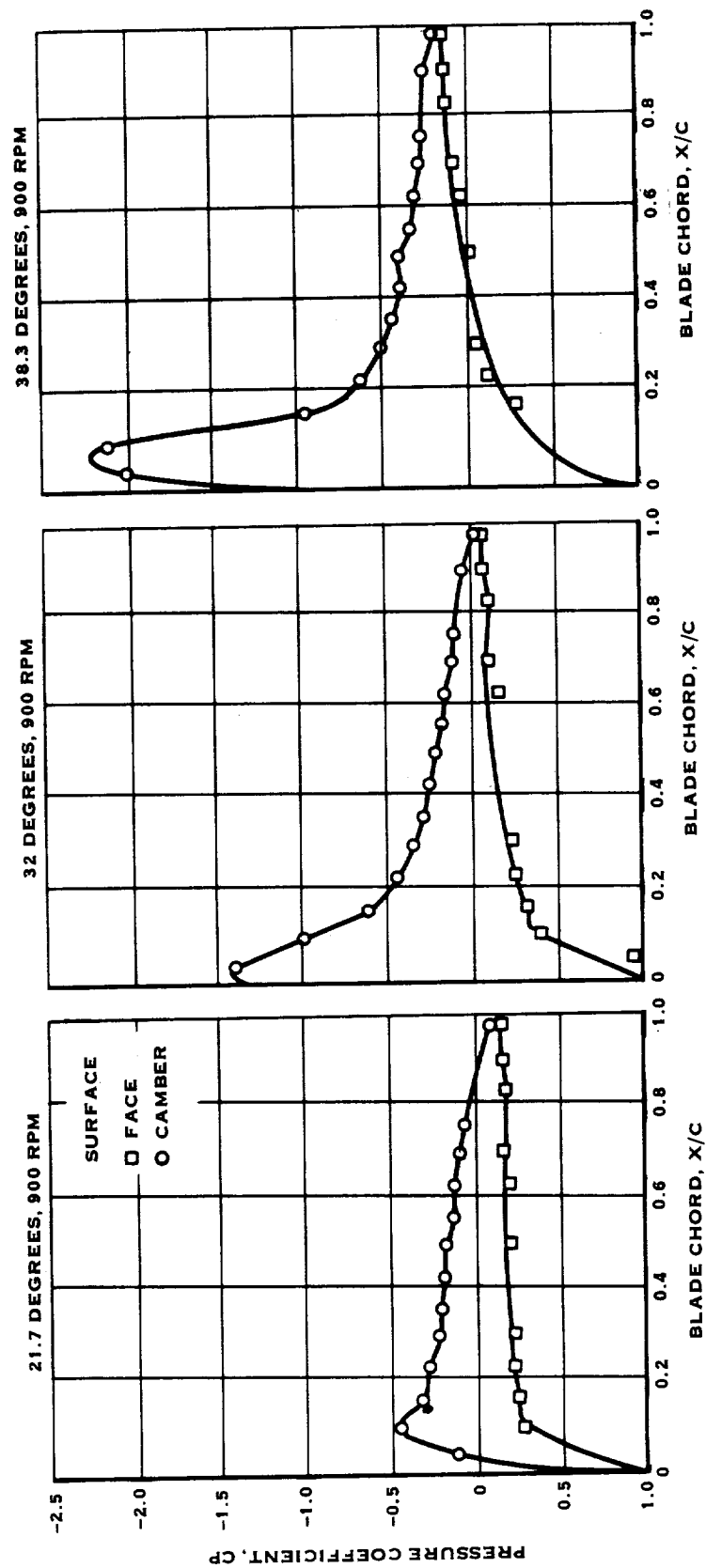
FIGURE 9.7 SR-7 PRESSURE DISTRIBUTION, r/R = 0.556
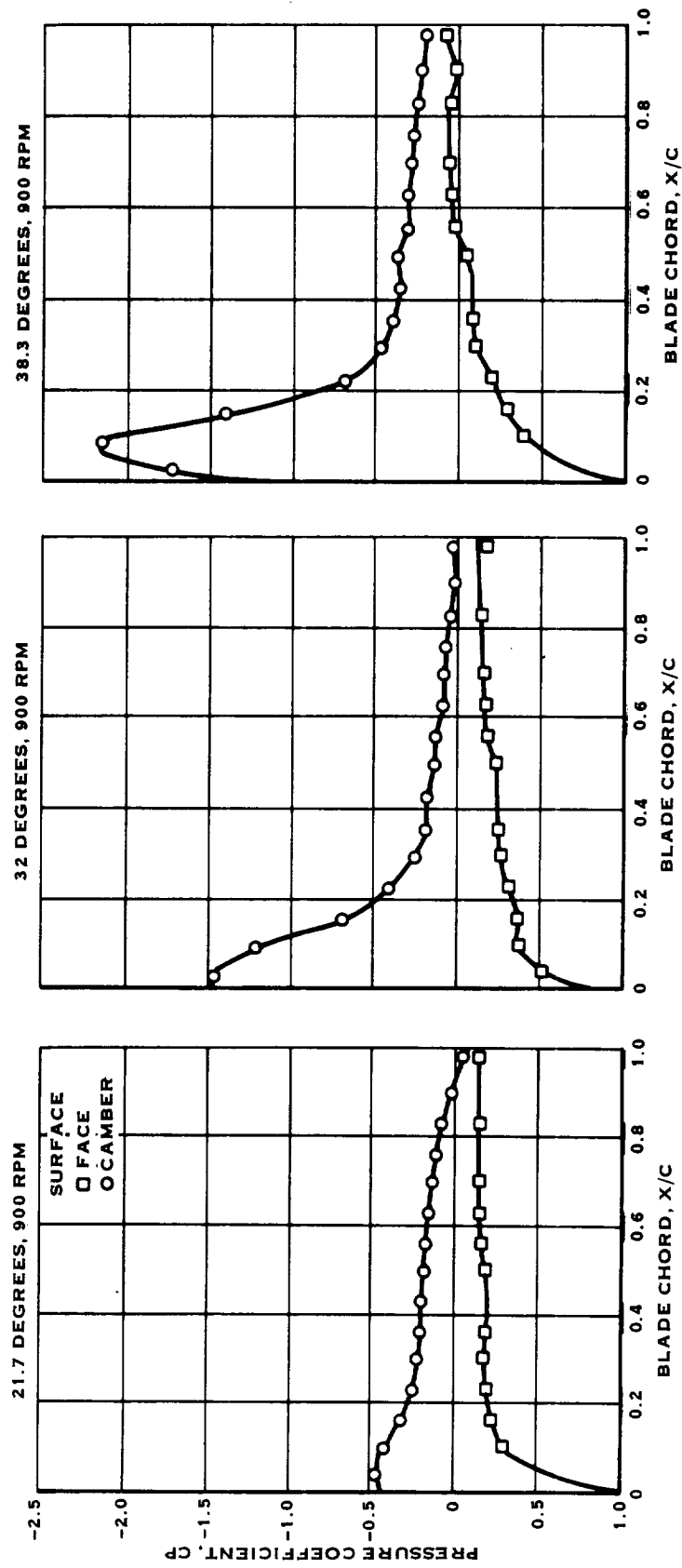
FIGURE 9.8 SR-7 PRESSURE DISTRIBUTION, r/R = 0.648
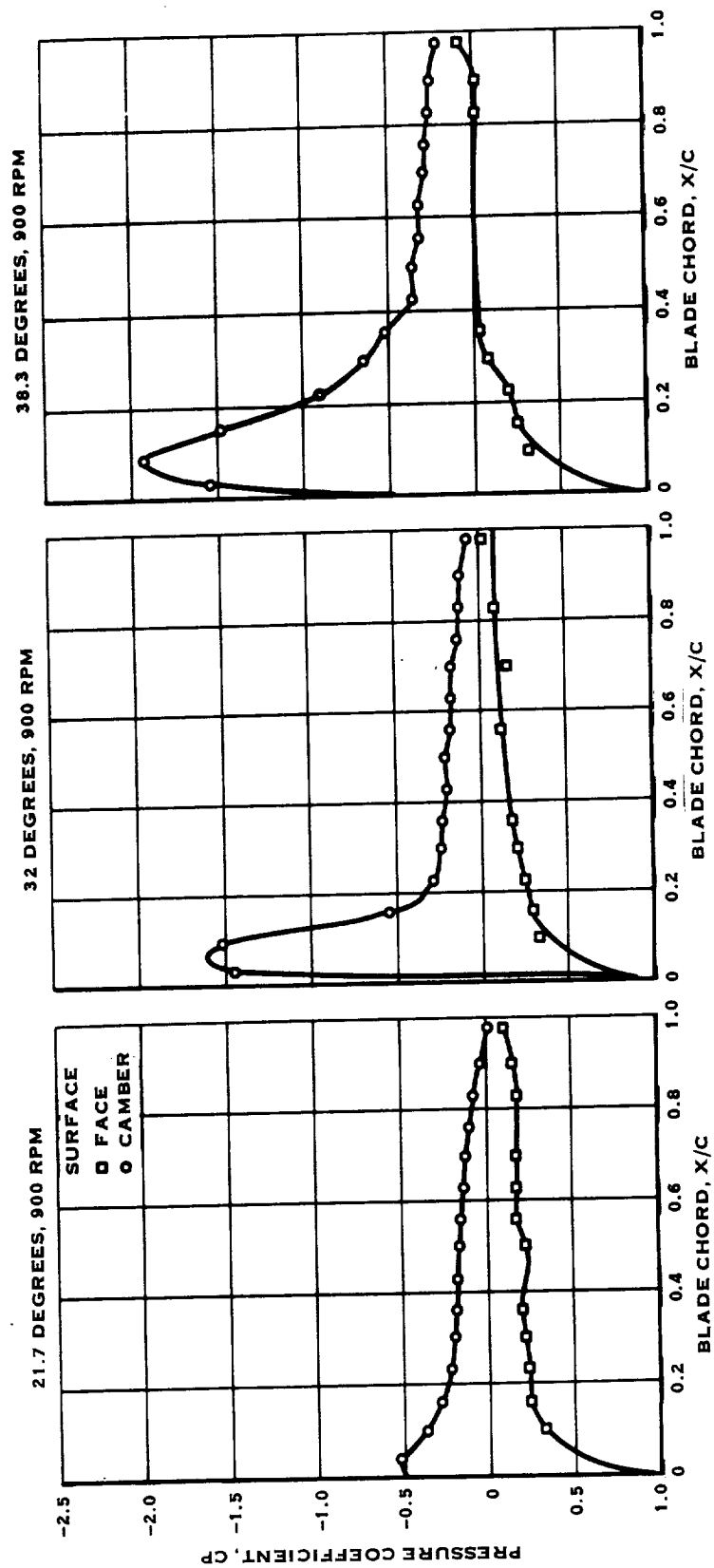
FIGURE 9.9 SR-7 PRESSURE DISTRIBUTION, r/R = 0.722
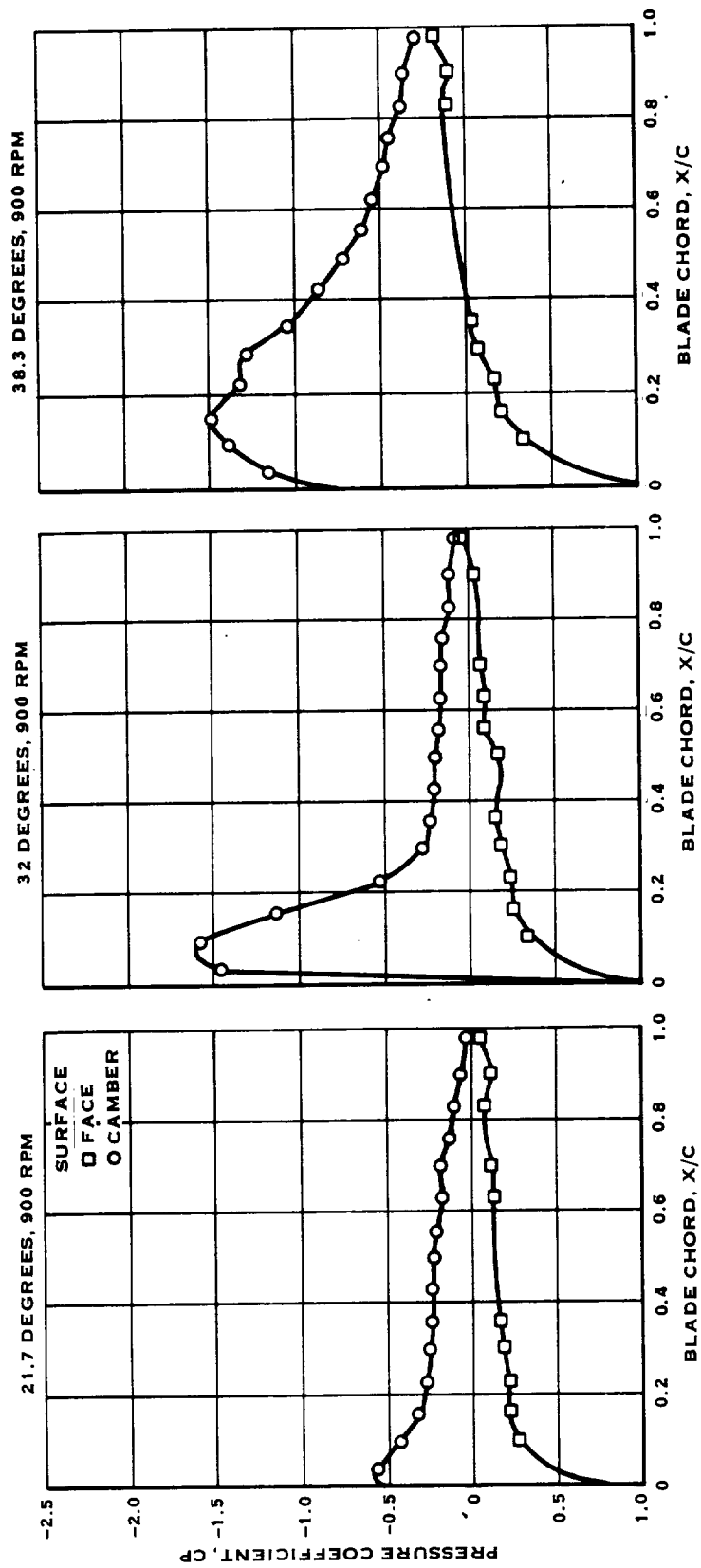
FIGURE 9.10 SR-7 PRESSURE DISTRIBUTION, r/R = 0.800
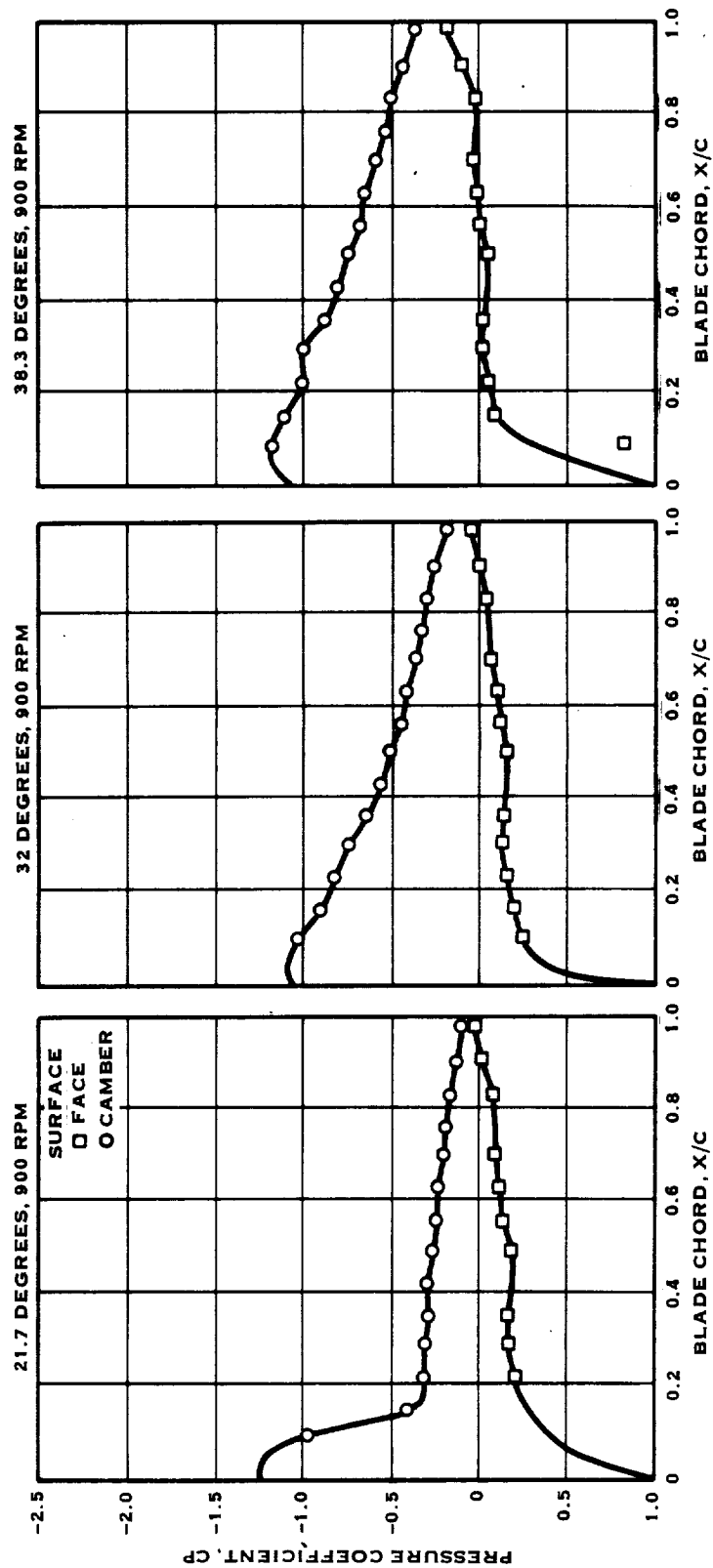
FIGURE 9.11 SR-7 PRESSURE DISTRIBUTION, r/R = 0.861
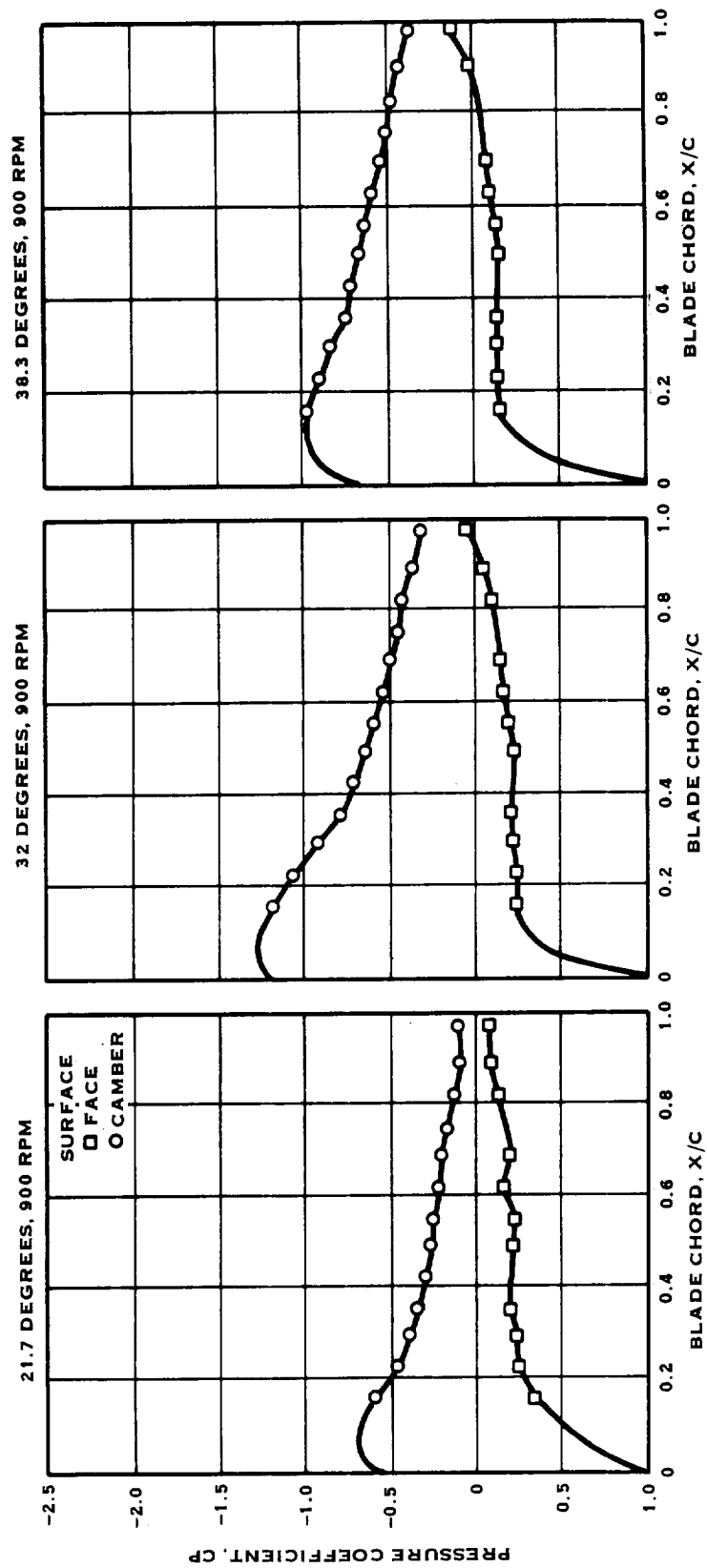
FIGURE 9.12 SR-7 PRESSURE DISTRIBUTION, r/R = 0.917
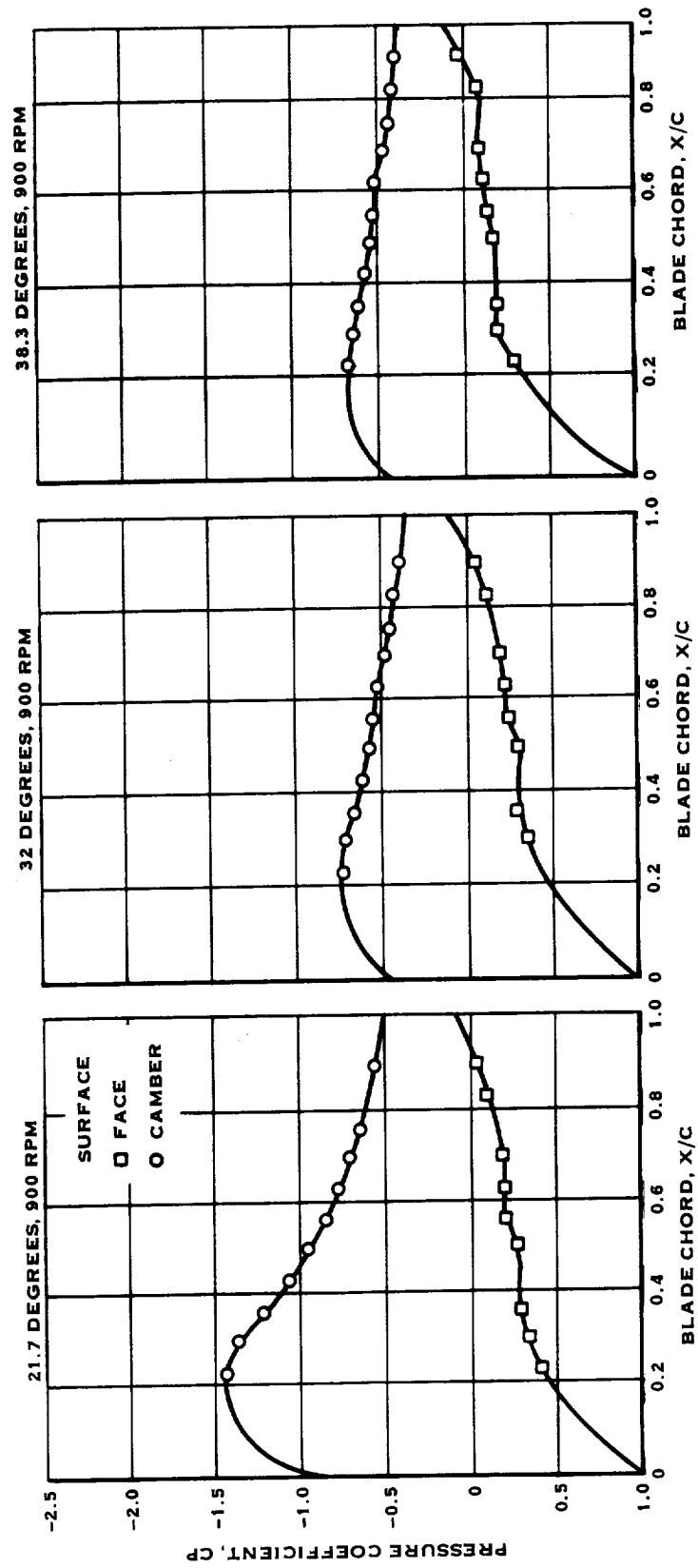
FIGURE 9.13 SR-7 PRESSURE DISTRIBUTION, r/R = 0.963

9.3 (Continued)

The variation of blade surface pressure distribution with blade angle indicates why measured thrust begins to fall short of predicted thrust for blade angles greater than 32°, as discussed in section 6.0. Data presented in Figure 9.4 for the inboard most station (r/R = .287) shows that the area between the face and camber side pressure distribution curves increases continuously as blade angle is varied from 22° to 38°. This implies that the airfoil section normal force coefficient increases continuously with blade angle from 22° to 38° at the inboard sections of the blade. Data presented in Figure 9.13 for the outboard most blade section, at which data was collected (r/R = .961), reveals that the area between the face and camber side pressure distribution curves decreases steadily, as blade angle is increased from 22° to 38°, implying that the section normal force coefficient also decreases continuously.

Figure 9.14 shows the distribution of the section normal force coefficient versus percent span on the blade for 900 RPM and a range of blade angles. The normal force coefficient was determined by integration of the pressure distribution data as described in section 9.2. For a blade angle of 22° a sharp rise in section normal force coefficient is noted near the tip of the blade (.93 < r/R < 1.0). For blade angles of 32° and 38° a decrease in normal force coefficient is noted in the tip region. Since thrust does not increase as the blade angle advances beyond 30°, it is concluded that the increase in loading in the inboard portion of the blade is being offset by the decrease in loading of the blade tip. The normal force coefficient distribution for 1300 RPM and a 32° blade angle is also compared to the 32° blade angle data taken at 900 RPM. This comparison shows minor variation of the section normal force coefficient with RPM as would be expected.

Figure 9.15 shows the variation of the SR-7L blade loading with span as determined from the normal force coefficient data for a 22° blade angle. Integration of the area under this curve yields a thrust of 6476N (1456 lb$_f$) as compared to the 7495N (1685 lb$_f$) thrust determined by the test rig thrust measurement system.

The calculated SR-7L blade loading distribution is overlayed on the experimentally determined distribution in Figure 9.16 for 900 RPM and a 22° blade angle. Comparison of these curves shows that the analytical technique predicts a higher loading inboard and lower loading outboard than was measured.

The analytical tools used to design the SR-7L Prop-Fan blade do not predict the sudden increase in section normal force coefficient in the vicinity of the blade tip which is illustrated in Figure 9.14 for a blade angle of 22°. The large spanwise gradient in section normal force coefficient suggests that it is the result of a very localized phenomenon. One explanation could be the generation of vortex lift at the blade tip. This may be caused by the same type of vortex flow, found on swept wing aircraft, occurring on the Prop-Fan Blades.
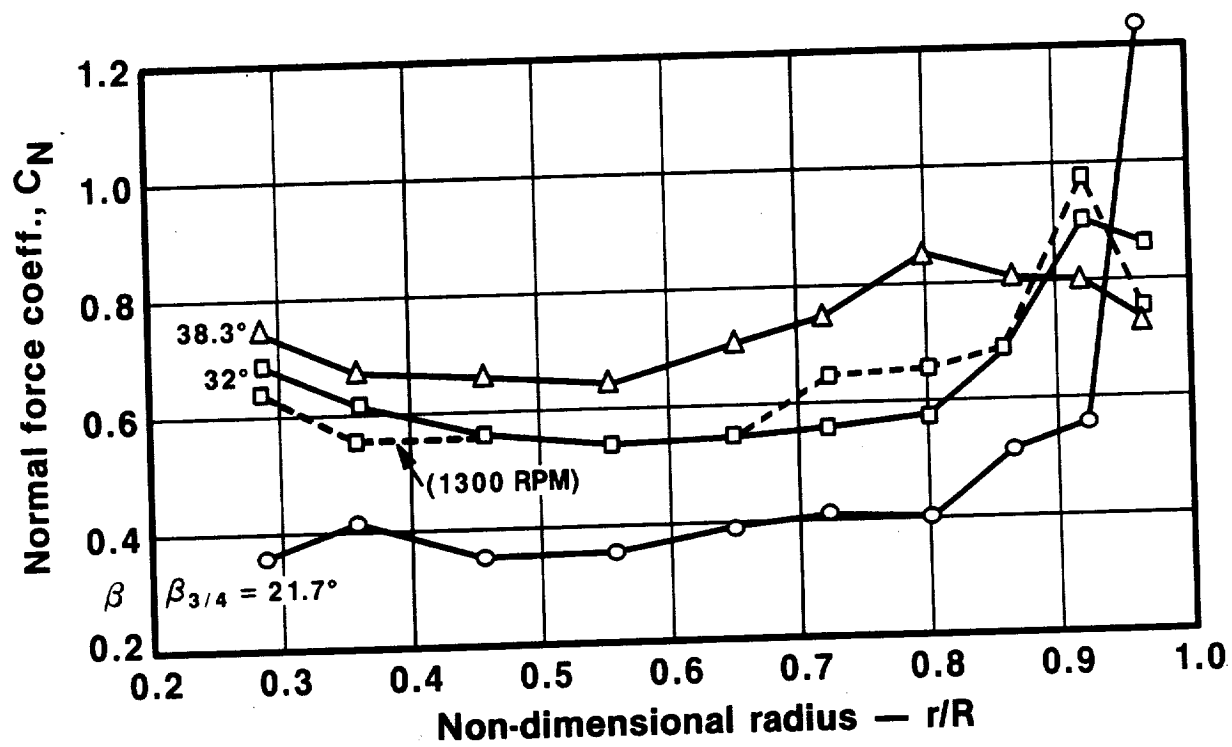
FIGURE 9.14 SR-7L BLADE NORMAL FORCE COEFFICIENT VS. RADIUS RATIO,
$RPM_{CORR} = 900$
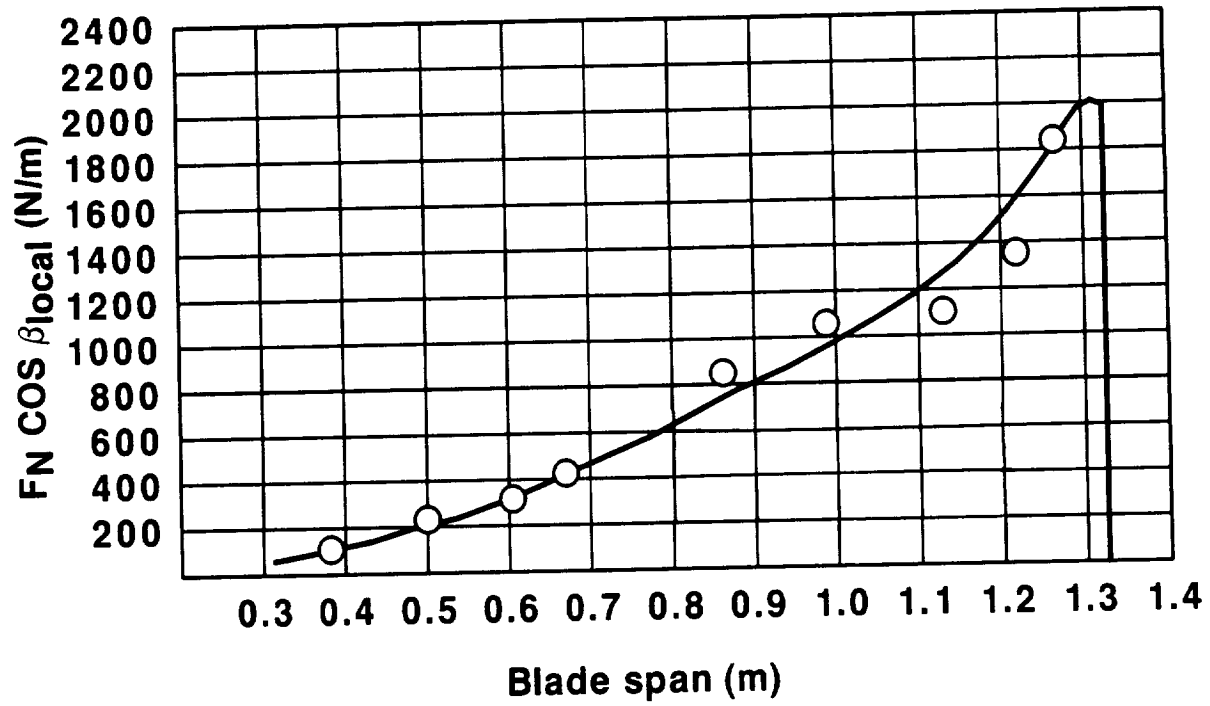
FIGURE 9.15 $F_N \cos \beta_{LOCAL}$ VS. BLADE SPAN, $\beta_{3/4} = 22°$, RPM$_{CORR}$ = 900, THRUST = 6476N
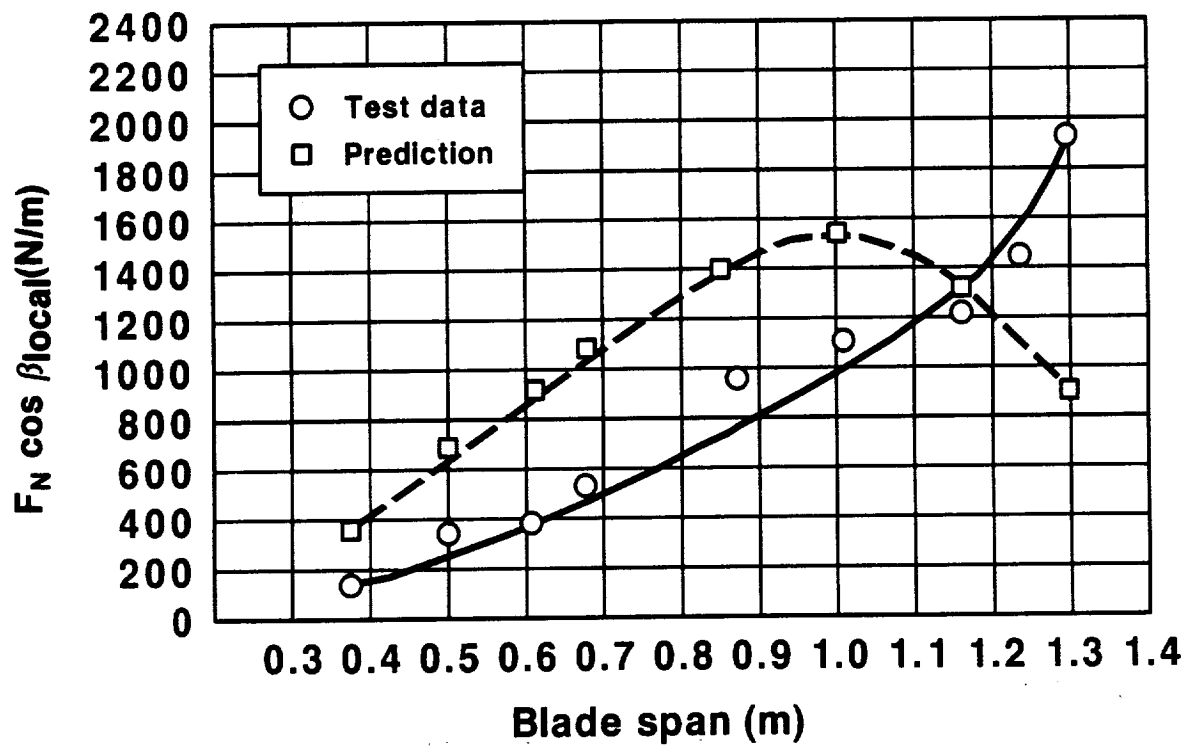
FIGURE 9.16 COMPARISON OF MEASURED AND PREDICTED BLADE LOADING, $\beta_{3/4} = 22°$, RPM CORR 900.

9.3 (Continued)

The vortex lift can be generated in two ways. A vortex sheet may separate
at the leading edge of the blade and become reattached on the suction sur-
face. The vortex reduces the pressure on the suction surface, thus increas-
ing lift. A similar flow pattern can occur along the tip edge of the blade.
The reduction of the blade loading to zero at the tip causes radial flow
that is outward on the blade pressure surface and inward on the blade suc-
tion surface. Flow going around the tip may separate causing the same type
of vortex to form on the blade suction surface (Reference 12).

For static operation it is hypothesized that as the blade angle, (β 3/4) is
increased beyond 30°, the suction surface vortex breaks down and the addi-
tional lift that it contributes at the tip is lost. The breakdown of the
vortex could also generate turbulence which may be the exciting force for
the blade buffet discussed in section 7.0 of this report.

10.0 BLADE SURFACE UNSTEADY PRESSURE TESTING

10.1 Test Procedure

The primary purpose of unsteady pressure testing was to evaluate the capability of transducers installed on the SR-7L blade to measure time varying pressures on both the face and camber side surfaces of the blades. If the transducers demonstrated sufficient accuracy and sensitivity, the unsteady pressure data could also be correlated with the blade structural dynamic behavior discussed in section 7.0. The impetus for developing the ability to monitor unsteady blade surface pressures was the wind tunnel and flight testing planned as a follow on to the Static Rotor Test. Operation of the Prop-Fan at a yaw angle relative to the flow was included in the agenda for the High Speed Wind Tunnel test. Operation at a yaw angle results in a continuous variation of the angle of attack seen by the blade as it rotates through 360°. This yields a 1P cylical variation of the surface pressure. Flight testing of the Large Scale Advanced Prop-Fan during the Prop-Fan Test Assessment Program, will also involve yawed and pitched flight attitudes. The proximity of the Prop-Fan to the aircraft wing and engine inlet also gives rise to a twice per revolution aerodynamic disturbance, resulting in a time dependent variation of the blade surface pressure,

Twenty six pressure transducers were installed in two rows on the face and camber sides of the blade, that was specially fabricated for unsteady pressure testing. The location of the transducers is shown in Figure 10.1. The unsteady pressure measurement blade is shown in Figure 10.2. The pressure transducers were mounted flush with the airfoil surface. The sensor and excitation wires from each transducer were embedded in the blade surface and run to attenuating resistors located on the surface of the blade root airfoil section. The function of the attenuating resistors was to establish the pressure signal gain for each of the transducers. The wires were then connected to signal conditioning electronics located inside the blade cuff.

The dynamic pressure range for the transducers used in the unsteady pressure measurement blade was $\pm$ 15 psi. The frequency response of the system was 0 to 1000 Hz. Prior to the Static Rotor Test an evaluation program was conducted to determine the sensitivity of the transducers to temperature, strain vibration and a centrifugal field. The results of this program indicated a maximum 2% error due to temperature in the range of 0 to 130°F and a maximum 0.92% error due to all other factors.

The unsteady pressure measurement blade was installed in position number six of the rotor. A counter-balance blade was installed in position number two to compensate for the slightly higher weight of the unsteady pressure blade as compared to the standard SR-7L blade. The pressure signals were transmitted from the rotary to the stationary field through the electronic data acquisition system. Strain gage 415 (reference Figure 7.1) was employed to monitor blade vibration. The unsteady pressure signals were recorded using the Honeywell 101 IRIG tape recorder. Real time monitoring of the unsteady pressure signals was accomplished using the four channel oscilloscope.

PRECEDING PAGE BLANK NOT FILMED

PAGE 104 INTENTIONALLY ...

Camber Side **Face Side**

STA 49
3.1° (r/R = 0.921)

STA 35
3° (r/R = 0.648)
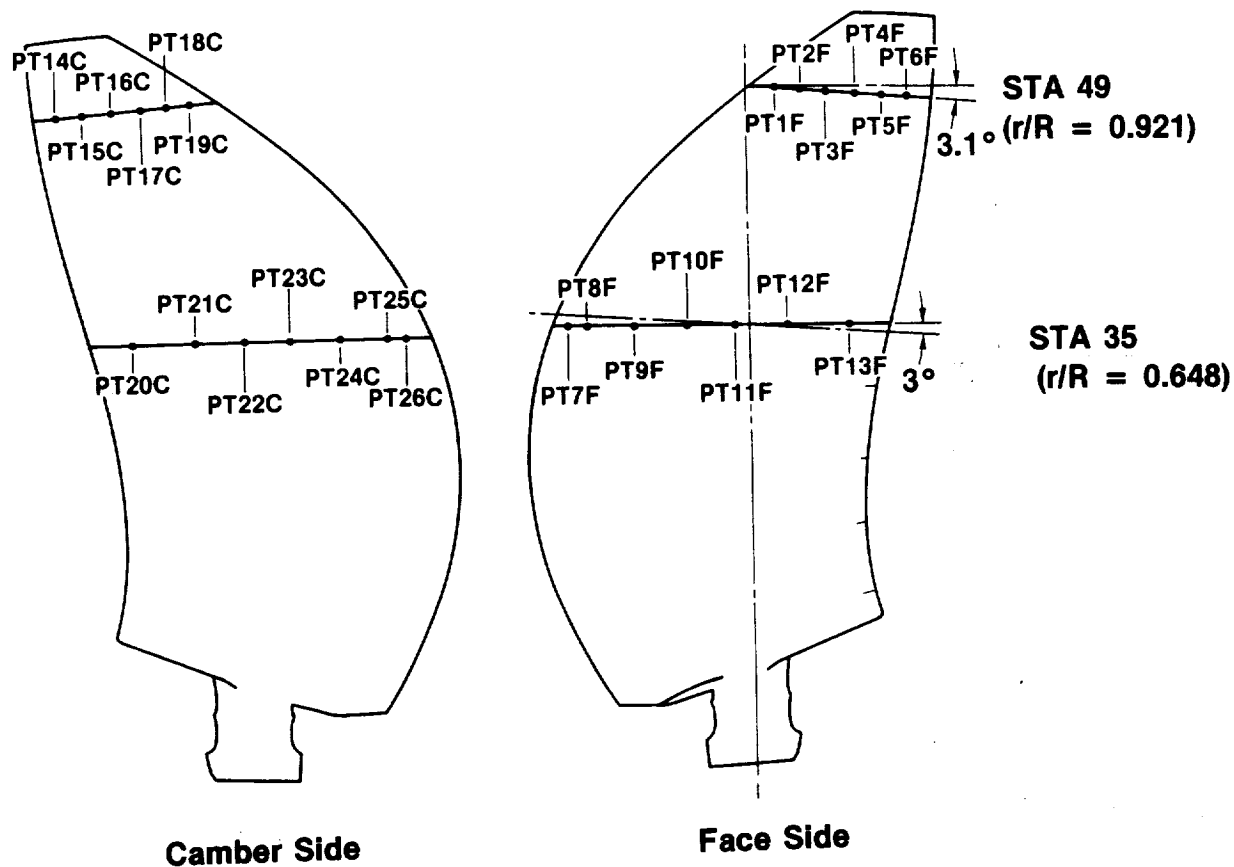
Locations — % Chord

PT1F & PT19C	16.58
PT2F & PT18C	29.85
PT3F & PT17C	43.11
PT4F & PT16C	56.38
PT5F & PT15C	69.64
PT6F & PT14C	89.54
PT7F & PT26C	4.93
PT8F & PT25C	10.00
PT9F & PT24C	23.33
PT10F & PT23C	36.66
PT11F & PT22C	49.99
PT12F & PT21C	63.32
PT13F & PT20C	83.33

FIGURE 10.1 UNSTEADY PRESSURE BLADE, TRANSDUCER LOCATIONS

106
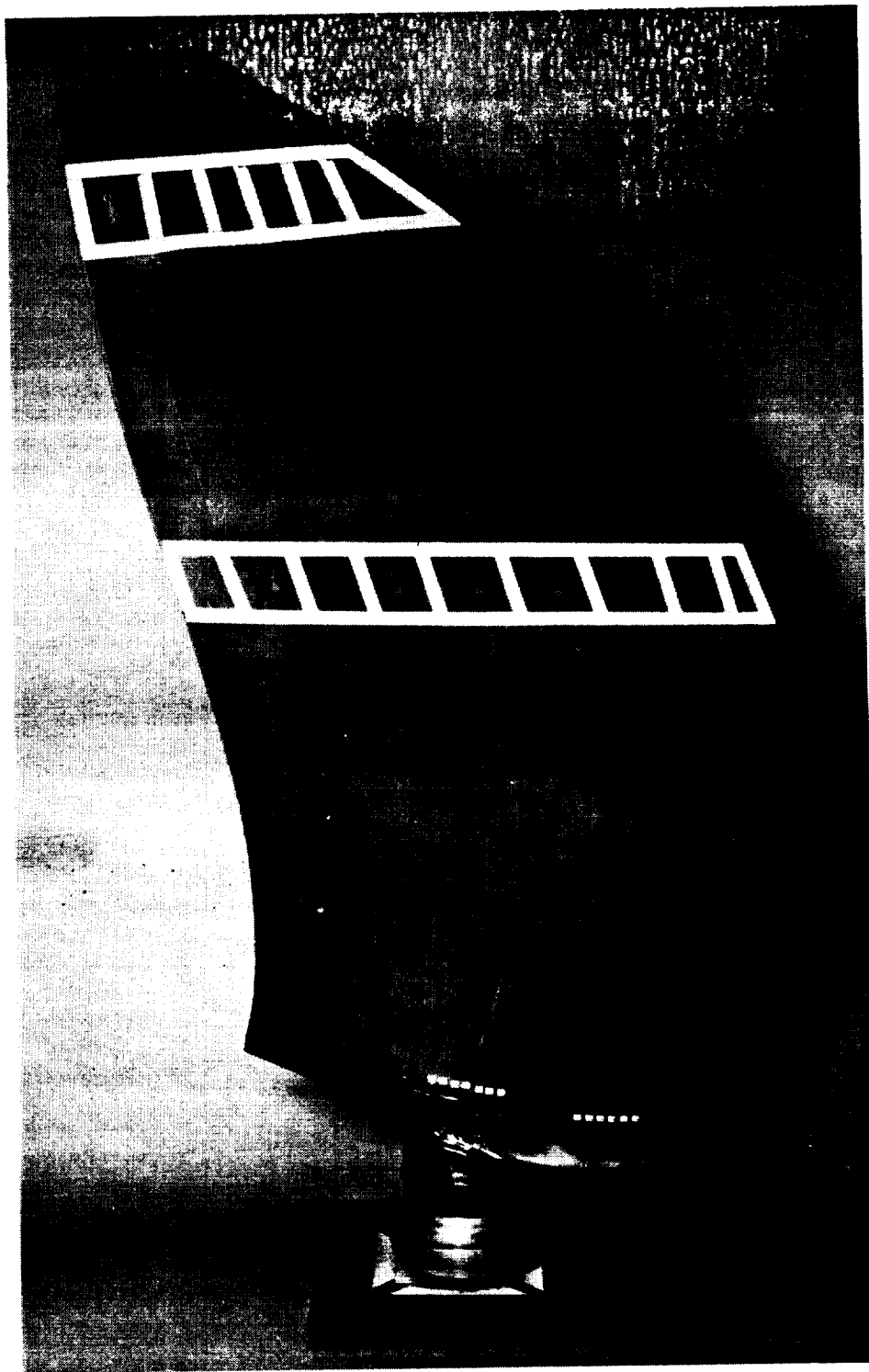
FIGURE 10.2 UNSTEADY PRESSURE BLADE

10.1 (Continued)

In order to produce a time variation of the pressure sensed by the transducers during a static test, an aerodynamic obstruction was erected in front of the Prop-Fan. The obstruction was a four inch diameter cylinder that spanned from the blade root to well beyond the blade tip. The centerline of the cylinder was located 24 inches in front of the blade pitch change axis. The wake generated by the inflow to the Prop-Fan, passing over the obstruction, was intended to create a once per revolution disturbance for the transducers to pass through. The Large Scale Advanced Prop-Fan is depicted with the obstruction in place in Figure 10.3.

Data from the pressure transducers was recorded at each Prop-Fan operating condition both with the obstruction in place and with the obstruction removed. The desired range of rotational speeds were run at a constant blade angle without the obstruction. The obstruction was then put in place and the same corrected speeds were rerun. The blade angle was then increased and the procedure repeated. The rotational speeds for data points were specified as RPM corrected for ambient temperature. This allowed pressure data to be compared for a constant blade surface Mach number rather than a constant propeller speed. The speed correction was calculated per equation 9.1. The test points run with the unsteady pressure measurement blade are listed in Table 10.1.

TABLE 10.1. TEST POINTS FOR UNSTEADY PRESSURE TESTING

β 3/4 (Deg.)	RPM	Temp. (°C)	Obstruction
21.9	594	9	None
21.9	891	9	None
21.9	1286	9	None
21.9	1484	9	None
21.9	1682	9	None
21.9	1880	9	None
21.9	594	9	4" diameter cylinder
21.9	891	9	4" diameter cylinder
21.9	1286	9	4" diameter cylinder
21.9	1484	9	4" diameter cylinder
21.9	1682	9	4" diameter cylinder
21.9	1880	9	4" diameter cylinder
31.7	592	8	None
31.7	887	8	None
31.7	1282	8	None
31.7	1478	8	None
31.7	1676	8	None

FIGURE 10.3 STATIC ROTOR TEST UNSTEADY PRESSURE MEASUREMENT
BLADE INSTALLED; CYLINDRICAL OBSTRUCTION IN PLACE, SECURED

TABLE 10.1.   TEST POINTS FOR UNSTEADY PRESSURE TESTING (Continued)

β 3/4 (Deg.)	RPM	Temp. (°C)	Obstruction
31.7	596	11	4" diameter cylinder
31.7	894	11	4" diameter cylinder
31.7	1291	11	4" diameter cylinder
31.7	1490	11	4" diameter cylinder
31.7	1688	11	4" diameter cylinder
38.2	596	11	None
38.2	894	11	None
38.2	1192	11	None
38.2	596	11	4" diameter cylinder
38.2	894	11	4" diameter cylinder
38.2	1192	11	4" diameter cylinder
32.0	600	15	4" cylinder with plate
32.0	900	15	4" cylinder with plate
32.0	1200	15	4" cylinder with plate
32.0	1700	15	4" cylinder with plate

10.2 Data Reduction Procedure

The unsteady pressure data was first reduced to plots of pressure versus time for a period of 80 msec, equivalent to from one to two revolutions of the Prop-Fan rotor depending on the rotational speed. A wave form averaging technique was employed so that the data presented represents an average taken over 400 revolutions of the rotor. A constant phase was maintained for the data acquired from each revolution, so that averaging enhanced data that was periodic in nature and tended to eliminate noise, due to its random nature.

Spectral analysis of unsteady pressure data was also conducted. The analysis was accomplished for data taken from each transducer at 1200 RPM, without the obstruction for blade angles of 22°, 32° and 38°. The purpose was to determine if the frequency content of the pressure signals corresponded to the frequency content of the blade vibration during the stall buffet phenomenon discussed in section 7.0. It was also desired to determine the location of the airfoil section, where the unsteady pressure amplitude first began to increase with increasing blade angle.

110

10.3 Results and Discussion

At the start of unsteady pressure testing it was determined that transducers
PT2F and PT13F were not functional. Pressure data obtained from transducer
PT7F with and without the cylindrical obstruction in place at a blade angle
of 32° is shown in Figure 10.4. Comparison of data with and without the ob-
struction did not show any indication that an aerodynamic disturbance was
sensed by the transducer. This data was typical for all of the functional
transducers on the blade. It was concluded that either the obstruction was
not generating a significant wake or the transducers were not passing through
the wake, due to a large radial component of the inflow to the Prop-Fan.
Radial inflow is typical of propeller static operation.

The aerodynamic obstruction was altered in order to generate a wake that
would be intersected by the blade stations containing the transducers. The
modification consisted of attaching plates to the cylindrical post as shown
in Figure 10.5. Tufts were also attached to the obstruction in an attempt to
visualize the inflow to the Prop-Fan passing around the obstruction. The
motion of the tufts was recorded on video tape.

When testing was resumed with the modified obstruction in place, a once per
revolution pressure pulse was detected by most of the transducers located on
blade station 35.0. The amplitude and the width of the pulses were variable
from transducer to transducer at that station. Figures 10.6 through 10.9
show plots of the surface pressure versus time at the transducer locations
where the pressure pulse was most pronounced.

The pressure pulse was not detected by any of the transducers on blade sta-
tion 49.0. A review of the videotape of the run indicated that the wake
eminating from the plate obstruction may not have been intersected by blade
station 49.0. Therefore the failure to detect the wake at that station does
not indicate a shortcoming of the instrumentation.

The transducers demonstrated the ability to detect pressure pulses of 13.80
Pascal (.2 psig) amplitude and durations of less than 10 milliseconds.
Therefore the transducer installation in the unsteady pressure measurement
blade provides sufficient sensitivity and frequency response for use in wind
tunnel or flight testing.

The spectral analyses of the pressure data taken without the obstruction in
place did not indicate any specific frequency content for the pressure data.
Instead, an increase in pressure amplitude over a broad frequency band is
noted as the blade angle is increased. If the breakdown of a tip vortex is
in fact what is exciting the blade buffet response, the transducers may not
be located far enough outboard on the blade to detect it.

111
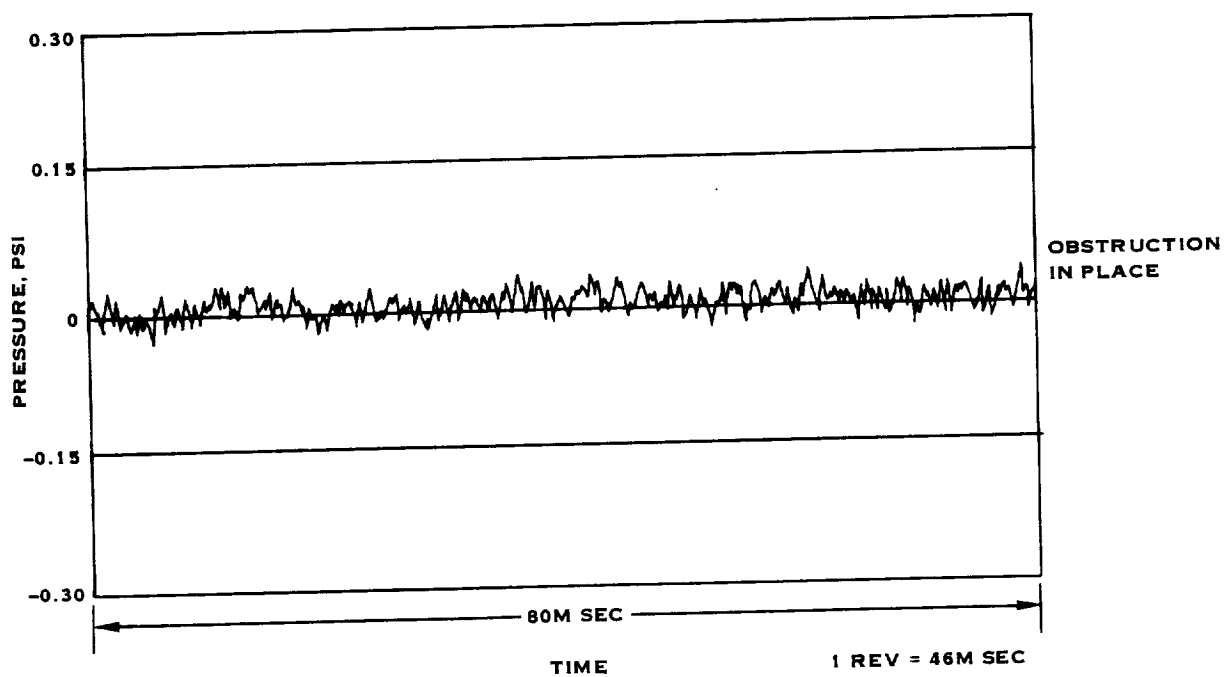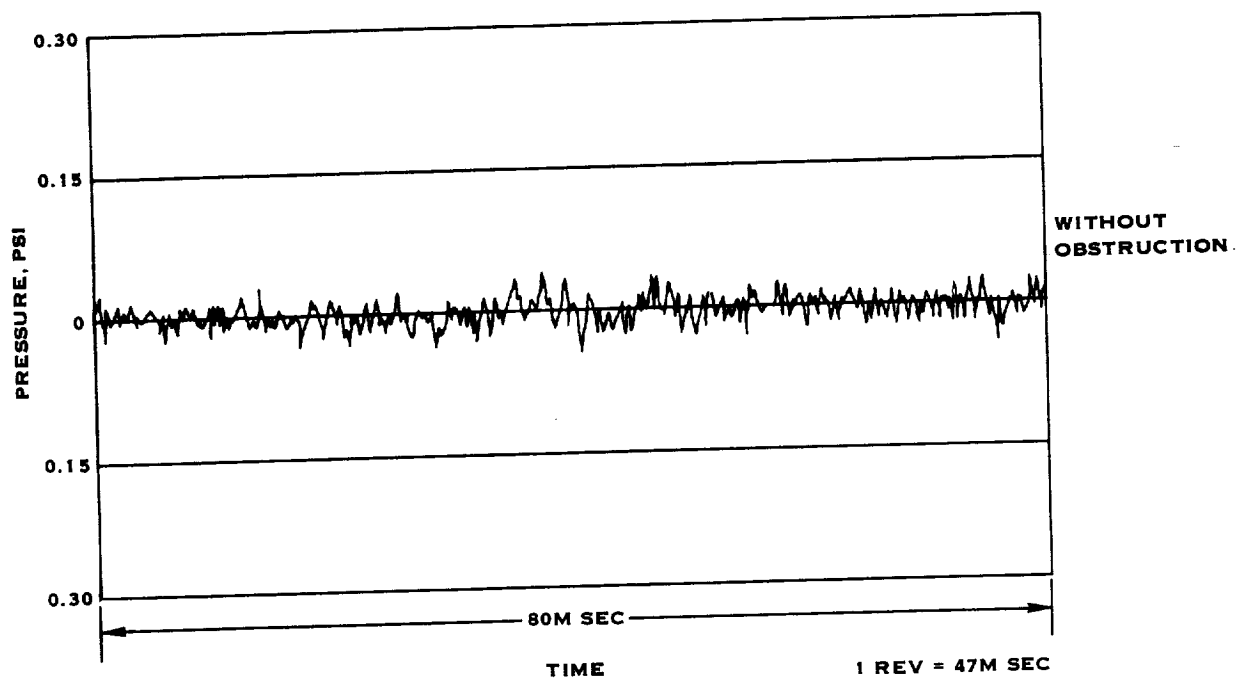
FIGURE 10.4 COMPARISON OF PRESSURE DATA WITH AND WITHOUT CYLINDRICAL OBSTRUCTION TRANSDUCER PT7F $\beta\frac{3}{4}$ = 32°, 1275 RPM

Prop-Fan
axis of
rotation

70.5"

18"

12"

18"

24"

Blade pitch
change axis
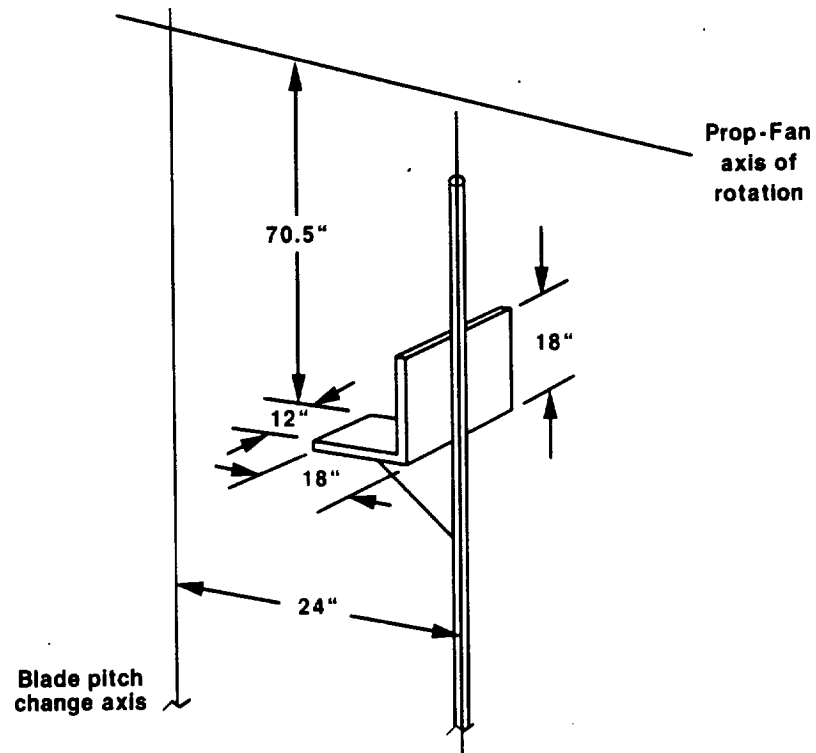
FIGURE 10.5 PLATE OBSTRUCTION

113
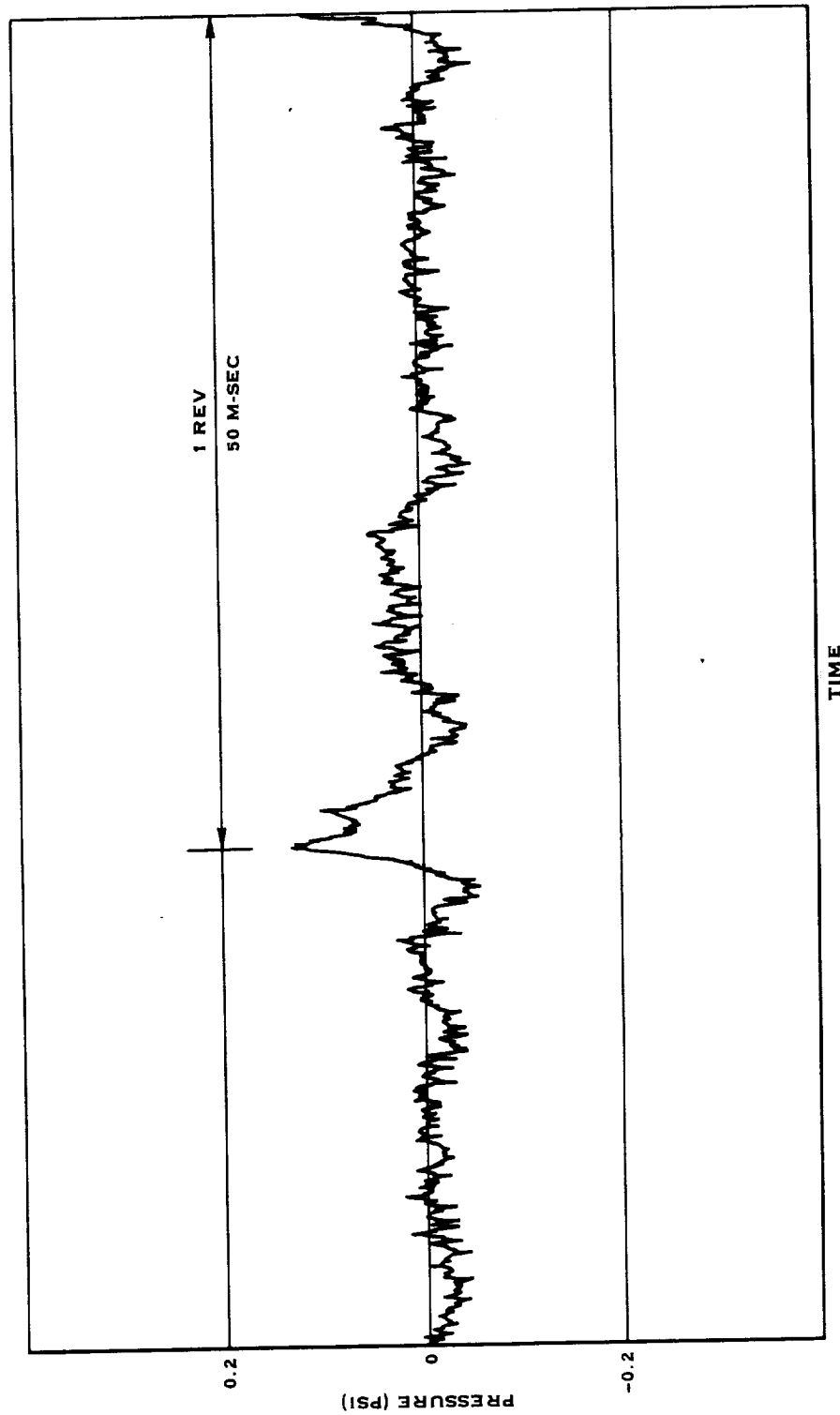
FIGURE 10.6 PRESSURE DATA, TRANSDUCER PT8F, PLATE OBSTRUCTION $\beta\frac{3}{4} = 32°$, 1200 RPM

114
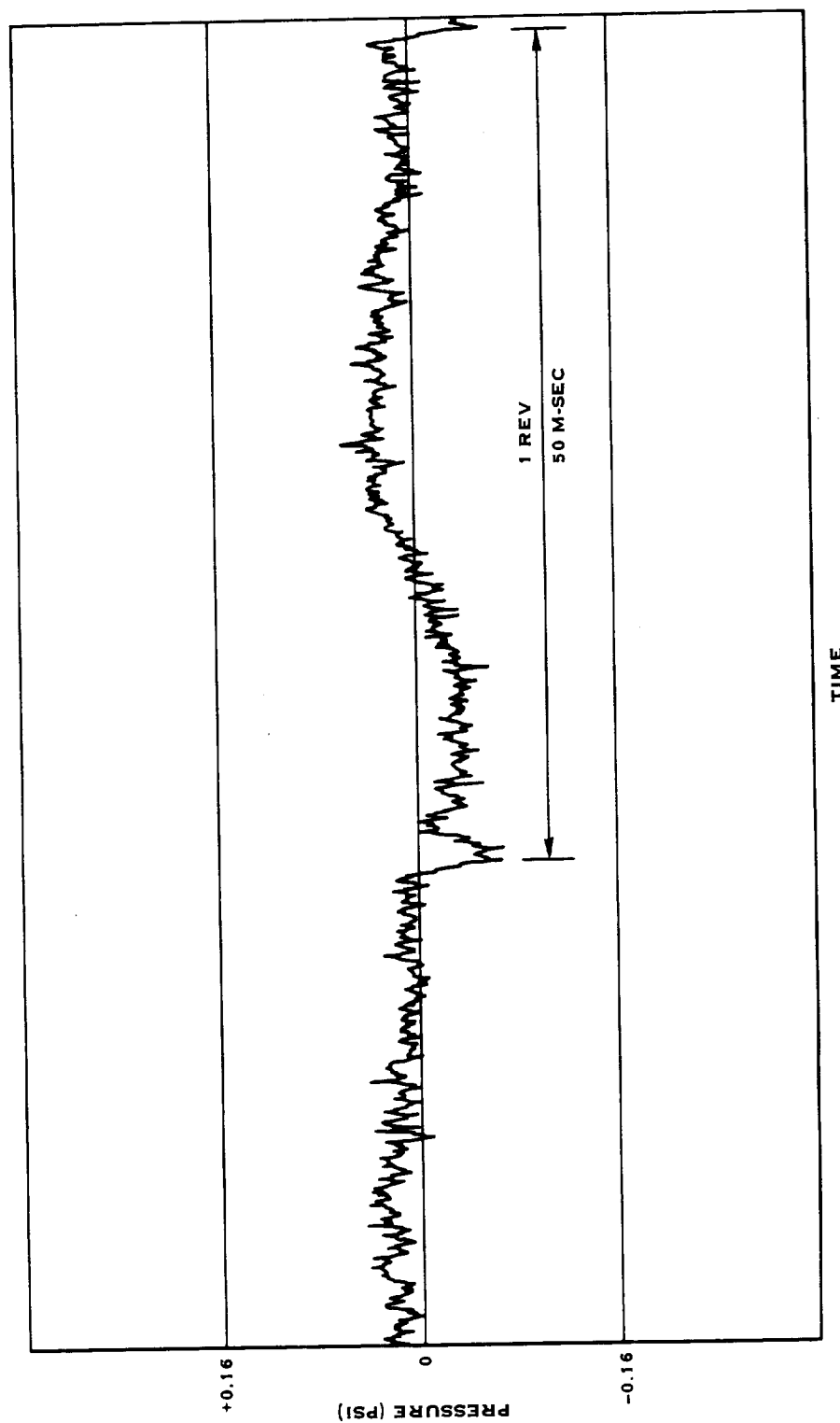
FIGURE 10.7 PRESSURE DATA TRANSDUCER PT9F, PLATE OBSTRUCTION, $\beta_{3/4} = 32°$, 1200 RPM

115
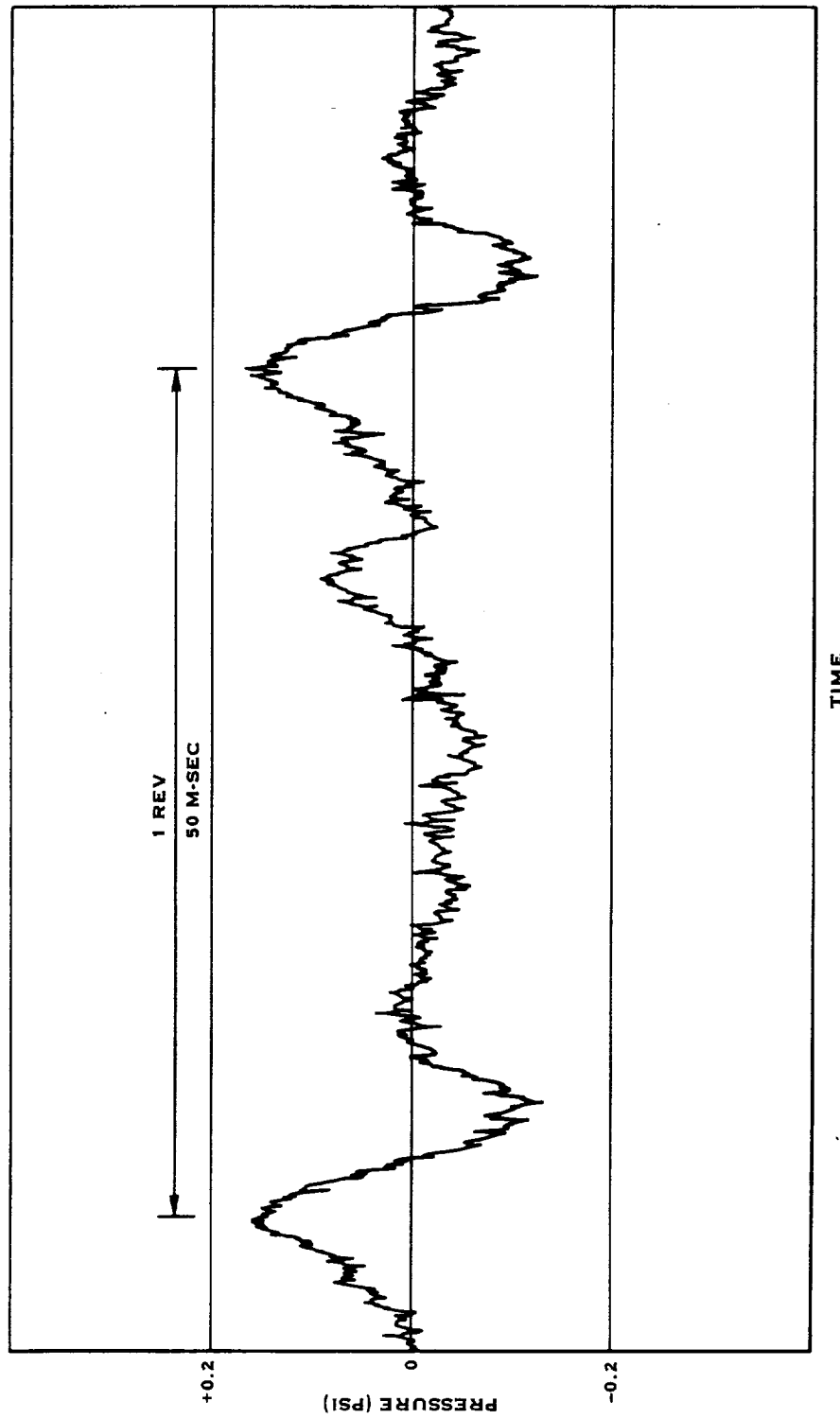
FIGURE 10.8 PRESSURE DATA, TRANSDUCER PT21C, PLATE OBSTRUCTION, $\beta\frac{3}{4} = 32°$, 1200 RPM

116
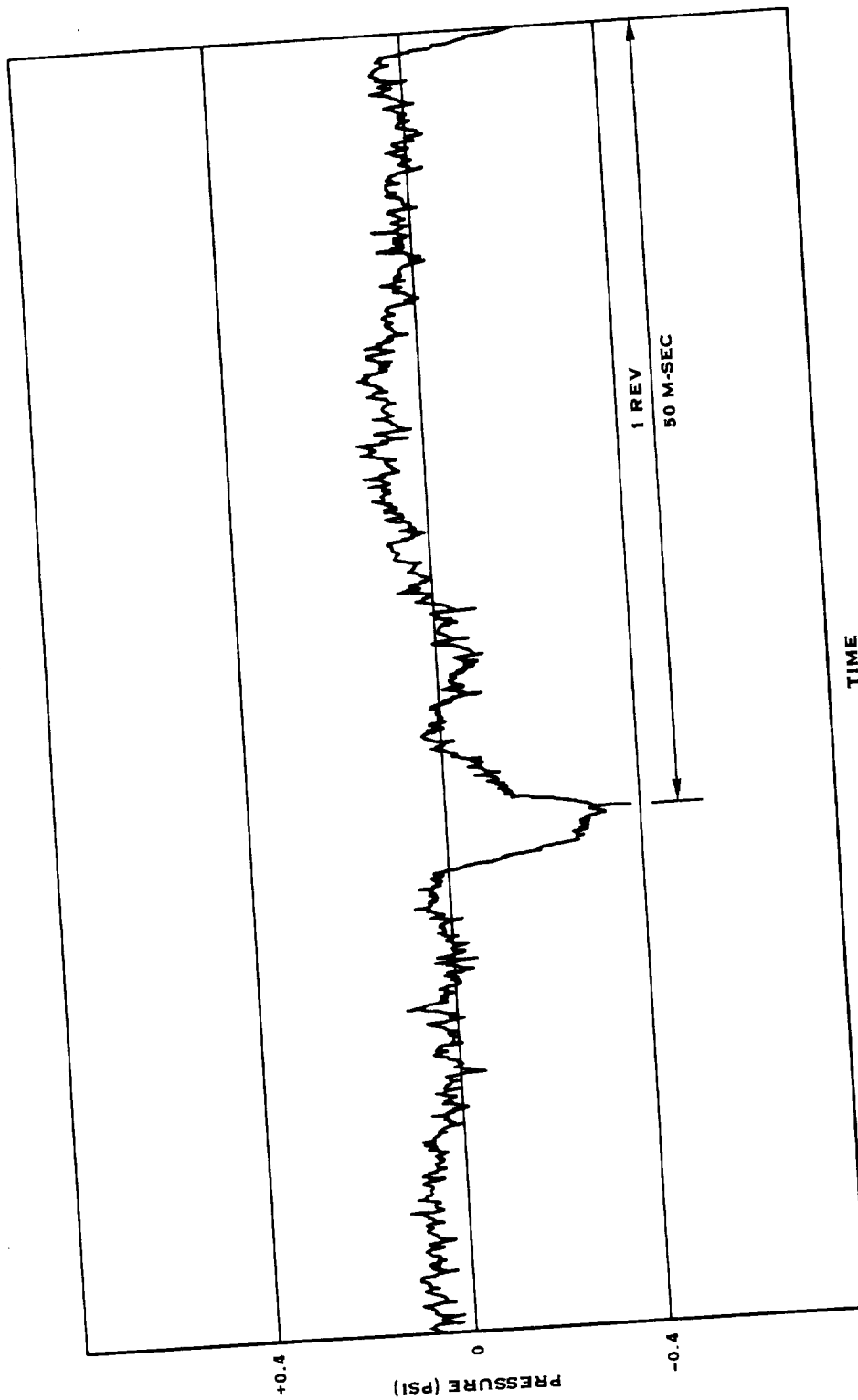
FIGURE 10.9 PRESSURE DATA, PT26C, PLATE OBSTRUCTION. $\beta\frac{3}{4} = 32°$, 1200 RPM

11.0 CONCLUSIONS AND RECOMMENDATIONS

The Static Rotor Test has provided an extensive evaluation of the performance characteristics of the SR-7L Large Scale Advanced Prop-Fan. All of the test objectives regarding acquisition of data were accomplished and fifty six hours of operating experience were attained. No problems were uncovered that were considered to be an impedance to the planned follow on wind tunnel or engine testing of the LAP. Results were obtained that differed from predictions in the areas of aerodynamic performance and blade loading distribution. High blade vibratory stresses in the blade structure did prevent operation at the design power of 4476 kW (6000 Hp) from being achieved at 100% speed. The conclusion and recommendation derived from each phase of the Static Rotor Test are presented in the following sections.

11.1 Aerodynamic Performance

Measured aerodynamic performance of the Prop-Fan corresponded well with analytical predictions for blade angles up to 30°. At blade angles above 30° the thrust produced and power absorbed by the Prop-Fan were lower than predicted. However the ratio of measured thrust to measured power at the static design point was actually higher than predicted. The characteristic shape of the LAP static performance curves were not significantly different from those observed for the SR-2, SR-3 and SR-5 Prop-Fan wind tunnel models. More research into the geometry of the wakes generated by Prop-Fans might improve the accuracy with which their static performance could be predicted.

11.2 Structural Dynamics

Blade vibratory stresses were found to increase significantly as blade angle was increased beyond 30°. This corresponded with the point at which measured and predicted aerodynamic performance began to deviate. The blade vibration was characterized as stall buffet rather than stall flutter because it was unsteady, non-sinusoidal and its onset was not sudden. The dominant frequency of vibration at the onset of buffet was 92.5 Hz which corresponds to the blade second flatwise bending normal mode. The mode of vibration was also found to vary with blade angle in the buffet region. The blade natural frequencies were accurately predicted by the design analytical tools. The variation of natural frequency with RPM and blade angle was also clearly observed.

11.3 Steady Stress, Deflection and Overspeed Testing

The analytical techniques used in the blade design process accurately predicted the distribution of steady state strain in the blade structure. The twist deflection of the blades was also predicted with reasonable accuracy. The difference between the desired and observed blade deflections did not have a significant impact on Prop-Fan aerodynamic performance.

PAGE 118 INTENTIONALLY

11.3 (Continued)

The structural integrity of the Prop-Fan was verified by successful operation at 120% of design speed and 100% design power for one hour. The low vibratory stresses observed during the overspeed test suggest that classical unstalled flutter will not be a problem at the design cruise condition.

11.4 Blade Surface Steady Pressure Measurement

The blade surface steady pressure data indicates that at low blade angles, the tip region of the blade is more highly loaded than was predicted by the design analysis. This may be the result of a vortex attached to the blade suction surface in the vicinity of the blade tip. The vortex would tend to reduce the suction surface pressure. As blade angle is increased beyond 30°, much of the tip loading is lost, contributing to the observed reduction and leveling off of thrust. The loss of loading may be due to the breakdown of the vortex or detachment of the vortex from the suction surface. Turbulence due to the breakdown of the vortex may also be the exciting force for the stall buffet phenomenon.

11.5 Blade Surface Unsteady Pressure Testing

The suitability of instrumentation, installed in one SR-7L Prop-Fan blade, to monitor time varying pressures on the blade surfaces was verified. The failure of transducers, installed on the 1.24 meter (49 inch) blade station, to sense a time varying pressure is attributed to that station not passing through the wake caused by the aerodynamic obstruction. The inflow to the Prop-Fan had a larger radial component than was expected resulting in the wake not being intersected by the outboard blade section. No correlation was found between the unsteady pressure data and the stall buffet. If the excitation of the blade is indeed the result of an aerodynamic phenomenon occurring near the blade tip, the transducers may not have been installed for enough outboard to detect it.

APPENDIX I

CORRECTED THRUST AND POWER AND IRP STRAIN

FOR AERODYNAMIC PERFORMANCE AND STRUCTURAL DYNAMIC TEST POINTS

DESCRIPTION	RUN NO.	BLADE ANGLE DEGREES	ROTATIONAL SPEED RPM	POWER KILOWATTS	THRUST NEWTONS
HOOK-UP II	4	22.10	600.	92.	3438.
"	5	22.10	700.	143.	4630.
"	6	22.10	800.	209.	6258.
"	7	22.10	900.	294.	7495.
"	8	22.10	1000.	394.	9919.
"	9	22.10	1100.	533.	12081.
"	10	22.10	1200.	693.	14505.
"	11	22.10	1300.	912.	16974.
"	12	22.10	1400.	1075.	19794.
"	13	22.10	1500.	1328.	22836.
"	14	22.10	1600.	1611.	25963.
"	15	22.10	1650.	1770.	27684.
"	16	22.10	1700.	1924.	29183.
"	17	22.10	1750.	2104.	31034.
"	18	22.10	1800.	2289.	32755.
"	19	22.10	1850.	2488.	34739.
"	20	22.10	1900.	2670.	36545.
"	21	0.20	600.	13.	44.
"	22	0.20	700.	16.	89.
"	23	0.20	800.	23.	133.
"	24	0.20	900.	28.	200.
"	25	0.20	1000.	35.	285.
"	26	0.20	1100.	43.	396.
"	27	0.20	1200.	53.	485.
"	28	0.20	1300.	61.	663.
"	29	0.20	1400.	70.	792.
"	30	0.20	1500.	110.	925.
"	31	0.20	1600.	101.	1059.
"	32	0.20	1650.	106.	1014.
HOOK-UP II	33	0.20	1700.	116.	1103.

DESCRIPTION	RUN NO.	BLADE ANGLE DEGREES	ROTATIONAL SPEED RPM	POWER KILOWATTS	THRUST NEWTONS
HOOK-UP II	34	0.20	1750.	129.	1103.
"	35	0.20	1800.	140.	1192.
"	36	0.20	1850.	148.	1148.
"	37	0.20	1900.	158.	1237.
"	40	34.10	700.	272.	5587.
"	41	34.10	1000.	782.	11623.
"	42	34.10	1100.	1029.	14038.
"	43	34.10	1200.	1328.	16676.
"	44	34.10	1300.	1696.	19491.
"	45	-2.00	600.	13.	-22.
"	46	-2.00	700.	19.	22.
"	47	-2.00	800.	22.	44.
"	48	-2.00	900.	30.	53.
"	49	-2.00	1000.	38.	67.
"	50	-2.00	1100.	44.	89.
"	51	-2.00	1200.	51.	111.
"	52	-2.00	1300.	60.	178.
"	53	-2.00	1400.	72.	222.
"	54	-2.00	1500.	89.	200.
"	55	-2.00	1600.	103.	222.
"	56	-2.00	1650.	110.	133.
"	57	-2.00	1700.	118.	133.
"	58	-2.00	1750.	129.	156.
"	59	-2.00	1800.	139.	133.
"	60	-2.00	1850.	151.	111.
"	61	-2.00	1900.	162.	111.
"	65	-5.70	600.	14.	44.
"	66	-5.70	700.	23.	71.
"	67	-5.70	800.	29.	22.
HOOK-UP II	68	-5.70	900.	38.	-71.

DESCRIPTION	RUN NO.	BLADE ANGLE DEGREES	ROTATIONAL SPEED RPM	POWER KILOWATTS	THRUST NEWTONS
HOOK-UP II	69	-5.70	1000.	51.	-116.
"	70	-5.70	1100.	58.	-280.
"	71	-5.70	1200.	72.	-302.
"	72	-5.70	1300.	86.	-280.
"	73	-5.70	1400.	101.	-280.
"	74	-5.70	1500.	122.	-325.
"	75	-5.70	1600.	138.	-374.
"	76	-5.70	1650.	148.	-418.
"	77	-5.70	1700.	160.	-512.
"	78	-5.70	1750.	169.	-560.
"	79	-5.70	1800.	183.	-583.
"	80	-5.70	1850.	193.	-605.
HOOK-UP II	81	-5.70	1900.	205.	-605.
HOOK-UP I	94	21.90	1000.	383.	9541.
"	95	21.90	1500.	1254.	21773.
"	96	21.90	1700.	1814.	27978.
"	97	30.30	700.	236.	4773.
"	98	30.30	800.	348.	7317.
"	99	30.30	900.	490.	9216.
"	100	30.30	1000.	669.	11351.
"	101	30.30	1100.	896.	14038.
"	102	30.30	1200.	1119.	16769.
"	103	30.30	1300.	1509.	19642.
"	104	30.30	1400.	1823.	22565.
"	105	30.30	1500.	2257.	26172.
"	106	30.30	1600.	2747.	29926.
"	107	30.30	1650.	2934.	31452.
"	108	30.30	1700.	3266.	33538.
"	109	30.30	1750.	3498.	35299.
HOOK-UP I	110	30.30	1800.	3841.	37755.

DESCRIPTION	RUN NO.	BLADE ANGLE DEGREES	ROTATIONAL SPEED RPM	POWER KILOWATTS	THRUST NEWTONS
HOOK-UP I	111	30.30	1850.	4148.	39654.
"	112	30.30	1900.	4547.	41691.
"	113	34.30	600.	177.	3923.
"	114	34.30	700.	279.	5400.
"	115	34.30	800.	400.	7201.
"	116	34.30	900.	576.	9185.
"	117	34.30	1000.	793.	11449.
"	118	34.30	1100.	1037.	13571.
"	119	34.30	1200.	1334.	16342.
"	120	34.30	1300.	1683.	19020.
"	121	32.10	700.	257.	5627.
"	122	32.10	800.	374.	7348.
"	123	32.10	900.	529.	9345.
"	124	32.10	1000.	714.	11347.
"	125	32.10	1100.	935.	13718.
"	126	32.10	1200.	1204.	16275.
"	127	32.10	1300.	1542.	19251.
"	128	32.10	1400.	1904.	22178.
"	129	32.10	1500.	2346.	25527.
"	130	32.10	1600.	2880.	28783.
"	131	32.10	1700.	3403.	32177.
"	132	33.50	700.	266.	5489.
"	133	33.50	800.	397.	7353.
"	134	33.50	900.	553.	9167.
"	135	33.50	1000.	748.	11258.
"	136	33.50	1100.	990.	13727.
"	137	33.50	1200.	1279.	16378.
"	138	33.50	1300.	1618.	19077.
"	139	33.50	1400.	1996.	22053.
HOOK-UP I	140	33.50	1500.	2446.	25265.

DESCRIPTION	RUN NO.	BLADE ANGLE DEGREES	ROTATIONAL SPEED RPM	POWER KILOWATTS	THRUST NEWTONS
HOOK-UP I	141	33.50	1600.	2974.	28752.
"	- 142	.33.50	1700.	3519.	32337.
"	143	38.10	600.	204.	3981.
"	144	38.10	700.	309.	5529.
"	145	38.10	800.	461.	7215.
"	146	38.10	900.	670.	9181.
"	147	38.10	1000.	901.	11338.
"	148	38.10	1050.	1014.	12370.
"	149	38.10	1100.	1205.	13704.
"	150	38.10	1200.	1509.	16164.
"	151	42.00	600.	224.	3861.
"	152	42.00	700.	364.	5613.
"	153	42.00	800.	536.	7250.
"	154	42.00	900.	774.	9470.
"	155	42.00	1000.	1071.	11578.
"	156	42.00	1100.	1392.	13913.
"	157	42.00	1200.	1774.	16489.
"	158	49.90	600.	308.	4163.
"	159	49.90	700.	495.	5729.
"	160	49.90	800.	729.	7597.
"	161	49.90	900.	1021.	9585.
"	162	49.90	1000.	1456.	11925.
"	163	49.90	1100.	1864.	14260.
"	164	49.90	1200.	2441.	16600.
"	165	55.00	600.	355.	3901.
"	166	55.00	700.	564.	5493.
"	167	55.00	800.	844.	7246.
"	169	55.00	900.	1166.	8883.
" .	170	55.00	1000.	1570.	10987.
HOOK-UP I	171	55.00	1100.	2165.	13673.

DESCRIPTION	RUN NO.	BLADE ANGLE DEGREES	ROTATIONAL SPEED RPM	POWER KILOWATTS	THRUST NEWTONS
HOOK-UP I	172	60.10	600.	433.	3972.
"	173	60.10	700.	679.	5258.
"	174	60.10	800.	978.	6779.
"	175	60.10	900.	1399.	8763.
"	176	60.10	1000.	1996.	10635.
"	177	60.10	1100.	2710.	12739.
"	178	5.90	600.	19.	885.
"	179	5.90	700.	31.	1210.
"	180	5.90	800.	39.	1490.
"	181	5.90	900.	52.	1908.
"	182	5.90	1000.	63.	2349.
"	183	5.90	1100.	81.	2816.
"	184	5.90	1200.	101.	3421.
"	185	5.90	1300.	125.	4025.
"	186	5.90	1400.	149.	4630.
"	187	5.90	1500.	184.	5400.
"	188	5.90	1600.	224.	6143.
"	189	5.90	1650.	239.	6516.
"	190	5.90	1700.	261.	6841.
"	191	32.20	1700.	3453.	33049.
"	192	6.10	1700.	268.	6997.
"	193	6.10	1750.	289.	7290.
"	194	6.10	1800.	315.	7811.
"	195	6.10	1850.	344.	8171.
"	196	6.10	1900.	369.	8580.
"	197	2.00	600.	14.	338.
"	198	2.00	700.	20.	427.
"	199	2.00	800.	26.	587.
"	200	2.00	900.	34.	743.
HOOK-UP I	201	2.00	1000.	43.	1014.

128

DESCRIPTION	RUN NO.	BLADE ANGLE DEGREES	ROTATIONAL SPEED RPM	POWER KILOWATTS	THRUST NEWTONS
HOOK-UP I	202	2.00	1100.	49.	1219.
"	203	2.00	1200.	61.	1401.
"	204	2.00	1300.	78.	1850.
"	205	2.00	1400.	89.	2166.
"	206	2.00	1500.	112.	2438.
"	207	2.00	1600.	131.	2753.
"	208	2.00	1700.	157.	3114.
"	209	2.00	1800.	181.	3385.
"	210	2.00	1900.	213.	3656.

DESCRIPTION	RUN NO.	GAGE 12 IRP MICRO STRAIN	GAGE 22 IRP MICRO STRAIN	GAGE 32 IRP MICRO STRAIN	GAGE 52 IRP MICRO STRAIN	GAGE 62 IRP MICRO STRAIN	GAGE 72 IRP MICRO STRAIN	GAGE 82 IRP MICRO STRAIN
HOOK-UP II	4	121.0	0.0	113.0	75.0	56.0	82.0	60.0
"	5	142.0	0.0	130.0	102.0	76.0	106.0	80.0
"	6	165.0	0.0	151.0	126.0	97.0	138.0	84.0
"	7	118.0	0.0	114.0	84.0	54.0	88.0	77.0
"	8	153.0	0.0	149.0	117.0	90.0	115.0	92.0
"	9	133.0	0.0	149.0	130.0	88.0	138.0	122.0
"	10	144.0	0.0	174.0	140.0	105.0	146.0	113.0
"	11	131.0	0.0	166.0	144.0	102.0	147.0	111.0
"	12	113.0	0.0	151.0	134.0	95.0	132.0	103.0
"	13	181.0	0.0	219.0	196.0	140.0	206.0	162.0
"	14	160.0	0.0	164.0	152.0	125.0	154.0	134.0
"	15	173.0	0.0	220.0	170.0	113.0	158.0	159.0
"	16	145.0	0.0	215.0	151.0	96.0	146.0	122.0
"	17	121.0	0.0	169.0	125.0	84.0	126.0	96.0
"	18	102.0	0.0	135.0	106.0	74.0	115.0	93.0
"	19	103.0	0.0	138.0	110.0	79.0	118.0	98.0
"	20	102.0	0.0	131.0	108.0	79.0	118.0	101.0
"	21	92.0	0.0	88.0	69.0	43.0	70.0	49.0
"	22	95.0	0.0	97.0	84.0	58.0	82.0	63.0
"	23	101.0	0.0	104.0	97.0	62.0	88.0	72.0
"	24	87.0	0.0	94.0	95.0	57.0	85.0	73.0
"	25	82.0	0.0	86.0	92.0	54.0	86.0	69.0
"	26	87.0	0.0	95.0	101.0	59.0	99.0	81.0
"	27	94.0	0.0	100.0	99.0	59.0	95.0	80.0
"	28	136.0	0.0	138.0	131.0	87.0	126.0	101.0
"	29	244.0	0.0	237.0	226.0	163.0	215.0	170.0
"	30	150.0	0.0	133.0	134.0	91.0	133.0	109.0
"	31	134.0	0.0	112.0	113.0	75.0	112.0	93.0
"	32	129.0	0.0	111.0	107.0	75.0	111.0	86.0
HOOK-UP II	33	119.0	0.0	113.0	103.0	74.0	113.0	87.0

DESCRIPTION	RUN NO.	GAGE 12 IRP MICRO STRAIN	GAGE 22 IRP MICRO STRAIN	GAGE 32 IRP MICRO STRAIN	GAGE 52 IRP MICRO STRAIN	GAGE 82 IRP MICRO STRAIN	GAGE 72 IRP MICRO STRAIN	GAGE 82 IRP MICRO STRAIN
HOOK-UP II	34	115.0	0.0	109.0	102.0	69.0	107.0	84.0
"	35	106.0	0.0	103.0	100.0	64.0	105.0	83.0
"	36	103.0	0.0	101.0	97.0	62.0	103.0	83.0
"	37	101.0	0.0	100.0	96.0	63.0	102.0	87.0
"	40	280.0	0.0	232.0	246.0	188.0	229.0	181.0
"	41	642.0	0.0	592.0	641.0	485.0	601.0	366.0
"	42	406.0	0.0	400.0	415.0	342.0	438.0	391.0
"	43	430.0	0.0	429.0	393.0	332.0	406.0	341.0
"	44	522.0	0.0	593.0	548.0	429.0	571.0	428.0
"	45	119.0	0.0	0.0	110.0	54.0	83.0	83.0
"	46	95.0	0.0	81.0	92.0	55.0	90.0	83.0
"	47	101.0	0.0	98.0	100.0	63.0	99.0	89.0
"	48	86.0	0.0	89.0	91.0	57.0	94.0	91.0
"	49	91.0	0.0	99.0	95.0	66.0	106.0	82.0
"	50	91.0	0.0	98.0	94.0	68.0	108.0	92.0
"	51	106.0	0.0	111.0	105.0	76.0	115.0	93.0
"	52	148.0	0.0	150.0	140.0	107.0	144.0	114.0
"	53	211.0	0.0	211.0	196.0	151.0	196.0	155.0
"	54	164.0	0.0	146.0	145.0	108.0	151.0	126.0
"	55	137.0	0.0	109.0	110.0	84.0	122.0	104.0
"	56	132.0	0.0	100.0	102.0	73.0	113.0	93.0
"	57	130.0	0.0	93.0	95.0	72.0	111.0	92.0
"	58	125.0	0.0	90.0	93.0	67.0	104.0	88.0
"	59	117.0	0.0	83.0	86.0	66.0	99.0	86.0
"	60	114.0	0.0	83.0	89.0	67.0	100.0	88.0
"	61	109.0	0.0	84.0	87.0	63.0	97.0	88.0
"	65	84.0	0.0	68.0	70.0	40.0	68.0	49.0
"	66	81.0	0.0	67.0	78.0	45.0	76.0	56.0
"	67	83.0	0.0	77.0	92.0	52.0	85.0	64.0
HOOK-UP II	68	71.0	0.0	73.0	93.0	47.0	82.0	71.0

DESCRIPTION	RUN NO.	GAGE 12 IRP MICRO STRAIN	GAGE 22 IRP MICRO STRAIN	GAGE 32 IRP MICRO STRAIN	GAGE 52 IRP MICRO STRAIN	GAGE 62 IRP MICRO STRAIN	GAGE 72 IRP MICRO STRAIN	GAGE 82 IRP MICRO STRAIN
HOOK-UP II	69	72.0	0.0	85.0	97.0	49.0	90.0	75.0
"	70	71.0	0.0	89.0	101.0	56.0	98.0	80.0
"	71	79.0	0.0	93.0	101.0	56.0	98.0	82.0
"	72	92.0	0.0	106.0	110.0	68.0	113.0	88.0
"	73	95.0	0.0	110.0	112.0	66.0	110.0	83.0
"	74	111.0	0.0	120.0	116.0	75.0	119.0	88.0
"	75	136.0	0.0	137.0	130.0	91.0	134.0	99.0
"	76	151.0	0.0	144.0	136.0	93.0	140.0	110.0
"	77	144.0	0.0	138.0	128.0	89.0	137.0	101.0
"	78	145.0	0.0	134.0	125.0	84.0	133.0	100.0
"	79	138.0	0.0	128.0	118.0	81.0	129.0	98.0
"	80	127.0	0.0	123.0	113.0	75.0	123.0	95.0
HOOK-UP II	81	118.0	0.0	121.0	105.0	71.0	116.0	88.0
HOOK-UP I	94	104.0	118.0	135.0	86.0	79.0	94.0	82.0
"	95	168.0	131.0	234.0	146.0	130.0	168.0	153.0
"	96	156.0	129.0	263.0	113.0	88.0	116.0	111.0
"	97	159.0	156.0	142.0	126.0	117.0	136.0	134.0
"	98	178.0	180.0	158.0	150.0	140.0	150.0	144.0
"	99	179.0	197.0	179.0	163.0	151.0	169.0	160.0
"	100	218.0	224.0	222.0	202.0	189.0	209.0	187.0
"	101	212.0	224.0	218.0	215.0	190.0	215.0	209.0
"	102	222.0	217.0	231.0	211.0	195.0	218.0	200.0
"	103	230.0	222.0	242.0	215.0	193.0	217.0	193.0
"	104	251.0	221.0	264.0	242.0	221.0	233.0	206.0
"	105	257.0	229.0	278.0	245.0	229.0	247.0	239.0
"	106	260.0	232.0	298.0	246.0	232.0	241.0	224.0
"	107	281.0	250.0	331.0	258.0	232.0	241.0	239.0
"	108	293.0	263.0	377.0	274.0	222.0	266.0	280.0
"	109	272.0	268.0	351.0	243.0	221.0	247.0	232.0
HOOK-UP I	110	256.0	248.0	321.0	235.0	215.0	239.0	215.0

132

DESCRIPTION	RUN NO.	GAGE 12 IRP MICRO STRAIN	GAGE 22 IRP MICRO STRAIN	GAGE 32 IRP MICRO STRAIN	GAGE 52 IRP MICRO STRAIN	GAGE 62 IRP MICRO STRAIN	GAGE 72 IRP MICRO STRAIN	GAGE 82 IRP MICRO STRAIN
HOOK-UP I	111	254.0	237.0	313.0	224.0	214.0	228.0	210.0
"	112	260.0	315.0	323.0	242.0	228.0	254.0	226.0
"	113	178.0	170.0	153.0	145.0	134.0	137.0	144.0
"	114	225.0	210.0	206.0	184.0	186.0	185.0	183.0
"	115	299.0	263.0	281.0	251.0	273.0	268.0	231.0
"	116	302.0	297.0	294.0	284.0	285.0	303.0	269.0
"	117	568.0	522.0	486.0	528.0	485.0	540.0	375.0
"	118	358.0	363.0	369.0	361.0	354.0	396.0	375.0
"	119	381.0	367.0	380.0	379.0	371.0	380.0	338.0
"	120	484.0	551.0	559.0	535.0	484.0	550.0	474.0
"	121	193.0	197.0	188.0	171.0	166.0	168.0	165.0
"	122	225.0	225.0	231.0	192.0	203.0	210.0	184.0
"	123	236.0	251.0	242.0	225.0	225.0	238.0	215.0
"	124	331.0	325.0	323.0	308.0	285.0	308.0	240.0
"	125	275.0	281.0	288.0	275.0	268.0	295.0	282.0
"	126	302.0	300.0	320.0	298.0	283.0	304.0	275.0
"	127	294.0	322.0	337.0	318.0	293.0	320.0	299.0
"	128	307.0	328.0	357.0	313.0	298.0	325.0	306.0
"	129	310.0	312.0	364.0	312.0	296.0	335.0	314.0
"	130	334.0	333.0	398.0	348.0	343.0	354.0	327.0
"	131	384.0	399.0	458.0	385.0	353.0	375.0	365.0
"	132	206.0	207.0	193.0	178.0	181.0	188.0	183.0
"	133	272.0	261.0	263.0	228.0	262.0	250.0	207.0
"	134	269.0	279.0	278.0	261.0	265.0	274.0	245.0
"	135	455.0	464.0	452.0	470.0	432.0	466.0	325.0
"	136	328.0	353.0	362.0	359.0	338.0	374.0	340.0
"	137	357.0	364.0	388.0	355.0	333.0	358.0	332.0
"	138	394.0	462.0	473.0	461.0	427.0	457.0	396.0
"	139	391.0	408.0	444.0	415.0	415.0	433.0	405.0
HOOK-UP I	140	387.0	389.0	443.0	391.0	390.0	414.0	373.0

133

PAGE# 12

DESCRIPTION	RUN NO.	GAGE 12 IRP MICRO STRAIN	GAGE 22 IRP MICRO STRAIN	GAGE 32 IRP MICRO STRAIN	GAGE 52 IRP MICRO STRAIN	GAGE 82 IRP MICRO STRAIN	GAGE 72 IRP MICRO STRAIN	GAGE 82 IRP MICRO STRAIN
HOOK-UP I	141	377.0	379.0	448.0	404.0	392.0	394.0	373.0
"	142	435.0	465.0	520.0	465.0	430.0	432.0	427.0
"	143	191.0	184.0	187.0	180.0	174.0	165.0	177.0
"	144	230.0	222.0	230.0	220.0	229.0	221.0	218.0
"	145	294.0	282.0	294.0	286.0	294.0	290.0	263.0
"	146	350.0	333.0	339.0	346.0	346.0	345.0	308.0
"	147	549.0	551.0	532.0	528.0	511.0	534.0	381.0
"	148	459.0	507.0	468.0	496.0	499.0	514.0	415.0
"	149	447.0	460.0	476.0	455.0	463.0	477.0	448.0
"	150	511.0	490.0	517.0	473.0	501.0	494.0	465.0
"	151	221.0	214.0	227.0	233.0	230.0	209.0	200.0
"	152	303.0	298.0	320.0	312.0	302.0	280.0	284.0
"	153	323.0	316.0	323.0	315.0	312.0	298.0	296.0
"	154	371.0	362.0	364.0	358.0	351.0	364.0	334.0
"	155	447.0	251.0	446.0	433.0	447.0	446.0	382.0
"	156	500.0	513.0	540.0	510.0	515.0	495.0	458.0
"	157	595.0	591.0	603.0	556.0	606.0	569.0	532.0
"	158	279.0	275.0	311.0	294.0	285.0	279.0	264.0
"	159	463.0	446.0	472.0	478.0	501.0	430.0	410.0
"	160	420.0	392.0	417.0	418.0	409.0	384.0	379.0
"	161	427.0	421.0	424.0	417.0	418.0	413.0	389.0
"	162	490.0	482.0	488.0	472.0	475.0	473.0	446.0
"	163	585.0	576.0	618.0	590.0	586.0	591.0	505.0
"	164	714.0	713.0	749.0	721.0	745.0	727.0	681.0
"	165	324.0	299.0	324.0	329.0	323.0	295.0	296.0
"	166	509.0	514.0	572.0	516.0	560.0	475.0	468.0
"	167	444.0	423.0	457.0	465.0	472.0	428.0	422.0
"	169	477.0	464.0	498.0	464.0	491.0	446.0	426.0
"	170	533.0	514.0	560.0	521.0	529.0	517.0	482.0
HOOK-UP I	171	741.0	687.0	738.0	681.0	753.0	694.0	685.0

134

DESCRIPTION	RUN NO.	GAGE 12 IRP MICRO STRAIN	GAGE 22 IRP MICRO STRAIN	GAGE 32 IRP MICRO STRAIN	GAGE 52 IRP MICRO STRAIN	GAGE 62 IRP MICRO STRAIN	GAGE 72 IRP MICRO STRAIN	GAGE 82 IRP MICRO STRAIN
HOOK-UP I	172	355.0	344.0	372.0	362.0	367.0	356.0	316.0
"	173	511.0	503.0	557.0	495.0	530.0	469.0	456.0
"	174	509.0	465.0	540.0	513.0	533.0	490.0	463.0
"	175	520.0	493.0	513.0	511.0	536.0	488.0	471.0
"	176	600.0	558.0	592.0	609.0	618.0	604.0	542.0
"	177	855.0	830.0	862.0	794.0	815.0	780.0	757.0
"	178	57.0	69.0	69.0	41.0	41.0	37.0	47.0
"	179	65.0	73.0	81.0	44.0	47.0	45.0	54.0
"	180	57.0	67.0	82.0	43.0	45.0	40.0	53.0
"	181	58.0	63.0	91.0	43.0	46.0	42.0	56.0
"	182	64.0	76.0	108.0	67.0	61.0	62.0	63.0
"	183	58.0	58.0	108.0	47.0	49.0	46.0	60.0
"	184	61.0	60.0	115.0	56.0	57.0	52.0	53.0
"	185	71.0	68.0	120.0	71.0	72.0	69.0	59.0
"	186	75.0	77.0	132.0	88.0	86.0	80.0	85.0
"	187	63.0	59.0	101.0	63.0	66.0	69.0	61.0
"	188	56.0	56.0	100.0	56.0	60.0	61.0	70.0
"	189	54.0	56.0	93.0	55.0	58.0	60.0	70.0
"	190	53.0	55.0	89.0	53.0	57.0	55.0	70.0
"	191	350.0	350.0	400.0	353.0	347.0	335.0	386.0
"	192	46.0	66.0	90.0	52.0	55.0	55.0	67.0
"	193	47.0	63.0	87.0	53.0	56.0	57.0	70.0
"	194	46.0	61.0	83.0	51.0	54.0	55.0	71.0
"	195	47.0	60.0	83.0	52.0	55.0	55.0	70.0
"	196	47.0	58.0	81.0	51.0	53.0	59.0	72.0
"	197	54.0	68.0	73.0	41.0	44.0	39.0	46.0
"	198	59.0	70.0	81.0	42.0	49.0	43.0	53.0
"	199	60.0	71.0	91.0	46.0	53.0	47.0	56.0
"	200	59.0	71.0	97.0	49.0	51.0	49.0	59.0
HOOK-UP I	201	63.0	68.0	106.0	60.0	53.0	50.0	64.0

DESCRIPTION	RUN NO.	GAGE 12 IRP MICRO STRAIN	GAGE 22 IRP MICRO STRAIN	GAGE 32 IRP MICRO STRAIN	GAGE 52 IRP MICRO STRAIN	GAGE 62 IRP MICRO STRAIN	GAGE 72 IRP MICRO STRAIN	GAGE 82 IRP MICRO STRAIN
HOOK-UP I	202	62.0	65.0	110.0	61.0	55.0	55.0	61.0
"	203	65.0	66.0	108.0	61.0	59.0	56.0	58.0
"	204	68.0	70.0	107.0	65.0	60.0	60.0	60.0
"	205	69.0	70.0	103.0	61.0	62.0	63.0	72.0
"	206	70.0	75.0	108.0	70.0	76.0	73.0	76.0
"	207	64.0	66.0	97.0	61.0	66.0	67.0	76.0
"	208	63.0	65.0	94.0	64.0	68.0	67.0	77.0
"	209	59.0	67.0	90.0	61.0	66.0	65.0	80.0
"	210	56.0	66.0	84.0	60.0	69.0	67.0	81.0

136

DESCRIPTION	RUN NO.	GAGE 73 IRP MICRO STRAIN	GAGE 24 IRP MICRO STRAIN	GAGE 76 IRP MICRO STRAIN	GAGE 89 IRP MICRO STRAIN	GAGE 81 IRP MICRO STRAIN	GAGE 812 IRP MICRO STRAIN	GAGE 813 IRP MICRO STRAIN
HOOK-UP II	4	100.0	67.0	39.0	77.0	59.0	52.0	53.0
"	5	123.0	85.0	43.0	96.0	83.0	77.0	73.0
"	6	197.0	108.0	44.0	93.0	73.0	67.0	84.0
"	7	121.0	85.0	45.0	94.0	80.0	65.0	72.0
"	8	164.0	116.0	47.0	95.0	84.0	75.0	85.0
"	9	189.0	131.0	51.0	103.0	93.0	88.0	128.0
"	10	162.0	149.0	56.0	110.0	125.0	105.0	99.0
"	11	156.0	162.0	61.0	114.0	127.0	106.0	90.0
"	12	167.0	162.0	57.0	98.0	105.0	85.0	88.0
"	13	293.0	297.0	67.0	100.0	89.0	95.0	191.0
"	14	195.0	233.0	73.0	105.0	100.0	94.0	138.0
"	15	198.0	261.0	92.0	104.0	90.0	104.0	160.0
"	16	199.0	321.0	94.0	94.0	85.0	95.0	128.0
"	17	159.0	249.0	74.0	89.0	85.0	82.0	95.0
"	18	150.0	204.0	72.0	87.0	83.0	81.0	86.0
"	19	149.0	183.0	72.0	91.0	85.0	84.0	85.0
"	20	153.0	195.0	81.0	99.0	93.0	89.0	87.0
"	21	82.0	58.0	38.0	71.0	54.0	50.0	44.0
"	22	92.0	66.0	39.0	82.0	69.0	59.0	54.0
"	23	112.0	69.0	42.0	97.0	83.0	68.0	63.0
"	24	106.0	70.0	44.0	96.0	30.0	66.0	69.0
"	25	111.0	69.0	44.0	74.0	73.0	61.0	56.0
"	26	133.0	77.0	47.0	72.0	77.0	68.0	76.0
"	27	112.0	81.0	48.0	83.0	85.0	77.0	68.0
"	28	131.0	102.0	51.0	106.0	119.0	105.0	83.0
"	29	199.0	168.0	56.0	191.0	220.0	188.0	145.0
"	30	159.0	122.0	55.0	108.0	119.0	107.0	94.0
"	31	147.0	123.0	58.0	92.0	97.0	92.0	81.0
"	32	155.0	124.0	63.0	87.0	93.0	87.0	78.0
HOOK-UP II	33	156.0	129.0	65.0	87.0	89.0	85.0	77.0

DESCRIPTION	RUN NO.	GAGE 73 IRP MICRO STRAIN	GAGE 24 IRP MICRO STRAIN	GAGE 76 IRP MICRO STRAIN	GAGE 89 IRP MICRO STRAIN	GAGE 81 IRP MICRO STRAIN	GAGE 812 IRP MICRO STRAIN	GAGE 813 IRP MICRO STRAIN
HOOK-UP II	34	140.0	134.0	68.0	88.0	87.0	86.0	74.0
"	35	137.0	136.0	66.0	81.0	80.0	84.0	70.0
"	36	133.0	135.0	67.0	81.0	80.0	81.0	68.0
"	37	135.0	137.0	70.0	89.0	88.0	90.0	72.0
"	40	342.0	211.0	83.0	132.0	143.0	140.0	203.0
"	41	926.0	677.0	153.0	196.0	206.0	222.0	445.0
"	42	702.0	572.0	185.0	212.0	225.0	240.0	470.0
"	43	663.0	627.0	221.0	226.0	250.0	243.0	408.0
"	44	891.0	907.0	237.0	241.0	255.0	261.0	521.0
"	45	110.0	98.0	46.0	74.0	83.0	64.0	80.0
"	46	89.0	59.0	51.0	83.0	83.0	75.0	74.0
"	47	110.0	78.0	47.0	88.0	89.0	93.0	79.0
"	48	107.0	70.0	47.0	86.0	91.0	80.0	77.0
"	49	139.0	72.0	48.0	87.0	82.0	80.0	81.0
"	50	136.0	78.0	50.0	91.0	92.0	79.0	86.0
"	51	139.0	88.0	52.0	95.0	93.0	88.0	84.0
"	52	164.0	113.0	56,0	121.0	114.0	111.0	101.0
"	53	220.0	162.0	58.0	164.0	155.0	155.0	140.0
"	54	187.0	141.0	59.0	123.0	126.0	114.0	117.0
"	55	181.0	136.0	62.0	98.0	104.0	90.0	91.0
"	56	172.0	137.0	69.0	93.0	87.0	86.0	82.0
"	57	162.0	148.0	71.0	87.0	82.0	81.0	83.0
"	58	146.0	148.0	66.0	77.0	75.0	72.0	73.0
"	59	138.0	137.0	63.0	73.0	69.0	69.0	68.0
"	60	139.0	137.0	64.0	72.0	65.0	67.0	66.0
"	61	142.0	136.0	65.0	71.0	65.0	67.0	68.0
"	65	78.0	51.0	37.0	70.0	55.0	50.0	41.0
"	66	83.0	56.0	39.0	75.0	65.0	52.0	53.0
"	67	92.0	60.0	40.0	82.0	72.0	64.0	59.0
HOOK-UP II	68	92.0	60.0	43.0	85.0	78.0	65.0	58.0

DESCRIPTION	RUN NO.	GAGE 73 IRP MICRO STRAIN	GAGE 24 IRP MICRO STRAIN	GAGE 76 IRP MICRO STRAIN	GAGE 89 IRP MICRO STRAIN	GAGE 81 IRP MICRO STRAIN	GAGE 812 IRP MICRO STRAIN	GAGE 813 IRP MICRO STRAIN
HOOK-UP II	69	103.0	64.0	45.0	90.0	83.0	75.0	66.0
"	70	115.0	67.0	47.0	96.0	81.0	79.0	69.0
"	71	120.0	79.0	48.0	98.0	83.0	82.0	70.0
"	72	135.0	88.0	51.0	97.0	93.0	87.0	76.0
"	73	134.0	96.0	52.0	93.0	88.0	90.0	77.0
"	74	151.0	113.0	57.0	98.0	97.0	95.0	86.0
"	75	170.0	135.0	60.0	109.0	115.0	110.0	90.0
"	76	169.0	147.0	60.0	119.0	127.0	117.0	99.0
"	77	172.0	150.0	63.0	113.0	116.0	110.0	95.0
"	78	168.0	155.0	64.0	109.0	114.0	105.0	90.0
"	79	165.0	150.0	66.0	104.0	108.0	97.0	91.0
"	80	165.0	158.0	70.0	99.0	98.0	94.0	85.0
HOOK-UP II	81	173.0	158.0	72.0	87.0	85.0	80.0	76.0
HOOK-UP I	94	142.0	110.0	33.0	66.0	50.0	62.0	75.0
"	95	245.0	231.0	46.0	120.0	69.0	102.0	190.0
"	96	173.0	223.0	53.0	102.0	88.0	104.0	123.0
"	97	212.0	146.0	56.0	97.0	119.0	109.0	154.0
"	98	248.0	197.0	72.0	135.0	118.0	123.0	179.0
"	99	279.0	245.0	87.0	143.0	127.0	132.0	202.0
"	100	340.0	301.0	100.0	115.0	142.0	136.0	213.0
"	101	344.0	333.0	106.0	140.0	153.0	153.0	239.0
"	102	361.0	363.0	119.0	173.0	163.0	164.0	253.0
"	103	367.0	395.0	127.0	165.0	156.0	160.0	249.0
"	104	401.0	445.0	135.0	175.0	171.0	168.0	266.0
"	105	425.0	479.0	142.0	185.0	178.0	183.0	296.0
"	106	404.0	486.0	146.0	172.0	162.0	173.0	269.0
"	107	391.0	522.0	152.0	178.0	178.0	189.0	305.0
"	108	428.0	589.0	159.0	188.0	185.0	212.0	340.0
"	109	423.0	579.0	155.0	173.0	186.0	199.0	296.0
HOOK-UP I	110	393.0	553.0	157.0	176.0	193.0	193.0	278.0

DESCRIPTION	RUN NO.	GAGE 73 IRP MICRO STRAIN	GAGE 24 IRP MICRO STRAIN	GAGE 76 IRP MICRO STRAIN	GAGE 89 IRP MICRO STRAIN	GAGE 81 IRP MICRO STRAIN	GAGE 812 IRP MICRO STRAIN	GAGE 813 IRP MICRO STRAIN
HOOK-UP I	111	383.0	552.0	155.0	180.0	186.0	185.0	267.0
"	112	420.0	579.0	169.0	195.0	198.0	198.0	292.0
"	113	205.0	135.0	43.0	104.0	127.0	122.0	159.0
"	114	294.0	187.0	58.0	125.0	151.0	142.0	213.0
"	115	410.0	261.0	79.0	191.0	192.0	192.0	287.0
"	116	479.0	330.0	98.0	165.0	201.0	192.0	328.0
"	117	829.0	620.0	119.0	223.0	210.0	235.0	484.0
"	118	618.0	498.0	142.0	238.0	229.0	250.0	484.0
"	119	596.0	554.0	165.0	256.0	258.0	252.0	437.0
"	120	861.0	868.0	193.0	288.0	277.0	280.0	623.0
"	121	256.0	179.0	59.0	138.0	148.0	137.0	192.0
"	122	337.0	229.0	76.0	161.0	153.0	154.0	229.0
"	123	375.0	288.0	97.0	129.0	160.0	149.0	256.0
"	124	506.0	407.0	112.0	145.0	179.0	168.0	285.0
"	125	466.0	391.0	129.0	206.0	199.0	200.0	354.0
"	126	468.0	465.0	145.0	234.0	246.0	231.0	345.0
"	127	518.0	534.0	151.0	216.0	214.0	215.0	376.0
"	128	530.0	590.0	175.0	217.0	213.0	218.0	388.0
"	129	553.0	633.0	195.0	224.0	229.0	236.0	394.0
"	130	565.0	698.0	213.0	237.0	249.0	244.0	398.0
"	131	587.0	803.0	227.0	255.0	256.0	264.0	440.0
"	132	288.0	180.0	58.0	151.0	148.0	149.0	225.0
"	133	389.0	253.0	77.0	177.0	179.0	177.0	251.0
"	134	422.0	319.0	96.0	151.0	187.0	176.0	285.0
"	135	702.0	525.0	115.0	179.0	210.0	209.0	393.0
"	136	586.0	476.0	141.0	210.0	254.0	240.0	419.0
"	137	562.0	529.0	158.0	269.0	287.0	273.0	421.0
"	138	707.0	701.0	181.0	281.0	290.0	280.0	505.0
"	139	666.0	710.0	192.0	273.0	278.0	274.0	513.0
HOOK-UP I	140	623.0	745.0	216.0	274.0	288.0	285.0	471.0

140

DESCRIPTION	RUN NO.	GAGE 73 IRP MICRO STRAIN	GAGE 24 IRP MICRO STRAIN	GAGE 76 IRP MICRO STRAIN	GAGE 89 IRP MICRO STRAIN	GAGE 81 IRP MICRO STRAIN	GAGE 812 IRP MICRO STRAIN	GAGE 813 IRP MICRO STRAIN
HOOK-UP I	141	628.0	782.0	232.0	282.0	294.0	281.0	456.0
"	142	702.0	901.0	240.0	298.0	306.0	314.0	528.0
"	143	218.0	147.0	41.0	160.0	183.0	172.0	184.0
"	144	299.0	199.0	58.0	181.0	211.0	201.0	239.0
"	145	397.0	279.0	75.0	230.0	266.0	252.0	308.0
"	146	502.0	361.0	95.0	235.0	272.0	268.0	350.0
"	147	815.0	618.0	118.0	242.0	287.0	276.0	448.0
"	148	751.0	598.0	126.0	280.0	318.0	310.0	502.0
"	149	681.0	577.0	138.0	331.0	369.0	363.0	540.0
"	150	723.0	662.0	164.0	342.0	393.0	362.0	553.0
"	151	238.0	157.0	40.0	187.0	222.0	203.0	202.0
"	152	334.0	232.0	54.0	254.0	316.0	291.0	276.0
"	153	370.0	279.0	69.0	260.0	319.0	295.0	305.0
"	154	492.0	382.0	90.0	277.0	335.0	307.0	366.0
"	155	625.0	485.0	113.0	305.0	364.0	333.0	433.0
"	156	699.0	603.0	142.0	371.0	435.0	399.0	518.0
"	157	774.0	748.0	167.0	439.0	519.0	477.0	604.0
"	158	310.0	203.0	40.0	234.0	286.0	270.0	272.0
"	159	438.0	323.0	56.0	403.0	493.0	450.0	394.0
"	160	424.0	329.0	70.0	373.0	455.0	410.0	377.0
"	161	488.0	405.0	85.0	374.0	462.0	405.0	400.0
"	162	584.0	485.0	104.0	432.0	510.0	460.0	462.0
"	163	695.0	632.0	129.0	511.0	600.0	535.0	549.0
"	164	831.0	803.0	154.0	696.0	831.0	728.0	700.0
"	165	333.0	211.0	40.0	245.0	299.0	293.0	303.0
"	166	483.0	365.0	58.0	449.0	561.0	519.0	455.0
"	167	455.0	335.0	69.0	409.0	510.0	460.0	412.0
"	169	527.0	424.0	86.0	417.0	510.0	457.0	436.0
"	170	605.0	522.0	105.0	470.0	576.0	510.0	498.0
HOOK-UP I	171	767.0	722.0	128.0	699.0	850.0	747.0	680.0

141

DESCRIPTION	RUN NO.	GAGE 73 IRP MICRO STRAIN	GAGE 24 IRP MICRO STRAIN	GAGE 76 IRP MICRO STRAIN	GAGE 89 IRP MICRO STRAIN	GAGE 81 IRP MICRO STRAIN	GAGE 812 IRP MICRO STRAIN	GAGE 813 IRP MICRO STRAIN
HOOK-UP I	172	390.0	240.0	44.0	278.0	344.0	322.0	324.0
"	173	495.0	365.0	58.0	435.0	543.0	496.0	445.0
"	174	523.0	371.0	71.0	431.0	539.0	496.0	460.0
"	175	560.0	433.0	86.0	437.0	542.0	485.0	474.0
"	176	686.0	558.0	105.0	511.0	634.0	561.0	553.0
"	177	815.0	829.0	131.0	749.0	914.0	818.0	761.0
"	178	48.0	65.0	23.0	54.0	53.0	48.0	41.0
"	179	54.0	68.0	24.0	60.0	61.0	56.0	46.0
"	180	54.0	69.0	24.0	56.0	51.0	49.0	43.0
"	181	57.0	72.0	25.0	55.0	53.0	48.0	42.0
"	182	99.0	83.0	26.0	80.0	56.0	62.0	65.0
"	183	66.0	76.0	26.0	83.0	53.0	57.0	57.0
"	184	69.0	81.0	26.0	65.0	55.0	57.0	53.0
"	185	78.0	86.0	28.0	82.0	78.0	78.0	64.0
"	186	121.0	106.0	28.0	81.0	54.0	71.0	87.0
"	187	89.0	93.0	30.0	91.0	72.0	81.0	71.0
"	188	78.0	92.0	30.0	85.0	64.0	75.0	63.0
"	189	79.0	98.0	32.0	86.0	65.0	75.0	60.0
"	190	76.0	94.0	31.0	73.0	61.0	70.0	57.0
"	191	565.0	738.0	206.0	244.0	233.0	260.0	458.0
"	192	76.0	96.0	32.0	85.0	47.0	77.0	71.0
"	193	75.0	99.0	30.0	87.0	52.0	76.0	71.0
"	194	75.0	97.0	32.0	89.0	52.0	73.0	68.0
"	195	73.0	95.0	32.0	90.0	53.0	75.0	68.0
"	196	80.0	97.0	33.0	88.0	50.0	74.0	45.0
"	197	52.0	67.0	24.0	56.0	51.0	47.0	40.0
"	198	57.0	71.0	26.0	59.0	53.0	50.0	44.0
"	199	64.0	77.0	26.0	59.0	55.0	51.0	47.0
"	200	67.0	80.0	27.0	78.0	56.0	61.0	58.0
HOOK-UP I	201	71.0	83.0	28.0	89.0	58.0	62.0	60.0

142

DESCRIPTION	RUN NO.	GAGE 73 IRP MICRO STRAIN	GAGE 24 IRP MICRO STRAIN	GAGE 76 IRP MICRO STRAIN	GAGE 89 IRP MICRO STRAIN	GAGE 81 IRP MICRO STRAIN	GAGE 812 IRP MICRO STRAIN	GAGE 813 IRP MICRO STRAIN
HOOK-UP I	202	75.0	90.0	31.0	98.0	54.0	64.0	67.0
"	203	81.0	97.0	32.0	91.0	55.0	68.0	63.0
"	204	83.0	102.0	32.0	96.0	58.0	69.0	73.0
"	205	87.0	108.0	34.0	94.0	67.0	73.0	69.0
"	206	97.0	113.0	34.0	102.0	68.0	84.0	79.0
"	207	93.0	119.0	36.0	92.0	57.0	74.0	79.0
"	208	95.0	121.0	39.0	82.0	54.0	76.0	75.0
"	209	94.0	127.0	41.0	88.0	56.0	73.0	75.0
"	210	97.0	133.0	42.0	87.0	55.0	77.0	77.0

APPENDIX II

PRESSURE COEFFICIENT DATA

BLADE SURFACE STEADY PRESSURE TEST

BLADE ANGLE: 21.7°

SPEED: 900 RPM

Cp

r/R		.04 (L.E.)	.10	.16	.23	.30	.36	.43	.50	.56	.63	.70	.76	.83	.90	.98 (T.E.)
.287	FACE	0.42	0.18	0.16	0.15	0.18	0.17		0.24	0.32	0.22	0.32	0.12	0.18	0.20	0.24
	CAMBER		-0.39	-0.57	-0.59	-0.47	-0.37	-0.28	-0.14	-0.07	-0.02	0.03				
.361	FACE	-0.86	0.18	-1.39	0.20	0.19	0.20		0.20	0.22	-0.49	-0.57	-0.21	0.22	0.25	0.22
	CAMBER	-0.26	-0.69	-0.55	-0.45	-0.36	-0.31	-0.24	-0.20	-0.13	-0.06	-0.03		0.06	0.14	0.20
.454	FACE	0.41	0.30	0.25	0.22	0.21	0.26		0.53		0.22	0.20		0.23	0.22	0.19
	CAMBER	-0.02	-0.50	-0.37	-0.31	-0.24	-0.23	-0.18	-0.17	-0.11	-0.10	-0.03		0.05	0.09	0.15
.556	FACE	0.85	0.29	0.25	0.22	0.21	0.91		0.20		0.19	0.17		0.18	0.16	0.15
	CAMBER	-0.11	-0.44	-0.31	-0.27	-0.21	-0.20	-0.18	-0.17		-0.12	-0.09	-0.06			0.09
.648	FACE		0.30	0.23	0.20	0.18	0.19		0.19	0.16	0.15	0.15		0.15	0.55	0.14
	CAMBER	-0.47	-0.42	-0.32	-0.25	-0.22	-0.20	-0.20	-0.18	-0.17	-0.15	-0.13	-0.11	-0.08	-0.02	0.05
.722	FACE		0.33	0.33	0.24	0.22	0.20		0.22	0.17	0.17	0.17		0.17	0.15	0.11
	CAMBER	-0.52	-0.37	-0.28	-0.22	-0.20	-0.19	-0.18	-0.17	-0.16	-0.14	-0.13	-0.10	-0.08	-0.04	0.01
.800	FACE		0.27	0.22	0.21	0.18	0.16		0.18	0.59	0.13	0.11		0.07	0.11	0.04
	CAMBER	-0.57	-0.44	-0.32	-0.28	-0.26	-0.25	-0.24	-0.24	-0.22	-0.18	-0.19	-0.14	-0.11	-0.07	-0.04
.861	FACE		-0.18	0.23	0.21	0.17	0.17		0.18	0.13	0.11	0.09		0.07	0.01	-0.03
	CAMBER		-0.97	-0.40	-0.31	-0.30	-0.28	-0.29	-0.26	-0.24	-0.23	-0.20	-0.19	-0.17	-0.13	-0.10
.917	FACE			0.33	0.24	0.22	0.18		0.20	0.21	0.14	0.18		0.11	0.06	0.05
	CAMBER			-0.60	-0.47	-0.40	-0.36	-0.31	-0.28	-0.27	-0.24	-0.22	-0.19	-0.15	-0.12	-0.13
.963	FACE				0.41	0.34	0.29		0.27	0.20	0.20	0.19		0.09	0.03	
	CAMBER				1.43	-1.36	-1.21	-1.06	-0.95	-0.85	-0.78	-0.71	-0.65	-0.64	-0.56	

x/c

147

BLADE ANGLE: 21.7°

SPEED: 1300 RPM

Cp

R/r		x/c: .04 (L.E.)	.10	.16	.23	.30	.36	.43	.50	.56	.63	.70	.76	.83	.90	.98 (T.E.)
.287	FACE	-0.01	0.23	0.23	0.19	0.26	0.23		0.30	0.28	0.28	0.27		0.28	0.27	0.22
	CAMBER		-0.75	-0.61	-0.56	-0.41	-0.32	-0.25	-0.14	-0.05	0.02	0.06	0.11	0.16	0.20	
.361	FACE	-0.08	0.21	-0.33	0.20	0.20	0.20		0.24	0.24	-0.24	0.03		0.26	0.27	0.23
	CAMBER	-0.36	-0.66	-0.49	-0.41	-0.35	-0.30	-0.24	-0.18	-0.12	-0.07	-0.01	-0.09	0.10	0.15	0.20
.454	FACE	0.64	0.31	0.27	0.25	0.22	0.35		0.68		0.24	0.22		0.25	0.24	0.20
	CAMBER	-0.08	-0.50	-0.36	-0.31	-0.26	-0.23	-0.18	-0.16	-0.11	-0.09	-0.03		0.05	0.10	0.16
.556	FACE		0.31	0.26	0.23	0.23	0.71		0.23	-0.14	0.22	0.20		0.19	0.18	0.16
	CAMBER	-0.14	-0.44	-0.28	-0.24	-0.20	-0.18	-0.16	-0.15	-0.12	-0.11	-0.08	-0.05	0.00	0.02	0.11
.648	FACE		0.30	0.23	0.21	0.20	0.20		0.20	0.17	0.16	0.16		0.25	0.63	0.28
	CAMBER	-0.41	-0.38	-0.28	-0.22	-0.21	-0.17	-0.20	-0.17	-0.17	-0.15	-0.14	-0.12	-0.08	-0.03	0.06
.722	FACE		0.31	0.25	0.24	0.23	0.20		0.23	0.18	0.18	0.19		0.19	0.17	0.12
	CAMBER	-0.51	-0.32	-0.21	-0.18	-0.18	-0.18	-0.18	-0.17	-0.16	-0.15	-0.14	-0.11	-0.08	-0.05	0.02
.800	FACE	0.28	0.26	0.22	0.22	0.18	0.15		0.19	0.37	0.14	0.14		0.10	0.14	0.06
	CAMBER	-0.45	-0.42	-0.33	-0.28	-0.26	-0.26	-0.25	-0.25	-0.23	-0.19	-0.19	-0.15	-0.12	-0.07	-0.02
.861	FACE		0.46	0.24	0.22	0.20	0.19		0.20	0.15	0.13	0.11		0.09	0.02	-0.02
	CAMBER		-0.70	-0.35	-0.34	-0.33	-0.31	-0.32	-0.29	-0.26	-0.25	-0.22	-0.20	-0.18	-0.12	-0.09
.917	FACE			0.36	0.29	0.26	0.24		0.27	0.29	0.25	0.23		0.18	0.16	0.09
	CAMBER			-0.51	-0.43	-0.39	-0.33	-0.31	-0.28	-0.29	-0.25	-0.23	-0.21	-0.17	-0.13	-0.15
.963	FACE				0.41	0.33	0.30		0.33	0.32	0.30	0.27		0.10	0.03	
	CAMBER				-1.12	-1.10	-0.95	-0.99	-0.87	-0.84	-0.77	-0.72	-0.65	-0.62	-0.56	

x/c

BLADE ANGLE: 21.7°

SPEED: 1500 RPM

Cp

r/R		.04 (L.E.)	.10	.16	.23	.30	.36	.43	.50	.56	.63	.70	.76	.83	.90	.98 (T.E.)
.287	FACE	0.10	0.23	0.22	0.19	0.24	0.22		0.29	0.30	0.26	0.25		0.25	0.29	0.24
	CAMBER		-0.61	-0.56	-0.53	-0.43	-0.31	-0.23	-0.07	-0.06	0.04	0.05	0.09	0.16	0.19	
.361	FACE	0.07	0.22	-0.05	0.19	0.20	0.20		0.23	0.23	-0.04	0.08		0.25	0.27	0.24
	CAMBER	-0.43	-0.66	-0.51	-0.40	-0.35	-0.31	-0.25	-0.18	-0.12	-0.06	-0.03	-0.06	0.09	0.14	0.18
.454	FACE	0.55	0.30	0.25	0.25	0.22	0.34		0.71		0.24	0.22		0.25	0.24	0.20
	CAMBER	-0.07	-0.51	-0.36	-0.30	-0.25	-0.24	-0.19	-0.16	-0.12	-0.09	-0.04		0.05	0.10	0.16
.556	FACE		0.31	0.26	0.23	0.23	0.63		0.22	-0.14	0.22	0.20		0.20	0.19	0.16
	CAMBER	-0.14	-0.43	-0.28	-0.24	-0.19	-0.18	-0.17	-0.15	-0.12	-0.11	-0.09	-0.06		0.01	0.11
.648	FACE	0.81	0.31	0.25	0.23	0.23	0.22		0.22	0.25	0.21	0.24		0.21	0.59	0.27
	CAMBER	-0.46	-0.36	-0.28	-0.22	-0.19	-0.18	-0.19	-0.16	-0.17	-0.14	-0.14	-0.12	-0.08	-0.03	0.06
.722	FACE		0.29	0.24	0.23	0.23	0.20		0.23	0.18	0.17	0.19		0.18	0.18	0.13
	CAMBER	-0.45	-0.30	-0.23	-0.20	-0.19	-0.18	-0.18	-0.18	-0.17	-0.16	-0.15	-0.11	-0.09	-0.05	0.02
.800	FACE	0.05	0.24	0.21	0.21	0.18	0.14		0.18	0.28	0.15	0.14		0.13	0.15	0.09
	CAMBER	-0.39	-0.40	-0.33	-0.28	-0.26	-0.26	-0.25	-0.25	-0.23	-0.21	-0.21	-0.16	-0.13	-0.08	-0.02
.861	FACE		0.50	0.23	0.19	0.15	0.14		0.16	0.13	0.12	0.11		0.10	0.06	0.01
	CAMBER		-0.49	-0.34	-0.34	-0.33	-0.31	-0.33	-0.29	-0.27	-0.26	-0.23	-0.22	-0.19	-0.14	-0.09
.917	FACE			0.36	0.28	0.26	0.22		0.30	0.29	0.25	0.24		0.18	0.14	0.08
	CAMBER			-0.51	-0.42	-0.42	-0.35	-0.32	-0.30	-0.32	-0.27	-0.25	-0.23	-0.19	-0.15	-0.16
.963	FACE				0.43	0.36	0.31		0.36	0.36	0.32	0.31		0.22	0.17	
	CAMBER				-1.09	-1.03	-0.89	-0.94	-0.81	-0.81	-0.74	-0.70	-0.63	-0.59	-0.55	

x/c

149

BLADE ANGLE: 21.7°

SPEED: 1700 RPM

Cp

r/R		.04 (L.E.)	.10	.16	.23	.30	.36	.43	.50	.56	.63	.70	.76	.83	.90	.98 (T.E.)
.287	FACE	0.53	0.28	0.25	0.21	0.25	0.23		0.32	0.38	0.29	0.27		0.30	0.33	0.85
	CAMBER	0.19	-0.63	-0.58	-0.55	-0.41	-0.32	-0.22	-0.12	-0.05	0.03	0.06	0.10	0.17	0.20	0.24
.361	FACE	0.45	0.28	0.06	0.22	0.22	0.24		0.24	0.24	-0.12	0.10		0.27	0.27	0.25
	CAMBER	-0.52	-0.66	-0.50	-0.39	-0.34	-0.30	-0.24	-0.18	-0.11	-0.06	-0.01	-0.03	0.10	0.16	0.20
.454	FACE	0.89	0.30	0.25	0.25	0.23	0.34		0.76		0.24	0.23		0.25	0.25	0.21
	CAMBER	-0.08	-0.50	-0.35	-0.29	-0.24	-0.24	-0.18	-0.16	-0.11	-0.08	-0.04		0.06	0.10	0.17
.556	FACE		0.31	0.26	0.24	0.24	0.58		0.22		0.22	0.20		0.20	0.20	0.17
	CAMBER	-0.14	-0.42	-0.27	-0.23	-0.20	-0.14	-0.14	-0.06	-0.11	-0.08	-0.08	-0.05		0.02	0.12
.648	FACE	0.35	0.28	0.24	0.21	0.20	0.20		0.21	0.19	0.17	0.19		0.18	0.49	0.21
	CAMBER	-0.48	-0.36	-0.28	-0.22	-0.19	-0.18	-0.19	-0.17	-0.17	-0.15	-0.14	-0.12	-0.08	-0.03	0.07
.722	FACE	0.71	0.29	0.24	0.23	0.22	0.20		0.23	0.19	0.18	0.19		0.19	0.18	0.13
	CAMBER	-0.53	-0.33	-0.24	-0.20	-0.19	-0.18	-0.18	-0.19	-0.18	-0.16	-0.16	-0.12	-0.09	-0.05	0.02
.800	FACE	-0.12	0.23	0.20	0.21	0.18	0.15		0.21	0.17	0.17	0.17		0.15	0.17	0.10
	CAMBER	-0.36	-0.37	-0.30	-0.27	-0.25	-0.26	-0.25	-0.26	-0.22	-0.22	-0.21	-0.17	-0.14	-0.09	-0.02
.861	FACE	0.39		0.23	0.21	0.19	0.18		0.22	0.20	0.18	0.17		0.14	0.06	0.04
	CAMBER	-0.45		-0.38	-0.37	-0.36	-0.33	-0.36	-0.31	-0.29	-0.28	-0.24	-0.23	-0.20	-0.14	-0.09
.917	FACE			0.38	0.29	0.28	0.24		0.34	0.27	0.24	0.27		0.20	0.08	0.02
	CAMBER			-0.60	-0.48	-0.43	-0.39	-0.34	-0.33	-0.34	-0.29	-0.27	-0.24	-0.20	-0.16	-0.18
.963	FACE				0.44	0.38	0.33		0.34	0.38	0.35	0.34		0.23	0.18	
	CAMBER				-0.93	-0.92	-0.84	-0.93	-0.86	-0.80	-0.75	-0.69	-0.63	-0.59	-0.55	
	x/c	.04	.10	.16	.23	.30	.36	.43	.50	.56	.63	.70	.76	.83	.90	.98
		L.E.														T.E.

150

BLADE ANGLE: 21.7°

SPEED: 1780 RPM

Cp

r/R		.04 (L.E.)	.10	.16	.23	.30	.36	.43	.50	.56	.63	.70	.76	.83	.90	.98 (T.E.)
.287	FACE	0.40	0.24	0.21	0.19	0.25	0.23		0.30	0.39	0.28	0.26		0.26	0.27	0.65
	CAMBER	0.09	-0.64	-0.59	-0.57	-0.43	-0.34	-0.25	-0.15	-0.07	0.01	0.05	0.08	0.15	0.18	0.23
.361	FACE	0.47	0.28	0.18	0.23	0.22	0.23		0.28	0.27	0.19	0.24		0.27	0.29	0.27
	CAMBER	-0.52	-0.62	-0.50	-0.40	-0.35	-0.32	-0.25	-0.20	-0.13	-0.07	-0.03	-0.04	0.10	0.15	0.19
.454	FACE	0.93	0.30	0.25	0.25	0.23	0.32		0.79		0.23	0.22		0.25	0.25	0.32
	CAMBER	-0.12	-0.45	-0.33	-0.28	-0.24	-0.23	-0.19	-0.16	-0.11	-0.09	-0.04		0.06	0.10	0.17
.556	FACE	0.95	0.30	0.26	0.24	0.24	0.52		0.22		0.22	0.20		0.20	0.19	0.17
	CAMBER	-0.14	-0.42	-0.26	-0.23	-0.19	-0.18	-0.16	-0.15	-0.12	-0.11	-0.09	-0.06		0.01	0.12
.648	FACE	0.57	0.28	0.23	0.20	0.20	0.19		0.20	0.18	0.17	0.17		0.17	0.44	0.15
	CAMBER	-0.50	-0.35	-0.28	-0.22	-0.19	-0.18	-0.19	-0.17	-0.17	-0.16	-0.15	-0.12	-0.08	-0.03	0.06
.722	FACE	0.82	0.29	0.24	0.23	0.22	0.20		0.24	0.19	0.19	0.20		0.19	0.18	0.13
	CAMBER	-0.52	-0.32	-0.24	-0.20	-0.19	-0.18	-0.18	-0.19	-0.18	-0.17	-0.16	-0.13	-0.10	-0.06	0.02
.800	FACE	0.11	0.23	0.20	0.21	0.19	0.16		0.23	0.28	0.21	0.21		0.16	0.18	0.10
	CAMBER	-0.35	-0.35	-0.29	-0.26	-0.25	-0.26	-0.25	-0.26	-0.24	-0.22	-0.22	-0.18	-0.14	-0.09	-0.02
.861	FACE		0.36	0.24	0.21	0.20	0.20		0.25	0.22	0.20	0.20		0.16	0.11	0.04
	CAMBER		-0.40	-0.37	-0.36	-0.36	-0.33	-0.36	-0.31	-0.30	-0.29	-0.25	-0.24	-0.20	-0.14	-0.09
.917	FACE			0.38	0.29	0.28	0.25		0.31	0.31	0.26	0.26		0.19	0.16	0.08
	CAMBER			-0.55	-0.44	-0.43	-0.37	-0.35	-0.33	-0.35	-0.30	-0.28	-0.26	-0.22	-0.17	-0.20
.936	FACE				0.43	0.37	0.32		0.39	0.38	0.30	0.21		0.14	0.07	
	CAMBER				-0.89	-0.93	-0.85	-0.89	-0.81	-0.80	-0.75	-0.69	-0.63	-0.60	-0.56	

x/c

151

BLADE ANGLE: 32°

SPEED: 900 RPM

Cp

r/R		.04 L.E.	.10	.16	.23	.30	.36	.43	.50	.56	.63	.70	.76	.83	.90	.98 T.E.
.287	1 FACE	0.72	0.06	0.01	-0.08	-0.06	-0.07		-0.02		-0.02	-0.01			-0.03	0.08
	CAMBER	-1.97	-1.34	-1.10	-1.05	-0.82	-0.73	-0.76	-0.57	-0.41	-0.30	-0.26	-0.23	-0.15	-0.14	-0.07
.361	2 FACE	1.05	0.30	0.37	0.11	0.12	0.10		0.05	0.06				0.05	0.09	0.07
	CAMBER	-1.79	-1.12	-0.83	-0.65	-0.56	-0.48	-0.50	-0.33	-0.25	-0.20	-0.16	-0.07	-0.05	0.02	0.06
.454	3 FACE	0.83	0.40	0.30	0.25	0.18	0.26		0.68		0.15	0.12	0.07	0.15	0.13	0.09
	CAMBER	-1.67	-1.27	-0.63	-0.42	-0.34	-0.31	-0.26	-0.22	-0.18	-0.14	-0.10		-0.04	0.01	0.07
.556	4 FACE	0.97	0.41	0.33	0.26	0.24	0.53		0.17	-0.21	0.17	0.11		0.11	0.08	0.07
	CAMBER	-1.37	-0.97	-0.59	-0.42	-0.33	-0.27	-0.23	-0.20	-0.16	-0.14	-0.10	-0.09		-0.04	0.03
.648	5 FACE	0.51	0.37	0.37	0.31	0.27	0.25		0.23	0.18	0.17	0.16		0.14	0.89	0.17
	CAMBER	-1.47	-1.21	-0.69	-0.40	-0.25	-0.19	-0.18	-0.14	-0.13	-0.09	-0.08	-0.07	-0.04	-0.02	0.03
.722	6 FACE	-0.14	0.33	0.29	0.25	0.21	0.18		0.33	0.12	0.26	0.15		0.09	0.31	0.02
	CAMBER	-1.45	-1.52	-0.55	-0.29	-0.24	-0.23	-0.20	-0.21	-0.18	-0.17	-0.17	-0.13	-0.12	-0.11	-0.07
.800	7 FACE	-0.16	0.33	0.25	0.23	0.18	0.15		0.16	0.08	0.09	0.06			0.03	-0.04
	CAMBER	-1.46	-1.58	-1.14	-0.53	-0.28	-0.24	-0.21	-0.21	-0.18	-0.17	-0.17	-0.16	-0.12	-0.12	-0.09
.861	8 FACE		0.24	0.19	0.15	0.12	0.13		0.14	0.11	0.09	0.06		0.03	-0.01	-0.06
	CAMBER		-1.03	-0.90	-0.81	-0.73	-0.64	-0.56	-0.51	-0.45	-0.42	-0.37	-0.34	-0.31	-0.27	-0.20
.917	9 FACE			0.24	0.24	0.22	0.21		0.22	0.19	0.16	0.14		0.09	0.04	-0.06
	CAMBER			-1.18	-1.06	-0.92	-0.79	-0.71	-0.64	-0.59	-0.54	-0.50	-0.45	-0.43	-0.37	-0.33
.963	0 FACE				0.84	0.36	0.31		0.31	0.26	0.24	0.21		0.13	0.06	
	CAMBER				-0.72	-0.70	-0.65	-0.60	-0.56	-0.54	-0.51	-0.47	-0.44	-0.42	-0.38	

x/c

152

BLADE ANGLE: 32°

SPEED: 1300 RPM

Cp

r/R		x/c = .04 (L.E.)	.10	.16	.23	.30	.36	.43	.50	.56	.63	.70	.76	.83	.90	.98 (T.E.)
.287	FACE	0.77	0.12	0.08	-0.03	0.05	-0.03		0.04	0.06	0.05	0.03		0.05	0.02	0.12
	CAMBER	-1.89	-1.25	-0.97	-0.93	-0.74	-0.63	-0.55	-0.43	-0.34	-0.23	-0.22	-0.14	-0.10	-0.06	-0.02
.361	FACE		0.41	0.15	0.21	0.16	0.16		0.13	0.12				0.13	0.11	0.12
	CAMBER	-1.87	-1.07	-0.80	-0.62	-0.53	-0.46	-0.35	-0.24	-0.19	-0.07	-0.03	0.31	0.02	0.08	0.09
.454	FACE	0.86	0.41	0.32	0.26	0.22	0.33		0.72		0.16	0.12		0.15	0.15	0.10
	CAMBER	-1.79	-1.08	-0.60	-0.44	-0.36	-0.32	-0.25	-0.22	-0.17	-0.13	-0.08	0.13	-0.00	0.03	0.06
.556	FACE	0.97	0.43	0.36	0.29	0.27	0.53		0.18		0.17	0.12		0.10		0.07
	CAMBER	-1.32	-0.96	-0.60	-0.41	-0.32	-0.26	-0.22	-0.19	-0.15	-0.13	-0.10	-0.07		-0.02	0.04
.648	FACE	0.28	0.39	0.34	0.29	0.24	0.21		0.20	0.17	0.15	0.14		0.12	0.59	0.12
	CAMBER	-1.35	-1.20	-0.67	-0.37	-0.27	-0.21	-0.19	-0.18	-0.15	-0.14	-0.11	-0.10	-0.06	-0.04	0.02
.722	FACE	0.78	0.44	0.34	0.29	0.28	0.29		0.65	0.29	0.42	0.30		0.16	0.50	0.06
	CAMBER	-1.04	-1.14	-0.70	-0.40	-0.29	-0.27	-0.23	-0.23	-0.20	-0.19	-0.17	-0.15	-0.13	-0.12	-0.08
.800	FACE	0.55	0.38	0.25	0.25	0.20	0.15		0.15	0.18	0.14	0.17		0.08	0.05	-0.01
	CAMBER	-0.94	-1.19	-1.04	-0.71	-0.51	-0.41	-0.37	-0.37	-0.33	-0.31	-0.29	-0.27	-0.21	-0.20	-0.12
.861	FACE		0.57	0.18	0.15	0.13	0.13		0.14	0.19	0.20	0.22		0.13	0.08	-0.01
	CAMBER		-0.72	-0.78	-0.73	-0.66	-0.61	-0.54	-0.50	-0.45	-0.41	-0.38	-0.35	-0.32	-0.26	-0.20
.917	FACE			0.28	0.25	0.30	0.27		0.37	0.41	0.38	0.36		0.25	0.22	0.08
	CAMBER			-0.97	-0.95	-0.91	-0.82	-0.74	-0.68	-0.61	-0.56	-0.52	-0.47	-0.44	-0.39	-0.35
.963	FACE				0.83	0.39	0.33		0.33	0.28	0.26	0.23		0.15	0.07	
	CAMBER				-0.72	-0.68	-0.64	-0.42	-0.34	-0.42	-0.42	-0.42	-0.43	-0.43	-0.39	

153

BLADE ANGLE: 32°

SPEED: 1500 RPM

Cp

r/R		x/c .04 (L.E.)	.10	.16	.23	.30	.36	.43	.50	.56	.63	.70	.76	.83	.90	.98 (T.E.)
.287	FACE	0.76	0.16	0.10	0.01	0.05	-0.02		0.08	0.08	0.07	0.06	0.06	0.06	0.06	0.16
	CAMBER	-1.90	-1.20	-0.92	-0.88	-0.70	-0.58	-0.51	-0.39	-0.30	-0.21	-0.15	-0.12	-0.06	-0.04	0.01
.361	FACE	1.77	0.42	0.28	0.23	0.20	0.17		0.17	0.16	0.87			0.16	0.17	0.15
	CAMBER	-1.72	-1.02	-0.76	-0.60	-0.50	-0.42	-0.34	-0.26	-0.19	-0.14	-0.10	-0.02	0.02	0.07	0.10
.454	FACE	0.87	0.42	0.31	0.27	0.22	0.33		0.72		0.16	0.11		0.15	0.14	0.11
	CAMBER	-1.97	-0.86	-0.58	-0.46	-0.37	-0.33	-0.27	-0.23	-0.16	-0.14	-0.09	0.14	-0.01	0.02	0.08
.556	FACE	0.96	0.44	0.35	0.29	0.27	0.53		0.20	-0.19	0.17	0.13		0.12	0.11	0.09
	CAMBER	-1.33	-0.97	-0.59	-0.40	-0.32	-0.25	-0.21	-0.18	-0.14	-0.12	-0.09	-0.07		-0.02	0.04
.648	FACE	-0.23	0.35	0.34	0.27	0.24	0.21		0.21	0.18	0.17	0.17		0.15	0.22	0.14
	CAMBER	-1.10	-1.10	-0.78	-0.45	-0.29	-0.23	-0.21	-0.22	-0.16	-0.17	-0.13	-0.11	-0.07	-0.05	0.01
.722	FACE	0.93	0.47	0.35	0.30	0.29	0.28		0.75	0.28	0.50	0.30		0.19	0.44	0.07
	CAMBER	-1.20	-1.33	-0.72	-0.35	-0.24	-0.25	-0.21	-0.21	-0.19	-0.18	-0.16	-0.15	-0.13	-0.12	-0.09
.800	FACE	0.36	0.38	0.26	0.25	0.20	0.16		0.17	0.19	0.16	0.17		0.10	0.08	
	CAMBER	-0.92	-1.12	-1.01	-0.75	-0.51	-0.41	-0.34	-0.33	-0.29	-0.27	-0.25	-0.23	-0.18	-0.17	-0.11
.861	FACE		0.69	0.22	0.16	0.17	0.17		0.20	0.24	0.26	0.24		0.13	0.12	
	CAMBER		-0.70	-0.71	-0.68	-0.63	-0.58	-0.53	-0.47	-0.44	-0.41	-0.37	-0.35	-0.32	-0.26	-0.20
.917	FACE			0.26	0.24	0.24	0.24		0.24	0.21	0.18	0.16		0.12	0.07	
	CAMBER			-0.98	-0.96	-0.92	-0.80	-0.74	-0.68	-0.62	-0.56	-0.51	-0.47	-0.44	-0.39	-0.34
.963	FACE															
	CAMBER															

x/c

154

BLADE ANGLE: 32°

SPEED: 1700 RPM

Cp

r/R		x/c .04 (L.E.)	.10	.16	.23	.30	.36	.43	.50	.56	.63	.70	.76	.83	.90	.98 (T.E.)
.287	FACE	0.57	0.15	0.12	0.04	0.08	0.01		0.06	0.10	0.10	0.08		0.07	0.06	0.17
	CAMBER	-1.91	-1.21	-0.96	-0.87	-0.68	-0.58	-0.47	-0.37	-0.29	-0.20	-0.15	-0.12	-0.05	-0.04	0.01
.361	FACE	0.94	0.35	0.23	0.21	0.19	0.17		0.15	0.14	0.50	0.88		0.15	0.16	0.14
	CAMBER	-1.62	-0.98	-0.74	-0.58	-0.49	-0.42	-0.54	-0.27	-0.19	-0.15	-0.10	-0.03	0.02	0.05	0.09
.454	FACE	0.87	0.42	0.33	0.30	0.25	0.36		0.74		0.18	0.14		0.17	0.17	0.13
	CAMBER	-1.90	-0.88	-0.56	-0.42	-0.33	-0.30	-0.23	-0.19	-0.13	-0.11	-0.06	0.19	0.03	0.06	0.10
.556	FACE	0.96	0.43	0.35	0.29	0.27	0.55		0.19		0.16	0.13		0.12	0.11	0.09
	CAMBER	-1.27	-0.89	-0.55	-0.41	-0.31	-0.25	-0.21	-0.18	-0.14	-0.12	-0.09	-0.07	0.00	-0.02	0.05
.648	FACE	0.24	0.39	0.35	0.30	0.26	0.24		0.23	0.21	0.20	0.19		0.16	0.24	0.17
	CAMBER	-0.99	-1.03	-0.78	-0.50	-0.33	-0.26	-0.21	-0.21	-0.16	-0.17	-0.14	-0.11	-0.08	-0.05	0.01
.722	FACE	0.47	0.42	0.32	0.28	0.23	0.19		0.59	0.13	0.41	0.13		0.11	0.50	0.02
	CAMBER	-1.06	-1.26	-0.72	-0.30	-0.22	-0.25	-0.23	-0.27	-0.20	-0.20	-0.17	-0.14	-0.12	-0.11	-0.08
.800	FACE	0.47	0.38	0.27	0.26	0.21	0.17		0.18	0.16	0.17	0.17		0.10	0.11	0.01
	CAMBER	-0.66	-0.81	-0.74	-0.58	-0.47	-0.41	-0.37	-0.36	-0.31	-0.30	-0.27	-0.24	-0.21	-0.18	-0.11
.861	FACE		0.78	0.22	0.18	0.21	0.19		0.20	0.22	0.22	0.20		0.12	0.09	0.01
	CAMBER		-0.71	-0.60	-0.56	-0.54	-0.50	-0.48	-0.43	-0.40	-0.38	-0.35	-0.33	-0.30	-0.25	-0.19
.917	FACE			0.28	0.26	0.30	0.28		0.26	0.23	0.30	0.32		0.13	0.17	0.04
	CAMBER			-1.11	-0.89	-0.85	-0.75	-0.71	-0.67	-0.61	-0.56	-0.51	-0.48	-0.44	-0.39	-0.35
.963	FACE				0.58	0.41	0.35		0.42	0.39	0.32	0.32		0.22	0.19	
	CAMBER				-0.57	-0.59	-0.54	-0.56	-0.50	-0.51	-0.50	-0.46	-0.44	-0.41	-0.38	

x/c

BLADE ANGLE: 38.3°

SPEED: 900 RPM

Cp

r/R		.04 (T.E.)	.10	.16	.23	.30	.36	.43	.50	.56	.63	.70	.76	.83	.90	.98 (L.E.)
.287	FACE	-0.50	-0.02	-0.18	-0.36	-0.31	-0.34	-0.95	-0.30	-0.32	-0.31	-0.25	-0.50	-0.28	-0.30	0.05
	CAMBER	-2.01	-1.78	-1.44	-1.28	-1.18	-1.04		-0.87	-0.81	-0.66	-0.61		-0.47	-0.44	-0.37
.361	FACE	-0.23	0.11	-0.13	-0.02	-0.13	-0.18	-0.68	-0.18	-0.20	-0.46	-0.45	-0.61	-0.16	-0.18	-0.20
	CAMBER	-2.67	-1.57	-1.18	-0.95	-0.84	-0.75		-0.60	-0.55	-0.46	-0.44		-0.28	-0.25	-0.20
.454	FACE	-0.38	0.22	0.12	0.08	0.03		-0.49	0.41		-0.11	-0.14	-0.30	-0.10	-0.09	-0.13
	CAMBER	-3.02	-1.75	-0.80	-0.66	-0.56			-0.47		-0.37	-0.29		-0.24	-0.21	-0.17
.556	FACE	-0.13	0.29	0.26	0.14	0.07	0.22	-0.39	0.02	-0.49	-0.03	-0.07	-0.26	-0.11	-0.11	-0.14
	CAMBER	-2.01	-2.13	-0.95	-0.63	-0.51	-0.44		-0.40	-0.33	-0.30	-0.27			-0.24	-0.17
.648	FACE	0.01	0.39	0.29	0.20	0.10	0.08	-0.35	0.05	-0.03	-0.05	-0.06	-0.27	-0.05	-0.02	-0.08
	CAMBER	-1.73	-2.16	-1.41	-0.68	-0.47	-0.40		-0.37	-0.31	-0.31	-0.28		-0.25	-0.22	-0.20
.722	FACE	-0.13	0.32	0.25	0.20	0.08	0.04	-0.36	0.58	0.13	0.41	0.16	-0.28	0.02	0.02	-0.08
	CAMBER	-1.55	-1.93	-1.48	-0.90	-0.65	-0.52		-0.36	-0.32	-0.32	-0.29		-0.26	-0.25	-0.21
.800	FACE	0.18	0.32	0.20	0.15	0.06	0.03	-0.87	0.77	0.71	0.58	0.60	-0.46	-0.12	-0.10	
	CAMBER	-1.17	-1.40	-1.50	-1.34	-1.30	-1.06		-0.73	-0.62	-0.56	-0.49		-0.39	-0.37	-0.30
.861	FACE		0.83	0.09	0.06	0.02	0.03	-0.79	0.05	0.01	-0.01	-0.03	-0.53	-0.03	-0.10	-0.18
	CAMBER		-1.16	-1.09	-0.99	-0.98	-0.86		-0.73	-0.67	-0.64	-0.58		-0.50	-0.44	-0.37
.917	FACE			0.16	0.14	0.14	0.13	-0.72	0.14	0.12	0.09	0.07	-0.52		-0.03	-0.14
	CAMBER			-0.97	-0.90	-0.84	-0.75		-0.67	-0.64	-0.60	-0.55		-0.49	-0.45	-0.39
.963	FACE				0.30	0.20		-0.57	0.18	0.14	0.12	0.10	-0.43	0.09	-0.01	
	CAMBER				-0.67	-0.64	-0.61		-0.54	-0.52	-0.51	-0.46		-0.41	-0.39	

x/c

156

REFERENCES

1. NASA Tech Mem. 83736 "Fuel Saving Potential of NASA Advanced Turbo Prop Program", September 1984.

2. NASA CR-3505 "Evaluation of Wind Tunnel Performance Testing of an Advanced 45° Swept Eight Bladed Propeller at Mach Numbers from .45 to .85", Hamilton Standard Division, UTC, March 1982.

3. NASA CR-174814 "Analysis and Test Evaluation of the Dynamic Response of Three Advanced Turboprop Models", Hamilton Standard Division, UTC, August 1985.

4. De George, C.L., J.E. Turnberg, and H.S. Wainauski, "A Report on the Initial Testing of the Large Scale Advanced Prop-Fan" Hamilton Standard Division, UTC, AIAA-86-1551.

5. NASA CR 174788 "Large Scale Advanced Prop-Fan Pitch Change Actuator and Control Design Report", Hamilton Standard Division, UTC, January 31, 1986.

6. S. Goldstein, "On the Vortex Theory of Screw Propellers", Royal Soc. London Proc. (1929), 440.

7. NASA CR 174790 "Large Scale Advanced Prop-Fan Blade Design", Hamilton Standard Division, UTC, September 1985.

8. Hamilton Standard Engineering Report 9790 "LAP Instrumentation Design Report" October 1984.

9. UTRC Report R81-335414 "Static Stall Flutter Tests of Hamilton Standard Prop-Fan Models", Goepner, B.W., January 1982.

10. Kaza, Krishna Rao V., and Kielb, Robert E. "Vibration and Flutter of Mistuned Bladed - Disk Assemblies", NASA TM 83634.

11. Gilmore, D.C., Measurement of the Surface Pressure Distribution on a Propeller Operating at Zero Advance Ratio", Canadair Limited Report.

12. Hanson, D. B., "Propeller Noise Caused By Blade Tip Radial Forces", Hamilton Standard Division, UTC AIAA-86-1892.

1. Report No. CR 180848	2. Government Accession No.	3. Recipient's Catalog No.
4. Title and Subtitle Large Scale Advanced Prop-Fan (LAP) Static Rotor Test Report		5. Report Date
		6. Performing Organization Code 73030
7. Author(s) C.L. De George, H.S. Wainauski J.E. Turnberg		8. Performing Organization Report No. HSER 116227
		10. Work Unit No.
9. Performing Organization Name and Address Hamilton Standard Division, UTC P.O. Box 1000 Windsor Locks, CT 06096		11. Contract or Grant No. NAS 3-23051
		13. Type of Report and Period Covered Contractor Report
12. Sponsoring Agency Name and Address NASA Lewis Research Center 21000 Brookpark Road Cleveland, OH 44135		14. Sponsoring Agency Code

15. Supplementary Notes
Project Manager: J. Notardonato, Advanced Turboprop Project Office
NASA Lewis Research Center
Cleveland, OH 44135

16. Abstract

This report discusses Static Rotor Testing of the SR-7L Large Scale Advanced Prop Fan (LAP). The LAP is an advanced nine foot diameter, 8 bladed propeller designed and built by Hamilton Standard under contract to the NASA-Lewis Research Center. The Prop-Fan employs thin swept blades to provide efficient propulsion at flight speeds up to Mach .85.

Static Testing was conducted on a 10,000 horsepower whirl rig at Wright Patterson Air Force Base. The test objectives were to investigate the Prop-Fan static aerodynamic and structural dynamic performance, determine the blade steady state stressers and deflections and to measure steady and unsteady pressures on the SR-7L blade surface.

The measured performance of the LAP correlated well with analytical predictions at blade pitch angles below 30°. A stall buffet phenomena was observed at blade pitch angles above 30°. This phenomena manifested itself by elevated blade vibratory stress levels and lower than expected thrust produced and power absorbed by the Prop-Fan for a given speed and blade angle.

17. Key Words (Suggested by Author(s)) Prop-Fan Static Rotor Test	18. Distribution Statement This document will remain under distribution limitation until December, 1988.
19. Security Classif. (of this report) Unclassified	20. Security Classif. (of this page) Unclassified	21. No. of Pages 160	22. Price*

NASA-C-168 (Rev. 10-75)